國立交通大學

材料科學與工程研究所

博 士 論 文

矽膠材料在微光學上的應用

Silicone materials for the application of microoptics

研 究 生：施騰凱

指導教授：陳家富、黃華宗　教授

中 華 民 國 九 十 六 年 11 月

矽膠材料在微光學上的應用

Silicone materials for the application of microoptics

研 究 生：施騰凱　　Student：Teng-Kai Shih

指導教授：陳家富 博士　　Advisor：Dr. Chia-Fu Chen

黃華宗 博士　　Dr. Wha-Tzong Whang

國 立 交 通 大 學

材料科學與工程研究所

博 士 論 文

A Thesis

Submitted to Institute of Material Science and Engineer College of Engineering

National Chiao Tung University

in partial Fulfillment of the Requirements

for the Degree of doctor of Science

in Material Science and Engineering

November 2006

Hsinchu, Taiwan, Republic of China

中華民國九十七年 11 月

國　立　交　通　大　學
研究所博士班
論文口試委員會審定書

本校 **材料科學與工程** 學系 施騰凱 君

所提論文 矽膠材料於微光學上的應用

Silicone materials for the application of microoptics

合於博士資格水準、業經本委員會評審認可。

口試委員：

指導教授：

系主任：　　　　　教授

中　華　民　國　九十六 年十一月 九 日

矽膠材料於微光學上的應用

研究生：施騰凱　　指導教授：陳家富 博士

黃華宗 博士

國立交通大學

材料科學與工程研究所

摘　　要

聚二甲基矽氧烷 (PDMS)有許多優異的特性並已經應用在很多不同領域，例如微機電、生醫和化學溶膠改質。本論文主要是應用矽膠高分子 PDMS 的特性去製作三種微光學元件：(1)折射式微透鏡；(2)反射式微透鏡；和(3)繞射光柵和相關元件。

在折射式微透鏡製作中,主要是利用準分子雷射在聚碳酸酯（PC）薄板上作圖案，接著利用旋轉塗佈機將聚甲基丙烯酸甲酯（PMMA）液體塗佈在圖案上，藉由薄膜重力形成微曲面，利用這曲面是當成微型透鏡模具,接著將 PDMS 液體倒入模具中，固化後形成微透鏡。藉由 PDMS 易脫膜的特性，PDMS 微透鏡可以輕易脫離聚甲基丙烯酸甲酯（PMMA）模具。而微透鏡的曲率和焦距可以藉由微孔的大小跟 PMMA 的膜厚來控制。

在反射式微透鏡製作中，主要是承接折射式微透鏡製作和 PDMS 的高反射率材料的研發。藉由光散射理論，PDMS 高分子混合奈米尺寸的二氧化鈦粉末形成高反射率材料，接著倒入 PMMA 模具，形成凸型的微透鏡。藉由 PDMS 二次翻模，可以分別製作出反射式 PDMS 凹、凸微透鏡。

在繞射光柵製作中，主要是基於金屬覆蓋於 PDMS 表面，這表面會自發展週期 1-2 微米波形結構的原理。在這裡，我們利用強酸使 PDMS 表面形成氧化層，進而導致波紋結構產生，藉由控制 PDMS 的彈性模數、強酸的比例和浸泡的時間，波紋的週期可以被控制。藉由外部拉力的引導，表面的波紋結構可以被整齊的排列以形成繞射光柵。

Silicone materials for the application of microoptics

Student：Teng-Kai Shih　　Advisor：Dr. Chia-Fu Chen

Dr. Wha-Tzong Whang

Institute of Material Science and Engineering

National Chiao-Tung University

Abstract

The silicone rubbery material, polydimethylsiloxane (PDMS), has attracted the attention of many material scientists recently as there are potential applications ranging from microelectromechanical systems (MEMS) to biology, due to its excellent physical and chemical characteristics. This thesis focused on the fabrication of microoptical elements by the use of PDMS polymer, included refractive microlenses, reflective microlenses and diffractive gratings.

For the fabrication of refractive microlenses, concave microlens molds were fabricated through spin-coating processes suspended liquid PMMA films on the micro-drilled holes, leading to the formation of the special curvature due to the weight of PMMA films. Then, liquid PDMS polymer was cast onto the PMMA concave molds. After curing PDMS polymer, the solidified PDMS microlens arrays could be easily stripped from the PMMA film due to the hydrophobic nature of PDMS polymer. With the change of diameters of microholes and thicknesses of PMMA films, the suspended height of films was surely controllable. Therefore, the curvature radiuses and shapes of microlens also depended on the diameters of microholes and the thicknesses of PMMA films.

For the fabrication of reflective microlenses, we connected the fabrication of refractive microlens and the preparation of high-reflectance material. Based on light scattering theory, PDMS rubber polymers mixed with nanoscale TiO2 powders to form directly high-reflectance materials. Finally, both of concave and convex elements could be fabricated through soft replica molding processes and these elements could directly reflect light without the deposition of metal coatings.

Wrinkles with the periodicity of 1-2 micrometer would be spontaneously developed on PDMS surface covered with a layer of gold films. Based on this phenomenon, a novel way to fabricate diffractive gratings could be proposed.　The surface layer of PDMS was

immediately oxidized, after it contacted with the acid solutions (H_2SO_4/ HNO_3). A bilayer system, a stiff layer (an oxidized PDMS film) was capped on the soft foundation (a PDMS film), would lead to the formation of wrinkles. By the control of elastic modulus of PDMS, the mixed ratio of strong acid solutions and the dipped duration, the periodicity of wrinkles could be adjusted. Wrinkles, which could be arranged orderedly through the guidance of external forces, were regarded as optical gratings.

致謝

本論文的完成首先要感謝指導教授陳家富博士，承蒙老師這些年來不論是在待人處事或是學業研究上的指導，使我受益匪淺。同時感謝實驗室學長在實驗上提供許多寶貴的意見以及監督，有如兄長一般無私的提攜讓我在實驗過程中成長許多。

感謝施士塵學長、羅鴻鈞學長、陳建銘學長、陳光中學長、劉厥揚同學、徐振航學長、洪淙琦學弟、王瑞豪學弟、陳宜輝學弟及莊方慈學弟在各方面的支持與鼓勵並在我攻讀博士的過程中，不斷地帶給我的歡樂與活力，謝謝你們陪我走過這段日子並帶給我許多美好的回憶。

另外深深感謝中正大學光機電整合研究所何正榮老師在實驗上的提攜，由於何老師的細心指導才能讓我茁壯至此。

最後深深地感謝我的家人，由於你們在背後的支持才能使我致力於學業研究上而能夠無所顧慮。僅將此論文獻給我所愛的家人。

Contents

Figure Caption

Table Caption

Chapter 1 Introduction

1.1 Preface

Growing needs and new applications of optical components and systems in multiple industries have driven the need for advances in fabrication and integration technologies for microoptics. New or increased functionality, smaller sizes, lower costs–these drivers are nearly universal for communications, sensors, biomedical applications, data storage, and a wide range of other technology-driven and consumer-driven industries. These factors drive needs for technical innovation, while fabrication volumes required for these markets place added emphasis on efficient manufacturing methods. The dual requirements of technical innovation and scalable, cost-efficient manufacturing present significant challenges for future developments in microoptical fabrication. Microoptic components offer a great deal of promise due to the ranges of functions that can be implemented as well as the ability to fabricate devices at the waferlevel using techniques leveraged from the microelectronics industry.

1.2 Types of microoptical elements

The term “microoptical elements” contains a nearly infinite variety of different surface profiles, shown in Fig.1-1. However, with respect to the different optical functions, we can classify the elements and define requirements for the corresponding fabrication technologies. Such a classification is, of course, not sharp and does not take into account the full variety of existing optical elements.

The first class consists of elements with continuous surface profiles such as lenses and prisms or, more general, beam-shaping elements with arbitrary shapes. The characteristic detail is large compared to the wavelength of light, and in order to analyze the optical function the optical function of these elements, the geometrical optical approach is sufficient. Ray tracing and the application of the law of refraction is the basis for modeling and design of these elements and that is why they are called refractive. However, with decreasing diameter or increasing deflection angle, wave-optical effects will affect the optical function more and more and have to be considered. Although from a physical point of view, optical elements are scalable with the wavelength, the size of

these elements is mostly determined by technical demands of setup or the device that admits the element. Thus, the aperture of these elements ranges from several microns to millimeters and the value for the total profile depth also varies over a wide range (<1μm to 1mm). The requirements for the profile accuracy for this class of elements are scaling with the wavelength and can be found usually between λ/5 and λ/20.

A second class of elements consists of periodic structures like binary and blazed gratings as well as beam splitters with a continuous profile. Computer-generated holograms (often used synonyms are kinoforms, diffractive optical elements, and holographic optical elements) also belong to this class. The characteristic details of these elements are larger than the wavelength of light, and for the analysis of its optical function, wave-optical methods have to be applied. Because diffraction of light is the basis for the functionality, these elements are called diffractive. In contrast to refractive elements, the accuracy of the transmitted (or reflected) wave front is related to the accuracy of the period d. If, for instance, the positioning error of a grating line is $d/10$, then the wave-front error will be $d/10$ in the 1^{st} and -1^{st} diffraction orders. The accuracy of the profile shape mainly influences the distribution of intensity between different diffraction orders. The size of diffraction elements ranges from some micrometers to some hundred millimeters, but the profile depth scales with the wavelength.

The third class of elements we want to distinguish consists of periodic structures too, but the feature size is, in contrast to the above-mentioned diffractive elements, lower than the wavelength of light. Therefore, for normal incidence, no propagating diffraction orders exist and the structure acts as an effective medium. The term “artificial materials” is often used for this class of elements, because they have optical properties (e.g., birefringence, locally varying refractive index, polarization) which are very different from the original properties of the used material. Examples for elements are phase-retarder plates, moth eye structures, or blazed binary gratings. For the analysis of these elements (especially the calculation of the wave front just behind the element), rigorous methods have to be applied. Since there exists up to now no algorithm which allows the backward calculation of a profile from a given wave front, the design of these elements has to utilize a systematic scanning of the parameter space. The accuracy of the optical function scales with the wavelength and depends mainly on the accuracy of the

grating parameters period d, fill factor f, and grating depth D.

1.3 Historical overview of microoptics fabrication

The history of microoptics dates back over 200 years. Diffraction gratings can be traced back to 1785, with the principles of these devices first attributed to Rittenhouse, an American astronomer. The principles of diffraction gratings were independently rediscovered by Fraunhofer in 1819. The earliest devices were amplitude gratings created as grids of fine wire or hair run between sets of parallel screws. Fraunhofer later ruled simple gratings in gold films on glass and directly in glass surfaces using a piece of diamond. Rowland made great advances in precision grating ruling engines in the 1880's. In 1910, Wood succeeded in ruling blazed phase gratings in copper plates with grooves of controlled shape. Diffractive "zone plates" with focusing power were hand-drawn as amplitude masks by Rayleigh in 1871, and later created as phase structures by Wood in 1898. An overview of early histories of diffraction grating fabrication can be found in [1]–[3]. Another important milestone in the history of diffractive optics is the development of holography by Gabor in 1948 [4]. Holograms are created on photographic film by recording the interference pattern of a light signal scattered off of an object and a coherent background signal, or reference. When the resulting hologram is illuminated only by the reference signal, an image of the object is reconstructed. This approach permits the creation of much more complicated diffraction patterns than can be achieved with mechanical ruling techniques. In the late 1960s and early 1970s, researchers developed techniques by which computer-generated holograms were created directly on photographic film by imaging of patterns plotted by computer on large paper sheets or CRT screens [5]. By subjecting the film to a bleaching process, surface relief patterns, or kinoforms, were created in the film emulsion [6]–[9]. Another key development in the history of diffractive optics was the invention of lithographic fabrication technologies for the manufacture of integrated circuits in the late 1950s. The convergence of principles of computer generated holography and lithographic fabrication methods form the basis for most modern diffractive optics. Diffractive optics fabricated using binary lithographic masks were first realized in the early 1970s [10]–[11], while lithographic direct-writing methods were demonstrated in the early late 1970s and early

1980s for fabrication of diffractive structures [12]–[14]. Efficient manufacturing techniques using binary lithographic masks were demonstrated in the mid 1980s by researchers at MIT's Lincoln Labs [15]–[16]. Unlike earlier lithographic masking approaches that generated phase steps from masks, this approach generated diffractive structures with up to phase levels from masks. Diffractive optical elements (DOEs) fabricated using this approach are commonly referred to as *binary optics* [17]. Ruling of circularly symmetric diffractive kinoforms ("diamond turning") was reported in the late 1980s [18].

The history of refractive microoptics is not nearly as long as that for diffractive optics. The seminal works in surface relief refractive microoptics are generally considered to be presentations of lithographic patterning and thermal reflow techniques by Popovic *et al.* in 1988 and Daly *et al.* in 1990 [19] – [20]. A timeline illustrating key milestones in the history of microoptical fabrication is presented in Fig. 1-2.

1.4 Application of microoptical elements

Microlens arrays find applications in large number areas. Some of these areas are now discussed.

1.4.1 Imaging

Microlens arrays have been used in a large range of imaging applications. These include photocopier imaging systems, oscilloscope cameras and other "close-up" imaging systems, [21]. Recently a technique known as microlens lithography has been proposed, [22]. This system uses a 1: 1 imaging system built using microlens arrays to copy a pattern to photoresist. Advantages of this method include an increased depth of focus and a larger working distance (1 mm) than customary proximity printing. One result of these advantages is that no wear occurs to the mask as would occur in contact lithography.

1.4.2 Integral photography

This interesting technique was invented by Gabriel Lippmann in 1908. It involved using microlens arrays as the imaging system on a camera. Thereby recording an array of images of a distant object on the photographic film. The images are the object as seen from the position of each of the lenses. The developed film is then projected using the same type of microlens array to form a three dimensional image of the object. A detailed

discussion of this technique has been given by Stevens and Davies, [23].

1.4.3 Astronomy

Microlens arrays have been used as components in atmospheric wavefront sensors, known as Shack-Hartmann arrays, [24]. These are used to improve the images obtainable using ground based telescopes. They provide a measurement of the wavefront distortion caused by the earth's atmosphere. This information is then used to deform either the main mirror or a smaller secondary mirror to remove the distortion. This method can be used to produce diffraction limited images of stars despite atmospheric distortion. An example of optimising refractive microlens arrays for this purpose has been shown by Artzner, [33].

1.4.4 Staked planar optics for display technology

In certain applications, stacking of complex systems will not be required, but the array property of the planar integrated optical components is employed. An application for microlens arrays is, for example, beam shaping for LED arrays or direction-sensitive coding displays. The latter example can be employed for security reasons as well as for enhancing the brightness of displays. A further simple concept of stacked planar optics for imaging, utilizing only microlens, has already been shown in Fig.1-3. The set-up consists in the limit of only three planar microlens arrays. However, this set-up will possibly trigger tremendous developments in flat panel display fabrication.

1.4.5 Micro-optical sensor

A wide range of optical measuring and sensing techniques have been applied on an industrial scale. These systems are typically based on bulk optics and by three-dimensional integration they can be reduced in size and improved in terms of stability. Microinterferometers for measuring distances or physical parameters such as temperature, pressure, distance etc. are examples of this type. Micro-optical integration also allows in situ implementation of parallel measuring devices or of redundancy.

1.4.6 Parallel pick-up systems

For optical diskapplications the high interconnection density of imaging can improve the rate of data transfer. With integrated planar pick-up systems based on microlenses and microprisms several hundreds of pixels can be read simultaneously.

1.4.7 Optical interconnections

Three-dimensional micro-integration can provide suitable technology for different levels

of communication. At the system-to-system level integrated connectors for parallel fiber interconnect can be built (shown in Fig.1-4). For flexible connectors the alignment again profits from the planar surfaces. However, a connection to a stacked planar is not straightforward. In this case, an intermediate set-up of cascaded image divisions has to reduce the high density of data points to be coupled into the fibers with larger physical dimensions.

1.5 Introduction of PDMS

Polysiloxanes(PDMS), which contain $[-Si(CH_3)_2O-]_x$ repeat units, are unique among inorganic and semi-inorganic polymers and are a commercially available clean room compatible type of silicone rubber with a wide range of applications. Additional structural information is presented in the sketch of PDMS shown in Fig.1-5. It is currently used, for instance, as the mechanical interconnection layer between two silicon wafers [26], and as the spring material in accelerometers [27]. Other possible applications are its use as the top elastomer on a tactile sensor such as that described in [28] without influencing the sensitivity of the device and as flexible encapsulation material in order to mechanically and chemically decouple sensors from their environment [29]. Furthermore, it could be used in sensors with integrated electronics due to its low curing temperature.

Some physical and chemical attributes of PDMS are, compared to other polymers, a low glass transition temperature ($Tg \approx -125$℃), a unique flexibility (the shear modulus G may vary between 100 kPa and 3 MPa[30]), very low loss tangent ($\tan\delta$ «0:001), small temperature variations of the physical constants (except for the thermal expansivity, $\alpha \approx 20 \times 10^{-5}\ K^{-1}$ [31]), high dielectric strength (~14 V μm^{-1} [31]), high gas permeability, high compressibility, usability over a wide temperature range (at least from −100 ℃ up to +100 ℃ [32]), low chemical reactivity (except at extremes of pH) and an essentially non-toxic nature.

An elastomeric stamp or mold, made of PDMS, is the key element that transfers the pattern to the substrate and this technique is widely called soft lithography. Soft lithography can be roughly classified four aspects：(1) replica molding (REM); (2) microcontact printing (μCP); (3) microtransfer molding (μTM),and (4)micromolding in

capillaries (MIMIC).[33]

An elastomeric stamp, mold, or mask having relief structures on its surface is the key element of soft lithography. It is usually prepared by replica molding (Fig.1-5 A) by casting the liquid prepolymer of an elastomer against a master that has a patterned relief structure in its surface. Several properties of PDMS are instrumental in the formation of high-quality patterns and structures in soft lithography. First, PDMS is an elastomer and conforms to the surface of the substrate over a relatively large area. PDMS is deformable enough such that conformal contact can even be achieved on surfaces that are nonplanar on the micrometer scale. The elastic characteristic of PDMS also allows it to be released easily, even from complex and fragile structures. Second, PDMS provides a surface that is low in interfacial free energy ($21.6*10^3$ Jm^{-2}) and chemically inert: Polymers being molded do not adhere irreversibly to or react with the surface of PDMS. Third, PDMS is homogeneous, isotropic, and optically transparent down to about 300 nm: UV cross-linking of prepolymers that are being molded is possible. Fourth, PDMS is a durable elastomer. We used the same stamp up to about 100 times over a period of several months without noticeable degradation in performance. Fifth, the surface properties of PDMS can be readily modified by treatment with plasma followed by the formation of SAMs to give appropriate interfacial interactions with materials that themselves have a wide range of interfacial free energies.

In microtransfer molding (μTM, see Fig. 1-5 B) a drop of liquid prepolymer is applied to the patterned surface of a PDMS mold and the excess liquid is removed by scraping with a flat PDMS block or by blowing off with a stream of nitrogen. The filled mold is then placed in contact with a substrate and irradiated or heated. After the liquid precursor has cured to a solid, the mold is peeled away carefully to leave a patterned microstructure on the surface of the substrate. The most significant advantage of mTM over other microlithographic techniques is the ease with which it can fabricate microstructures on nonplanar surfaces, a characteristic that is essential for building three-dimensional microstructures layer by layer.

Capillary filling is a very simple and well-known phenomenon, and the dynamics of wetting and spreading of liquids in capillaries has been studied systematically. The flow of a liquid in a capillary occurs because of a pressure difference between two

hydraulically connected regions of the liquid mass, and the direction of flow decreases this difference in pressure. In circular capillaries, the flow of a wetting liquid occurs initially in thin films that wet the capillary symmetrically; in noncircular capillaries the most rapid flow usually occurs in the corner regions. Micromolding in capillaries (MIMIC) represents another non-photolithographic method that forms complex microstructures on both planar and curved surfaces. In MIMIC (see Fig. 1-5 C) the PDMS mold is placed on the surface of a substrate and makes conformal contact with that surface; the relief structure in the mold forms a network of empty channels. When a low-viscosity liquid prepolymer is placed at the open ends of the network of channels, the liquid spontaneously fills the channels by capillary action. After filling the channels and curing the prepolymer into a solid, the PDMS mold is removed, and a network of polymeric material remains on the surface of the substrate. However, MIMIC does have several limitations: 1) It requires a hydraulically connected network of capillaries; it cannot, therefore, form isolated structures or patterns on contoured surfaces. 2) Although capillary filling over a short distance (c.a.1 cm) can be achieved quickly and efficiently, the rate of filling over a large distance decreases significantly due to the viscous drag of the fluid in the capillary. 3) Since the rate of filling is proportional to the cross-sectional dimension of the capillary, the extremely slow filling of small capillaries may limit the usefulness of MIMIC in certain types of nanofabrication. Nevertheless, several groups have demonstrated that appropriate liquids could wet and fill nanometer-sized capillaries over short distances. 4) The forward ends of capillaries may fill incompletely if the hydraulic drag is sufficiently high. Interestingly, capillaries with closed ends may fill completely if they are short; the gas in them appears to escape by diffusing into the PDMS.

Solvent-assisted micromolding (SAMIM) is a technique that allows fabrication of patterned, quasi-three-dimensional microstructures on the surfaces of polymeric substrates. It can also be used to modify surface morphologies of polymers. The operational principle of this technique shares characteristics with both replica molding and embossing (see Fig.1-5 D). An elastomeric PDMS mold is wetted with a solvent that is a good solvent for the polymer, and is brought into contact with the surface of the polymer. The solvent dissolves (or swells) a thin layer of the polymer, and the resulting

(probably gellike) fluid comprising polymer and solvent conforms to the surface topology of the mold. While the mold is maintained in conformal contact with the substrate, the polymer solidifies as the solvent dissipates and evaporates (probably by diffusion through the mold) to form relief structures with a pattern complementary to that on the surface of the mold. SAMIM is an experimentally simple procedure. The key elements are wetting of the PDMS mold by a liquid that is a solvent for the polymer to be molded and conformal contact between the solvent-coated elastomeric mold and the substrate. The choice of solvent for a polymer determines the effectiveness and success of SAMIM. The solvent should rapidly dissolve or swell the surface of the polymer; it should not, however, swell the PDMS mold and thereby distort the mold and/or destroy the conformal contact between the polymer and the mold.[126] In general, the solvent should have a relatively high vapor pressure and a moderately high surface tension (e.g., methanol, ethanol, and acetone) to ensure rapid evaporation of the excess solvent and minimal swelling of the PDMS mold. Dyes and inorganic salts can also be added to the solvent; they are subsequently incorporated into the resulting microstructures. Solvents with low vapor pressures (e.g., ethylene glycol and dimethyl sulfoxide) are not well suited for SAMIM. Surface modification[122] of the PDMS mold may be required when solvents with high surface tensions are used since they only partially wet the PDMS surface. Many nonpolar solvents (e.g., toluene and dichloromethane) cannot be used in SAMIM because they can swell the PDMS mold.

1.6 Motivation of this thesis

While there is a continuing need for low volume, custom fabrication of microoptics, the need for volume manufacturing continues to increase. This demand necessitates the development of efficient, scalable manufacturing techniques, such as automated processing and micro-replication that are capable of producing large volumes at reasonable costs. Similarly, there will be a continued drive to improve the performance of microoptical components for many applications. This requirement can be met in multiple ways, including both analog and digital surface fabrication methods. However, all of these methods will benefit from tighter process controls to increase performance and reduce process variability.

The challenge to the industry going forward is to develop the technology, procedures, and infrastructure to address all of these general challenges at the same time. We now present a discussion of various paths on this “roadmap” for microoptical fabrication. Multiple examples of the technical challenges and motivations facing the industry are presented, along with discussions of the fabrication technologies that have promise in addressing feature sizes and materials issues.

Since many researcher have been utilized the rubber polymer, PDMS, to act as a replica mold or a optical material, due to its fascinating properties, such as low surface energy, thermal curing property, its refractive about 1.41 and soft nature. Based on these fascinating properties, we will use the interesting materials (PDMS) to fabricate optical elements such as microlenses, gratings and other components in this study.

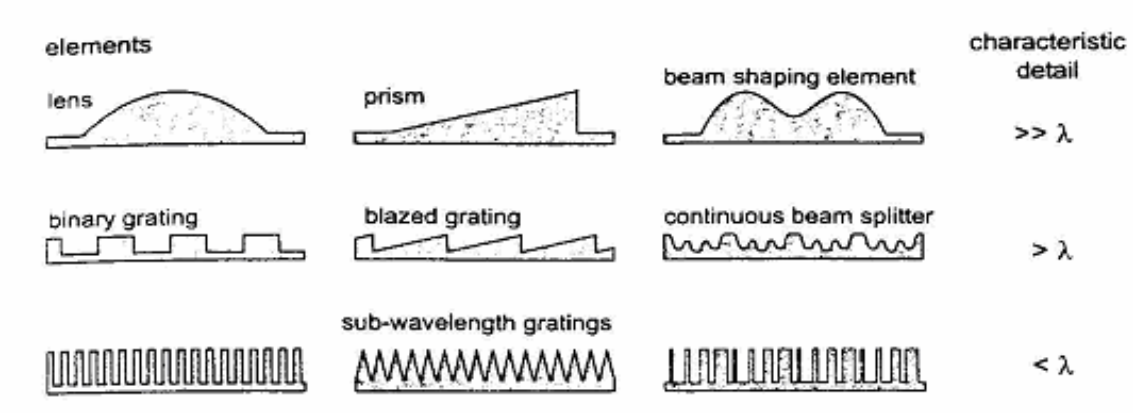

Fig.1.1 Profile of optical elements to be fabricated

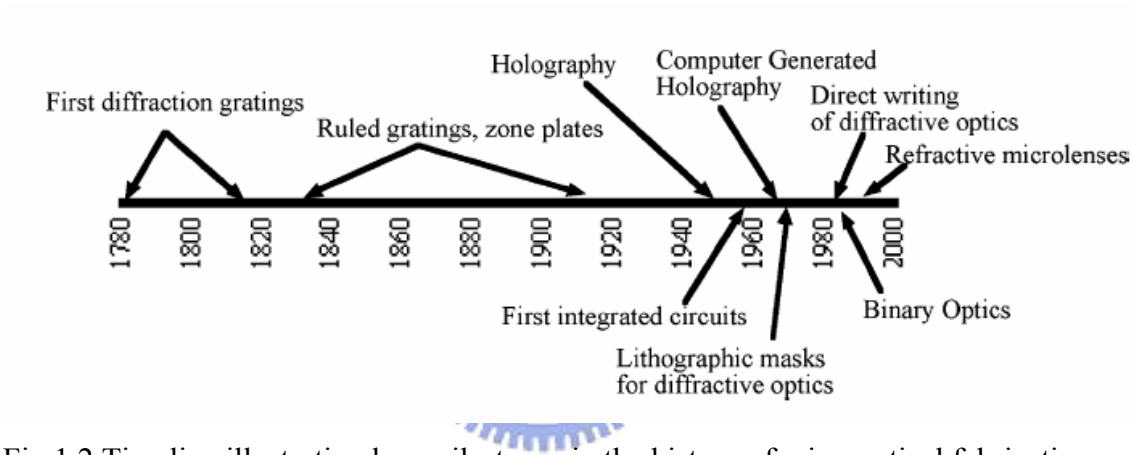

Fig.1.2 Timeline illustrating key milestones in the history of microoptical fabrication

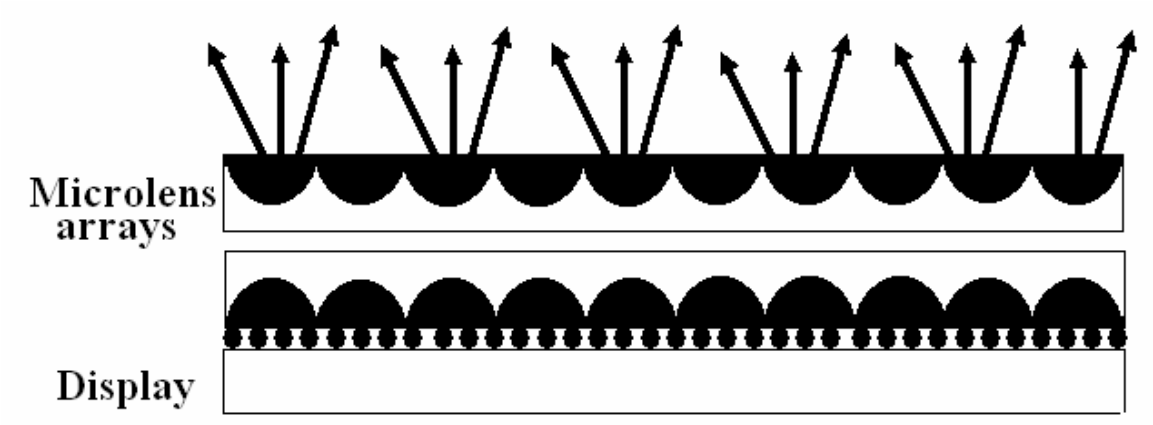

Fig.1.3 Direction-sensitive display for various applications

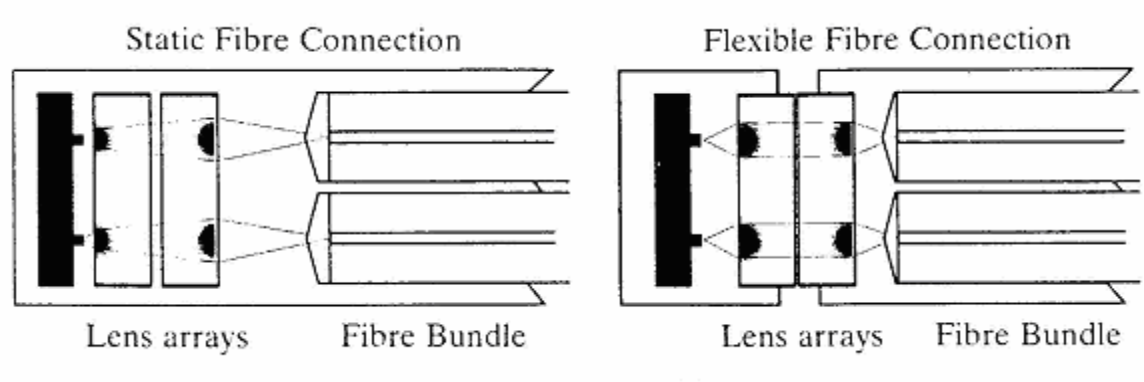

Fig.1.4 Static and flexible fiber connectors with planar microlens arrays

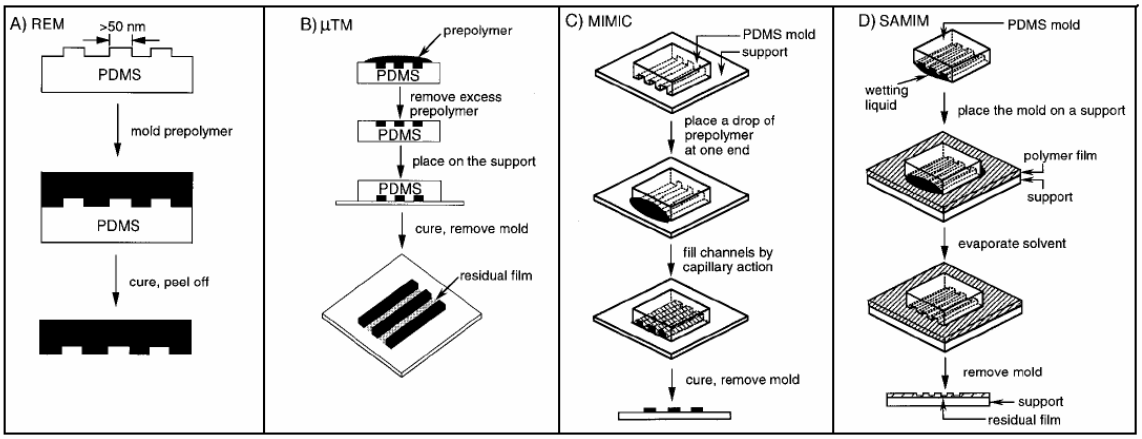

Fig.1-5 Schematic illustration of procedures for A) replica molding, B) microtransfer molding, C) micromolding in capillaries, and D) solventassisted micromolding.

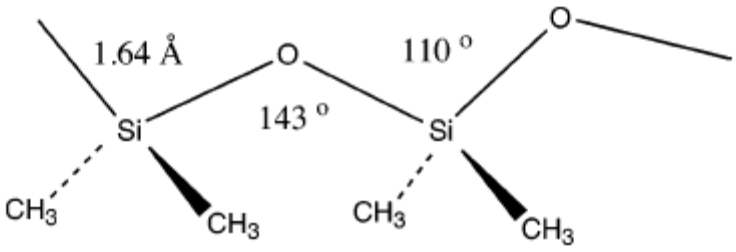

Fig.1.6 Sketch of a portion of a PDMS chain, showing some structural information relevant to its high flexibility

Chapter 2 Literature review for microlens fabrication

2.1 Introduction of microoptics

There are many applications that only became accessible for optical solutions via microoptics. However, the scaling of size and the addition of new functionalities also affect the methods necessary for theoretical treatment in design and analysis of the systems. The reason for this mainly lies in the change of the influence of different physical effects on the optical performance during the scaling process. Although typical feature sizes are reduced, the wavelength used often remains unchanged. Especially, the strength of refraction and diffraction change in their influence on the optical function. This will be demonstrated by the simple example of the scaling of a lens with low numerical aperture (NA). The arrangement under consideration is sketched in Fig 2.1(a). The lens shall have a constant NA of 0.05, but its diameter and focal length are scaled down from position 1 to 3. By calculating the intensity distribution onto the optical axis along the z direction in the surrounding of the focus position, we obtain the curves shown in Fig.2.1 (b) for the three different nominal focal length f_1=1.6mm, f_2=0.8mm, and f_3=0.4mm. As can be seen, the position of the highest intensity moves toward the lens as the lens size decreases. This cannot be explained if only refraction at the lens surfaces is taken into consideration. This effect is caused merely by the increasing influence of diffraction at the lens aperture. The edge of the lens acts like the zone of a Fresnel zone plate and thus, delivers an additional optical power to the lens. This diffractive powder increases as the lens diameter decreases. In most cases of practical relevance, the optical function has to be treated as a superposition of both physical effects- refraction and diffraction. The modeling techniques used for design and analysis of microoptical systems must take care of this.

2.2 The modeling of light propagation

In order to get some rough ideas about the validity of the different approaches, we first have to make some systematic considerations about the crucial points in the modeling of light propagation through a microoptical system. For this purpose, we do not care about the light sources itself, but start the consideration with an electromagnetic field given at

the entrance of the system. Inside of the system, we have to distinguish between the modeling of propagation surfaces. The most common techniques for the modeling of these two cases are ray tracing and a wave-optics approach. However, both have different strengths and weaknesses in the two modeling regions.

2.2.1 Ray tracing

The model of ray tracing is based on the solution of the eikonal equation, which can be derived directly from Maxwell's equations under the assumption of very large values of $k_0 = 2\pi / \lambda$, with λ being the wavelength. This approximation is justified in case where the changes in E and H are small compared with the magnitudes of both fields over domains whose linear dimensions are of the order of λ. Consequently, the fields behave locally as a plane wave. For the modeling of optical systems, these plane waves are represented by rays whose propagation directions are given by the local directions of the pointing vector S. In isotropic media, this direction is coincident with the direction of the k-vector of the local plane wave E_l, given by

$$E_l = A\exp(ikr) \quad (1)$$

with A being the local field amplitude. For the sake of simplicity, we restrict ourselves in the following to the case of isotropic media and, thus, the consideration of the k-vector is sufficient. The light rays are, therefore, orthogonal to the geometrical wave fronts.

In the case of propagation through homogeneous media, the direction of the k-vector remains unchanged and the position of the ray after a certain propagation distance can be calculated by simple geometrical considerations. If absorption or amplification is neglected, the energy carried by the ray remains unchanged, too.

In the surrounding of inhomogeneties in optical systems, the directions of the k-vector at the different positions on the wave front changes according to the certain form of the inhomogeneity. For the case of highest importance, which is the steplike change of the refractive index at a smooth surface separating two homogeneous media, the behavior of the k-vector can be either derived directly from the eikonal equation or by assuming local plane interfaces and using the fresnel equations. The advantage of the second approach is the possibility to include energy changes due to Fresnel losses. For

the change of the ray direction, we obtained, in both cases, the laws of refraction and reflection:

$$n_i \sin\theta_i = const. \quad (2)$$

$$\theta_1 = \pi - \theta_2 \quad (3)$$

Respectively, which θ_i being the angle between the ray and local surface normal in region i.

Many optical functions in microoptics are realized by microstructured surfaces. These have naturally strong surface profile variations and cannot be considered as local plane interfaces. Furthermore, the fields interacting with such elements can also not be considered to have a plane wave front locally. Typical examples of such elements are gratings and diffractive structures. Usually, the method of ray tracing breaks down at such inhomogeneities. Of course, there are special cases in which a new direction with the surface can be calculated by a proper model. An example is a structure for which the local inhomogeneity can be approximated by a known grating equation according to

$$n_2 \sin\theta_2 - n_1 \sin\theta_1 = \frac{m\lambda}{p} \quad (4)$$

for the one-dimensional case, with m being the diffraction order and p the local period. However, even for this case of local periodicity, the new wave front is represented by a number of plane waves or diffraction orders having different propagation directions or k-vector. In some cases, only one direction is of interest for the further propagation through the system. Furthermore, detailed information about the distribution of energy between the diffraction orders cannot be obtained by this simple approach. In addition, for certain elements such as computer-generated holograms, a local periodicity is often not existent and, as a consequence, a change of the k-vector is hard to calculate.

Although in most cases of practical interest in conventional optics the assumption made during derivation of the eikonal equation mentioned at the beginning of this section is completely adequate in the field of microoptics, naturally the number of cases where it fails increase. In general, one can state that ray tracing is approaching difficulties in cases where string local changes in the field amplitude and phase occur and thus, fields and surface can no longer be considered a local plane.

2.2.2 Wave-Optics Representation

The validity problems of ray tracing mainly arise from the fact that diffraction phenomena during propagation of the fields are not considered for the single rays. To include this, one must use a propagation operator for fields other than the simple geometrical consideration of ray directions. Examples are the well-known propagation operators for wave propagation in homogeneous media. The most popular ones are the angular spectrum operator and the Fresnel wave-propagation formula. These operators are used to calculate the evolution of the spatial dependency of a spatial field component U(x,y,z), these formulas cannot be solved in a closed analytical form and numerical methods have to be applied. For this purpose, the complex field amplitude is usually discretized on sample points located on a regular mesh. The resulting data volume is much larger compared with the number of parameters required for a ray-tracing approach, because one single ray at a certain position also contains information in its k-vector about the surrounding wave-front area. Often, powerful computational equipment is needed to handle this required data volume and perform the wave-optical analysis with sufficient accuracy.

One more general problem for the wave-optical approach is the treatment of the interaction between fields and inhomogeneities. There is no general method existent and a separate model for each has to surface type be used. For very few cases, a rigorous or even analytic expression exists. The best known example is the interaction of plane waves with plane surfaces expressed by Fresnels formulas. The interaction of plane waves with periodic structures can be handled, for instance, by so-called Fourier-expansion methods in a rigorous manner. However, for most other surface types, certain more or less serious approximations have to be made in order to be able to handle the interaction problem. A very simple and handy method is the so-called thin-element approximation. In this approximation, the optical element under consideration is mathematically enclosed by two planes which itself are oriented perpendicular to the optical axis which is directed along the z axis. Then the optical path between the two planes is calculated along the z direction and converted into a phase function $\varphi_e(x,y)$ for each (x,y) position. Absorption is included by a proper real amplitude $t(x,y)$. As a result, one obtains the complex transmission function

$$T(x,y) = t(x,y)e^{j\varphi_e(x,y)} \qquad (5)$$

And the transmission of $U(x,y,z)$ through the element can be express by

$$U(x,y,z_+) = T(x,y)U(x,y,z_-) \quad (6)$$

With z_- and z_+ being the positions directly in front and directly behind the element, respectively. Equation (6) can easily be inverted, which is the big advantage of the thin-element approach, especially in design procedures. However, t becomes obvious that diffraction effects and position changes of wavefront parts during propagation inside the element are completely neglected. Thus, in most cases, thin-element approximation represents even more of a simplification than the ray-tracing approach.

2.3 Literature review

The term “continuous-relief micro-optics” covers a wide range of refractive and diffractive microstructures offering a variety of optical characteristics arranging from on-axis focusing of a collimated light beam to the formation of complex holographic images. Fig.2.3 illustrates the basic structure type and shows some examples of typical continuous-relief planar micro-optical elements. Although the elements can be dominantly refractive (as microlenslets and lenslet arrays), diffractive (such as kinoforms and grating microstructures) or a combination of both (for example, Fresnel microlenses), we will pay attention to focus the fabrication of refractive microlenses and diffractive gratings in this study. First, the literature of refractive microlenses is induced in next section.

A relative large number of ways to make small refractive-type lenses has been employed over the last 10 years. Each has had some perceived advantage. Some are relatively inexpensive and utilize an existing technology, while other require new material with special properties and unusual fabrication techniques. The particular application must determine the best material and fabrication technique according to the choices, glass/plastic, single element/array and aspheric/spherical. Here, we will try to generalize these fabrication methods and classify these methods according to the mechanism of fabricated process.

2.3.1 Literature review of refractive microlenses fabrication

The study of microlenses has been an area of activity for many years. Hooke studied the effect of melting the ends of Venetian glass rods to produce microscope objectives in the 17th century [34]. One of the more recent methods used to produce arrays of microlens arrays is the photoresist reflow method, suggested by Popovic in 1988 [35]. Therefore, some of the special methods used to produce refractive microlens shall now be discussed in more detail.

(A) The use of surface tension for microlens fabrication

The use of surface tension is a common method to fabricate refractive lenses. Based on the use of surface tension, the developed methods for microlens fabrication are listed below.

- Single-layer photoresist reflow method [36]

The simplest and most ingenious way to create microlenses is to make a resist pattern in the shape of disks. Fig.2.4 shows the microlens fabrication flowchart by single-layer photoresist reflow method. In this case one exposes the resist of thickness L through a mask made up of clear circles with diameter D. Upon development, this turns into the disk shape. One now merely heats the substrate to melt the photoresist. The surface force controls the shape and a segment of a sphere represents the minimum energy surface.

- Double-layer photoresist reflow method [37]

Fig.2.4 shows the microlens fabrication flowchart by double-layer photoresist reflow method. Two polymer layers were coated onto a silicon substrate. The upper layer was a photoresist. The lower layer was a polyimide material. The polyimide was expected to form a pedestal to sustain the ball lens after the heat reflow process. Once the patterned polymer is heated above its glass transition temperature, the melting polymer surface will change into a spherical profile for minimizing its surface energy. A successful micro-ball array was formed in the photoresist through the different glass transition temperatures between two polymer materials. The interactive force between two material interfaces caused by surface tension causes the upper profile to form a spherical profile. This also forms the polyimide pedestal into a trapezoid with arc sides.

- Vertical photoresist reflow method [38]

Vertical reflow microlenses (VRM) are fabricated by combining the thermal reflow

method with succeeding silylative treatment on the lens surface (shown in Fig.2.6). By virtue of the strong adhesive force and cohesion, the VRM is formed by hanging the photoresist on a standingwall and then reflowing the photoresist. In order to enhance the thermal stability and reliability, the reflowed VRM is exposed to a silylative reagent to form a hard shell.

- Liquid microjet method [39]

Fig.2.7 shows the microlens fabrication flowchart by liquid microjet method. The use of the microjet technology, developed primarily for printing, has also been adapted to making microlenses. The analogous microjet system used a piezoelectric ceramic with a microchannel machined in it with a nozzle on one end connected to a reservoir on the other. An electrical pulse bends the channel and forces a droplet through the aperture. The droplet is directed to a substrate which is mounted on an XYZ micropositioner; the liquid drop solidifies on contact with the substrate and surface tension causes a spherical surface to form.

- Liquid dipping method [40]

Fig.2.8 shows the microlens fabrication flowchart by liquid dipping method. Polymeric vertical microlenses (PVMs) using photoresist material SU-8 are fabricated with a simple and low-cost process. By virtue of the strong adhesive force and liquid cohesion, the PVMs are formed by hanging the liquid SU-8 on walls by a dip method. Then, in order to enhance the thermal stability and reliability of the PVMs, the lenses are baked and exposed in the ultraviolet light to crosslink the SU-8.

- Hydrophobic effect [41]

Fig.2.9 shows the microlens fabrication flowchart by hydrophobic effect. In the first step, an adhesive hydrophobic layer is mechanically applied to the substrate. Regardless of what material is used, the substrate can then be lithographically patterned and the hydrophobic layer selectively etched from the exposed regions. The substrate is then dipped into and withdrawn from a UV-curable-monomer solution, the monomer will self-assemble into lenses on the hydrophilic domains. After a UV cure the lenses become hard and stable.

- Laser heating [42]

One method makes use of a laser whose emission wavelength is strongly absorbed

such as to produce local melting at the focal spot. Fig.2.10 shows the microlens fabrication flowchart by laser heating method. The explanation put forward for the formation of the bump is that the glass is initially melted and then resolidified. Since the soft glass with the higher temperature has a lower density, the excess volume wells up out of the colder solid substrate glass and reforms upon solidification into a lenslike shape.

(B) The application of Diffusion for microlens fabrication

- Bulk micromachining technology [43]

Fig.2.11 shows the microlens fabrication flowchart by bulk micromachining technology. Boron diffusion and etching selectivity with respect to boron density in an ethylenediamine pyrocatechol (EDP) etchant are utilized. When the EDP etchant meets the heavily boron doped p++ layer (above $2.5*10^{19}$ atoms/cm3), the etching is nearly self-stopped. As a result, Si microlens is formed.

- One-Step wet etching technology [44]

Refractive semiconductor microlenses were fabricated by using a diffusion-limited chemical etching technique based on Br2 solution. Fig.2.12 shows the microlens fabrication flowchart by One-Step wet etching technology. In this etching process, the etched profile is heavily dependent on the diffusion dynamics of the etching species, especially around etch-mask boundaries where the differential change in diffusion (and thus in etching rate) is rapid. The process for microlens fabrication also utilizes the nature of the diffusion-limited etching.

- Isotropic etch of ICP technology [45]

Fig.2.13 shows the microlens fabrication flowchart by isotropic etch of ICP technology. The isotropic etching properties of an inductively coupled plasma (ICP) etcher for masked and maskless etching steps in reference to fabrication of a silicon microlens mold. The silicon etching is performed with a continuous SF6 based ICP. For the masked etching step a consistent picture of the profile evolution is obtained, including a relation between the etching depth, the radius of curvature of the profile, the etching time and the size of the mask opening. For the maskless etching step, the optimal etch is purely isotropic.

(C) Photolithgraphy for microlens fabrication

- Proximity printing method [46]

Fig.2.14 shows the microlens fabrication flowchart by proximity printing method. This way to fabricate microlens arrays is presented by controlling the printing gap in the UV lithography process. The proximity printing bends the UV light away from the aperture edges and produces a certain exposure in the photoresist outside the aperture edges due to the diffraction effects. This causes the photoresist bottom in two adjacent patterns to link together after development. The fabricated microlens diameter has the same size as the pitch distance between the two apertures.

- Diffusion photolithography technology [47]

Fig.2.15 shows the microlens fabrication flowchart by diffusion photolithography technology. This simple and effective method to fabricate a plastic microlens array with controllable shape and high fill-factor, which utilizes the conventional lithography and plastic replication, is presented. The only difference from conventional lithography is the insertion of a diffuser that randomizes paths of the incident ultraviolet (UV) light to form lens-like 3D latent image in a thick positive photoresist. After replication of the developed concave microlens mold onto the polydimethylsiloxane (PDMS), PDMS microlens arrays are achieved.

- Gray-tone photolithography technology [48]

Fig.2.16 shows the microlens fabrication flowchart by gray-tone photolithography technology. The principle of a gray-tone mask for fabricating the microlenses involves modulation of the incident light by a different transparent area on the mask and by the number of laser pulses. Conventionally, there are three methods used to encode a 3D profile into the gray-tone mask layout: (1) pulse width modulation (PWM), (2) pulse density modulation (PDM) and (3) a combination of PWM and PDM. Fig. 2.16 illustrates the different layouts between PWM and PDM and modulation of transmissions of thus designed gray-tone masks. When the transmission of the mask changes from 25% to 50%, the transparent holes in PWM broaden, while the area of the transparent holes remains constant but the density increases in PDM. Base on the energy distribution through gray-tone mask in the UV lithography process, the microlens structures can be directly fabricated.

(D) Swell volume for microlens fabrication

• Deep lithography with protons [49]

Fig.2.17 shows the microlens fabrication flowchart by deep lithography with protons. In the first step of the microlens fabrication process, the PMMA sample is bombarded with an 8.3 MeV proton beam which is generated by a cyclotron and is shaped by a highaspect-ratio noncontact metal mask, featuring a high precision circular aperture. The shape of this aperture is directly projected onto the PMMA sample where the impinging high-energy protons split the polymer chains and create free radicals, hence reducing the molecular weight of the polymeric material. In the second step, the in-diffusion of the monomer causes a volume expansion which results in hemispherical surfaces because of the circular footprint of the irradiated zones. Because the degraded PMMA chains are incapable, because of their length, to diffuse towards the plates in the monomer vapor, the surface evolution of the PMMA plates is only determined by the diffusion of the monomer vapor in the bombarded zones and its accompanying volume expansion. The final shape of the swollen regions is determined by a balance between the internal stresses caused by the diffused monomers in the outwards direction, the surface tension and the gravitation force acting on the swollen layer.

• Ultraviolet-cured polymer [50]

The selected lens materials used for the UV-curing method should have a large change in volume without any physical damage during photopolymerization. Fig.2.18 shows the microlens fabrication flowchart by ultraviolet-cured polymer. First, the selected materials are poured into a cell that consists of a flat glassbottomed plate. A chromium mask with periodically arranged circular apertures deposited on a glass substrate is then placed on top of the cell. Next, the liquid monomer is irradiated from the upper side for 1 min with a metal-halide lamp that has a radiation spectrum ranging from 200 to 400 nm. The UV light induces photopolymerization, and the medium increases in density as it changes from the liquid to the solid phase. Because of this contraction effect, the molecules in the shaded regions of the medium moved into the irradiated regions to join the polymerization process, forming protrusions on both surfaces of the polymer at positions corresponding to the circular apertures.

• Photothermal process [51]

A photochemical modification to fabricate microlenses is presented by the use of a

special photosensitive glass. The basis of the effect is generated by a photonucleation of phase crystallization within the glass which produces a physical change in density. The total crystal content is of the order of 10-20% volume. Under the appropriate exposure pattern this density change can be used to produce surface features that ultimately act as lenses. A schematic of the process is shown in Fig.2.19. The photopatterning is done by conventional photolithographic technologies. After the glass is exposed, it is heated to about 600℃ to effect the crystallization. The results are circular regions where the light is blocked, surrounded by crystallization regions of higher density. The effect of this is to squeeze the soft unexposed glass beyond the surface that then forms a minimum energy surface. The surface bumps are formed on both.

- Vacuum-ultraviolet F_2 laser [52]

A photochemical modification to fabricate microlenses is presented. Fig.2.20 shows the microlens fabrication flowchart by vacuum-ultraviolet F_2 laser. The silicone surface irradiated by an F_2 laser beam swells and is modified to SiO_2 by means of photochemical reaction. When the surface is irradiated under a suitable condition of short laser pulses, it becomes smooth and spherical.

(E) The use of PDMS for microlens fabrication

- Micro-transfer molding with soft mold[53]

A novel technique for fabricating polymeric microlens arrays based on micro-transfer molding with soft mold is presented. Fig.2.21 shows the microlens fabrication flowchart by micro-transfer molding with soft mold. The soft mold with a micro-holes array is made by casting a pre-polymer of PDMS against a silicon master. The silicon master of the micro-cylinders array is prepared using photolithography and deep reactive ion etching. During the micro-transfer molding operation, the surface of the soft mold of the micro-holes array is filled with liquid UV curable photopolymer, and the soft mold is then pressed against the flat substrate with a slight pressure for a period of time. After the soft mold is removed from the substrate, surface tension causes the liquid photopolymer cylinders to assume a spherical shape. Finally, the liquid photopolymer is cured by UV irradiation at room temperature. A substrate with a microlens array pattern can be successfully fabricated.

- Organic selective-area patterning method [54]

A novel method to fabricate a polymer microlens array based on a selective-area patterning method is presented. Fig.2.22 shows the microlens fabrication flowchart by organic selective-area patterning method. The surfaces of glass substrates were defined as either hydrophilic or hydrophobic regions by microcontact printing of self-assembled monolayers (SAMs). After spin coating of the prepolymer on the substrate, the microlenses were self-organized on the defined regions. Finally, the microlenses were completed by UV curing.

- Soft roller stamping process [55]

An innovative technique for rapid fabrication of ultraviolet-cured polymer microlens arrays based on soft roller stamping process is presented. Fig.2.23 shows the microlens fabrication flowchart by soft roller stamping process. In this method, a soft roller with microlens array cavity is made by casting a pre-polymer of polydimethylsiloxane (PDMS) in a plastic master of microlens array. The plastic master is prepared using gas-assisted hot embossing of polycarbonate (PC) film over a silicon mold with micro-holes array. The microlens array cavity on the soft roller is filled with liquid UV curable polymer first. The roller rolls and stamps over the traveling transparent substrate. The microlens array pattern is formed. At the same time, the pattern on the substrate is cured by the UV light radiation while traveling through the rolling zone.

(F) The use of microspheres for microlens fabrication

- Microballs severed directly as microlens[56]

Self-assembled 2-D arrays of microspheres act as dense-packed arrays of microlenses and generate hexagonal dense arrays of micropatterns. Fig.2.24 shows the microlens fabrication flowchart by microballs severed directly as microlens. Use of 2-D microballs arrays, which can cause directly incident illumination to converge or diverge and can generate 2-D periodic optical patterns. These 2-D microballs arrays for photolithography and demonstrated that the lens arrays can generate 2-D arrays of uniform micropatterns over areas of several square centimeters.

- Microballs severed directly as molds [57]

A facile, reproducible soft-lithography-based method for fabricating hexagonally

close-packed microlens arrays by templating the surface of a colloidal monolayer, which is formed by spin-casting monodisperse polystyrene microsphere, is described. Fig.2.25 shows the microlens fabrication flowchart by microballs severed directly as molds. The relief structure of colloidal monolayers has successfully generated PDMS elastomers with hexagonal arrays of hemispherical air voids. Closely packed hemispherical microlens arrays were imprinted on ultraviolet-curable photopolymers which are bound on glass substrates.

- Replication by the use of microball [58]

Fig.2.26 shows the microlens fabrication flowchart by replication form microballs. Microporous polymer films with a hexagonal arrangement of pores were prepared by simple casting of various polymer solutions under humid conditions. Hexagonally packed micropores were prepared by using condensed water droplets as templates on the surface of polymer solutions. Spherical micro lens arrays (MLAs) were fabricated simply by molding from the resulting honeycomb structures. By peeling off the upper layer with adhesive tape, the pillars were severed, forming pins on each layer, and a hexagonal array of pincushion structures was generated by this procedure. Hemispherical MLAs were also fabricated by molding the pincushion structures.

- Suspension method [59]

A technique for producing ordered microlens arrays which is based entirely on self-assembly of charged latex particles spread at the oil–water interface is developed. Fig.2.27 shows the microlens fabrication flowchart by suspension method. The method includes using of a gel trapping technique and replication of the ordered particle monolayers by casting with curable PDMS. Microlens arrays have been fabricated by taking an inverse replica of the PDMS template with a photopolymer. This method allows immediate control of the microlens array lattice constant by using different amounts of particles spread at the original oil–water interface.

2.3.2 Literature review of diffractive gratings

Gratings are often used for dispersing light onto a detector for spectrometry, or for wavelength selection in an integrated demultiplexer. The fabricated methods for gratings are quite traditional, such as laser direct writer lithography or e-beam technique,

Interference lithography technique and diamond turning. In this section, we will introduce some traditional technique and some novel technique for gratings fabrication.

- Laser or e-beam direct writer lithography [60][61]

Laser or e-beam direct writer lithography technique, which forms cell patterns without the use of masks, stamps, etching, or other lithographic tools, is finding favors and applications in many areas relating to microfabrication processes. Its applications include processes such as the structuring of three-dimensional features, the development of prototypes, the manufacturing of small-scale components, and so on. The required microstructure to be fabricated is defined by surface-relief data generated by custom or commercial optical design programs. The data is converted to beam intensity values using calibration run measurements which define the relationship between the beam intensity and corresponding relief height of the resist film after development. The writing process then exposes the resist-coated substrate by scanning the substrate under the focused beam, with accurate and synchronized computer control of stage movement and beam intensity. The controlled development of the exposed resist film then results in the desired surface-relief microstructure.

- Interference lithography [62]

Interference lithography, which enables one to obtain large-scale periodic structures in a single exposure, can be regarded as a useful alternative to direct laser writing. Instead of tight focusing, it utilizes high spatial frequencies of an interference field, created by overlapping multiple coherent light waves. In most systems, two mutually coherent waves interfere to form a one-dimensional fringe pattern, which is recorded in a photoresist film. The period of the fringes is given by $p = \lambda/2 \sin\theta$, where θ is the half angle between the two interfering beams and λ has the usual meaning. Interference lithography with X-rays has potential for extremely high resolution due to the small wavelengths in this spectral region. Development of Synchrotron Radiation sources as extremely bright X-ray sources has enabled the practical implementation of X-ray interferometers for patterning purposes. Recently, a Lloyd's mirror interferometer was used to record fringe patterns with periods as small as 38 nm. While this mirror interferometer has potential for extremely high resolution, it is limited in terms of the

printed area due to the temporal coherence requirement.

Two-dimensional structures such as arrays of holes, posts or grids, can be obtained by a multiple exposure interference lithography scheme in which the sample is turned between the exposures to record crossed fringe patterns. The technique is widely used in practice but it has some weaknesses. Perhaps most importantly, the fringe patterns of successive exposures are added incoherently resulting in a latent image with reduced modulation. This decreases the process latitude making the method too sensitive to potential variations in process parameters. In addition, the double exposure procedure brings extra complexity and inconvenience to the process. Multi-beam IL techniques can overcome both limitations by creating a strongly modulated two-dimensional interference pattern in a single exposure.

- Laser-assisted etching or deposition [63][64]

In this approach, the focused laser beam results in a local enhancement of the deposition or etching rate, and suitable control of the scanning laser beam intensity can produce microrelief structures with submicron resolution. Most techniques of this type require laser scanning in a liquid or gas cell in which the deposition or etching of the substrate takes place.

The inventors have developed and demonstrated a number of implementations of the basic technique using a vector scan laser writing system integrated with a photochemical reactor cell. Surface-relief microstructures were fabricated on Si substrates by the pyrolithic deposition of polysilicon from a mixture of N_2 and SiH_4. The laser used was an Argon laser operating at =515nm and delivering in excess of 1W power in the focused laser spot of about 2 μm diameter. Fine grating structures and individual lines with a cylindrical profile were written on Si and on amorphous Si films on quartz and glass substrate. Improved control of the surface-relief profile was obtained using laser-enhanced etching. In addition, laser-assisted etching or deposition produces surface-relief microstructures and requires no further processing.

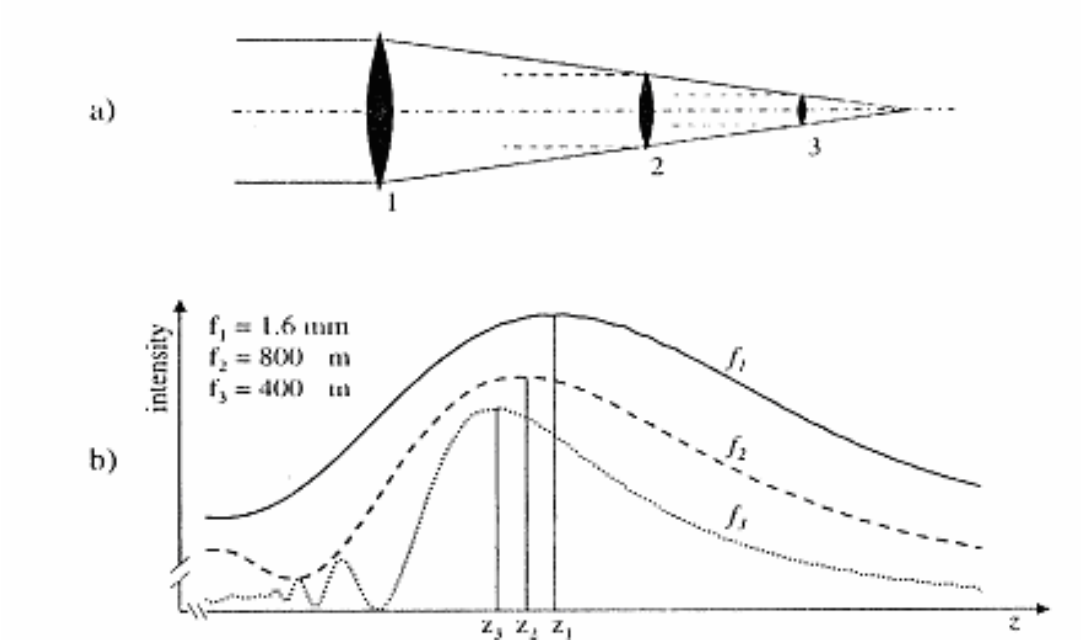

Fig.2.1 (a) Arrangement for investigation of the lens-scaling effect and (b) the corresponding change of focus position for a constant numerical aperture of 0.05

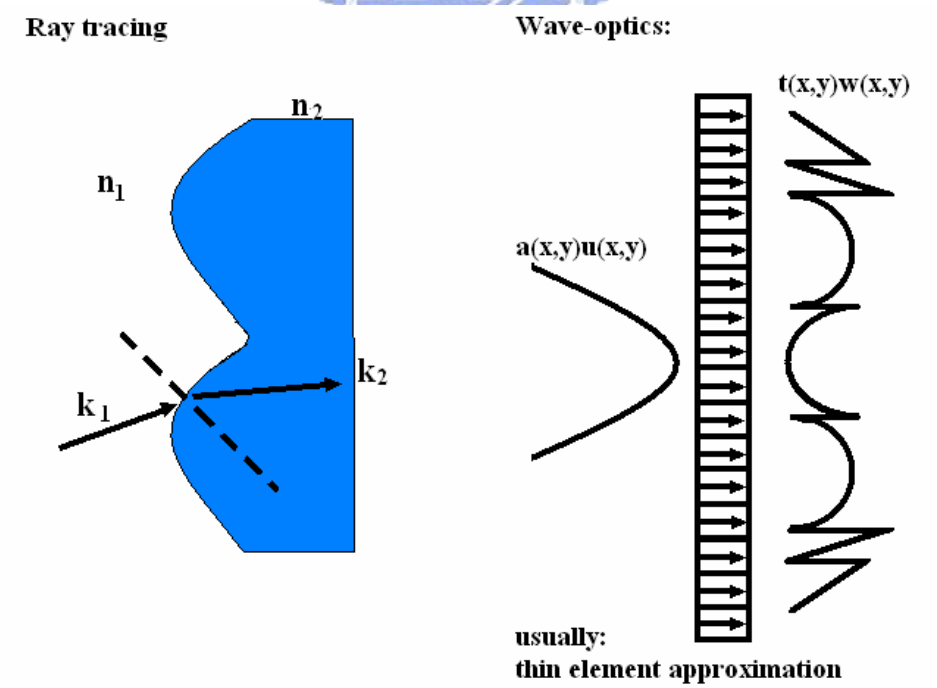

Fig.2.2 Different methods for representation of fields and surfaces or elements for ray-tracing and wave-optical approaches

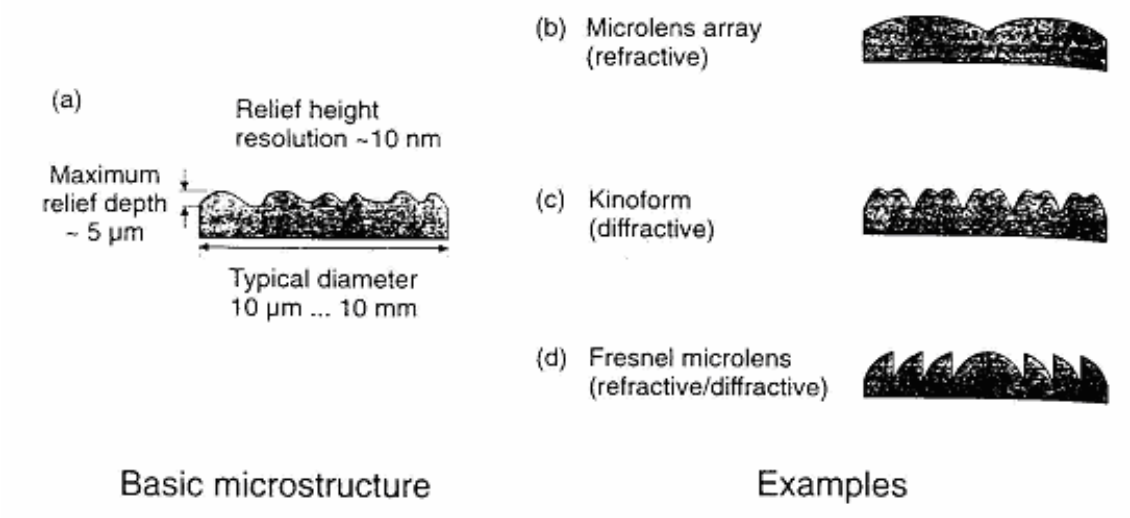

Fig.2.3 Coutinuous-relief micro-optical elements:Basic microstructure (a) of planar phase elements which can be fabricated by direct-writing techniques. Depending upon the microstructure and feature sizes, the elements can have optical properties which are dominantly refractive (b), diffractive (c) or mixed (d)

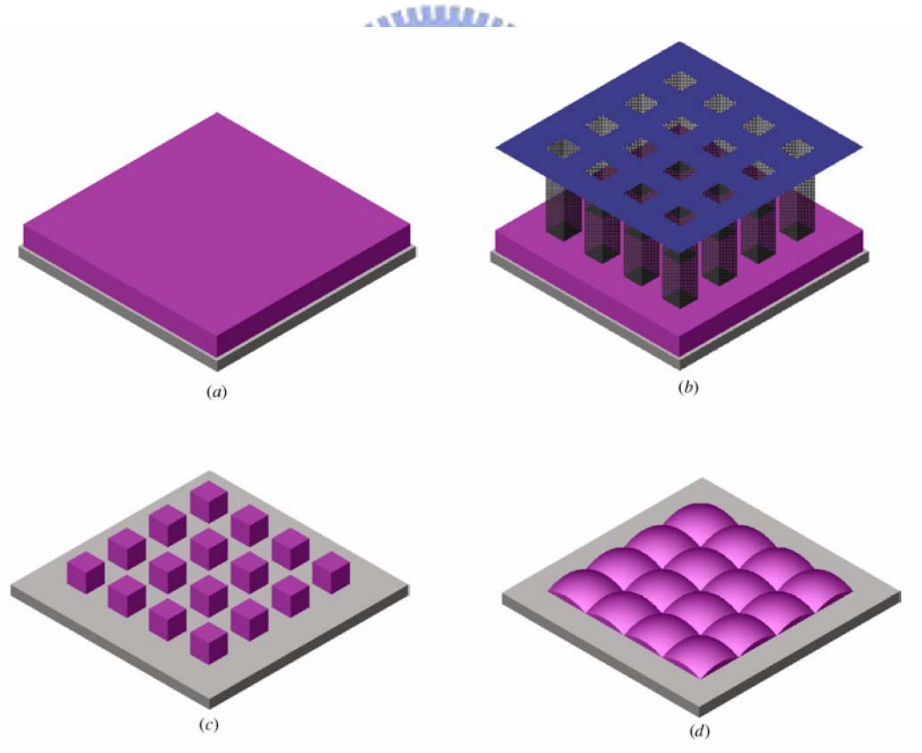

Fig.2.4 Schematic of square microlens array fabrication process; (*a*) a photoresist layer coated on the Si wafer, (*b*) lithography process to pattern square lens array through the mask, (*c*) photoresist pattern after development, (*d*) square microlens array after heat reflow.[36]

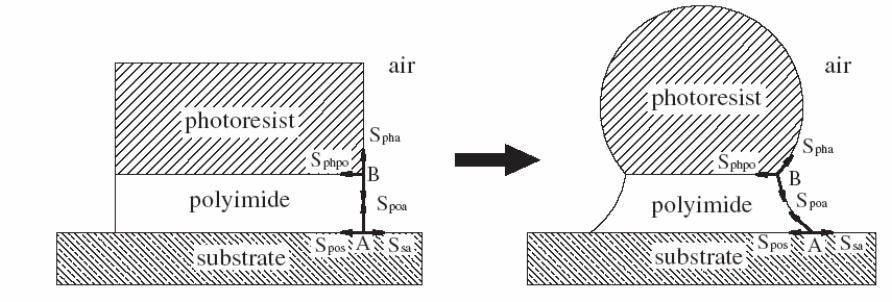

Fig.2.5 Illustration of a micro-ball lens formation in the thermal reflow process. [37]

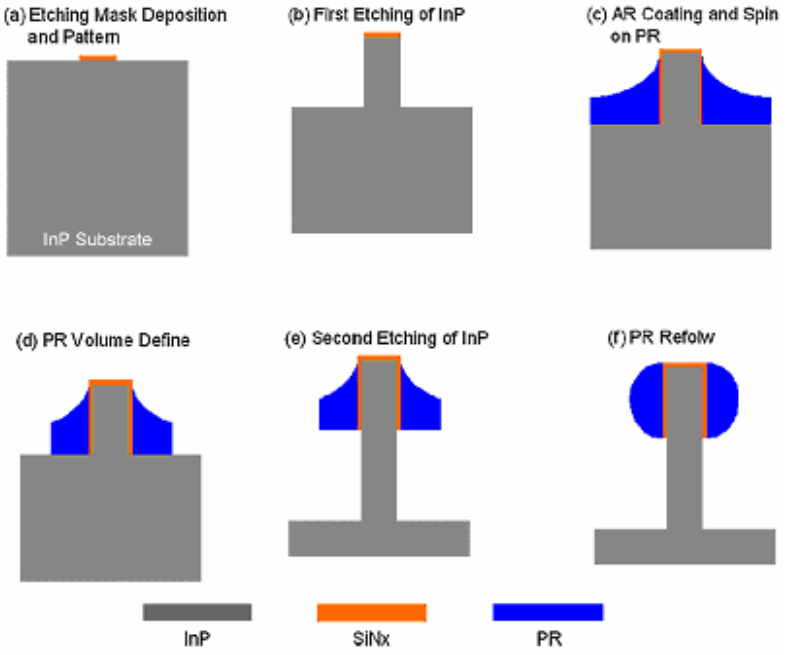

Fig.2.6 Flow chart of VRM fabrication process [38]

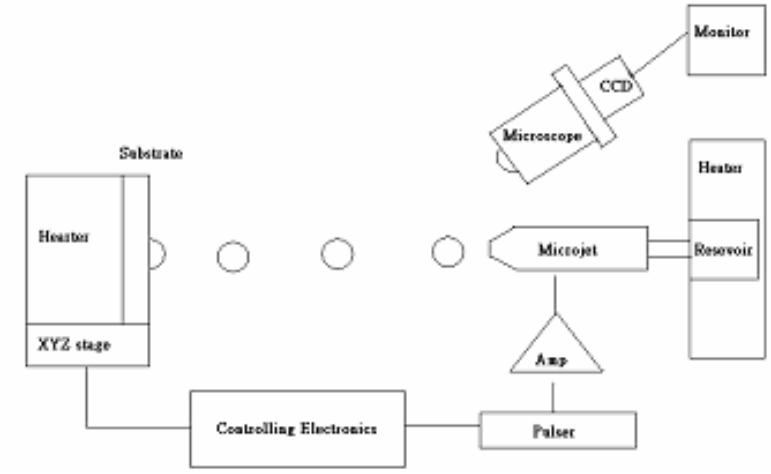

Fig.2.7 Schematic of droplets on microjet system used to manufacture microlens [39]

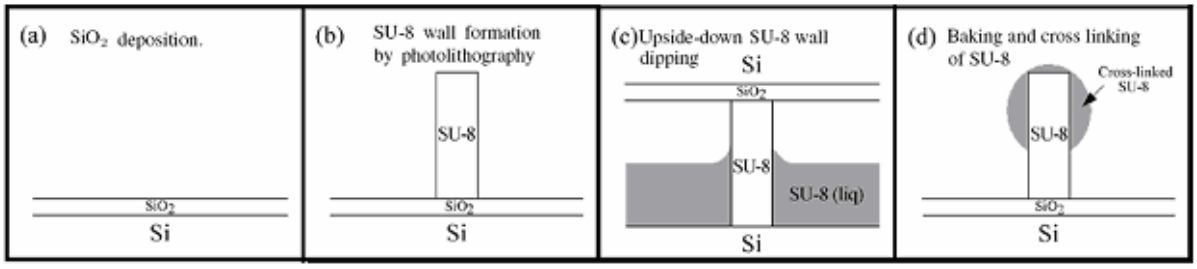

Fig.2.8 Schematic diagram of the PVM process by dipping method [40]

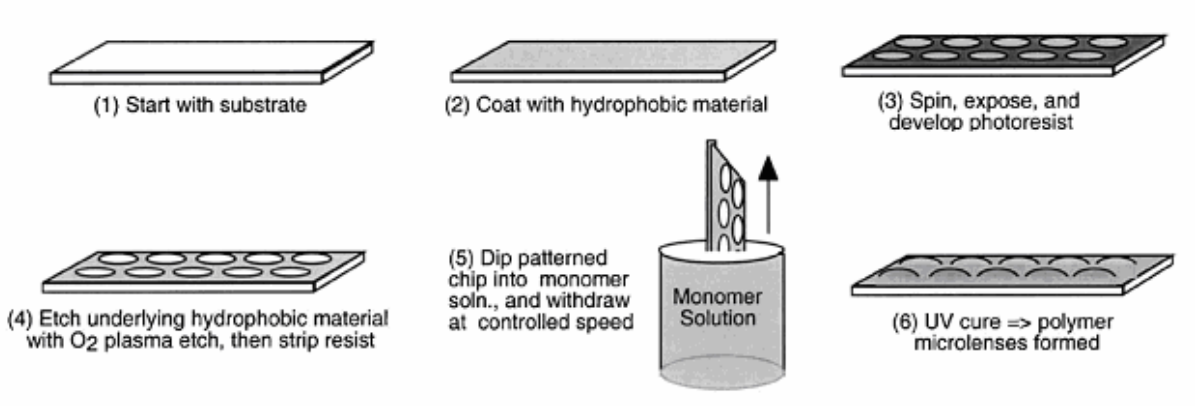

Fig.2.9 Process flow for hydrophobic patterning [41]

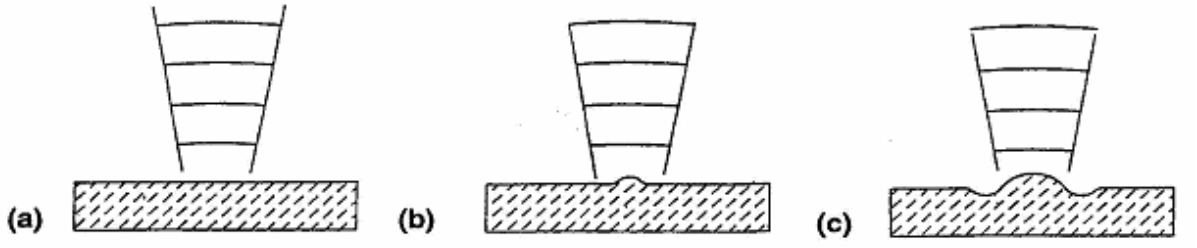

Fig.2.10 Schematic drawing of how lens forms by local laser heating. In (b) the temperature is sufficient to soften the central region; in (c) with higher temperature being achieved, the onset of the large deformation is seen. [42]

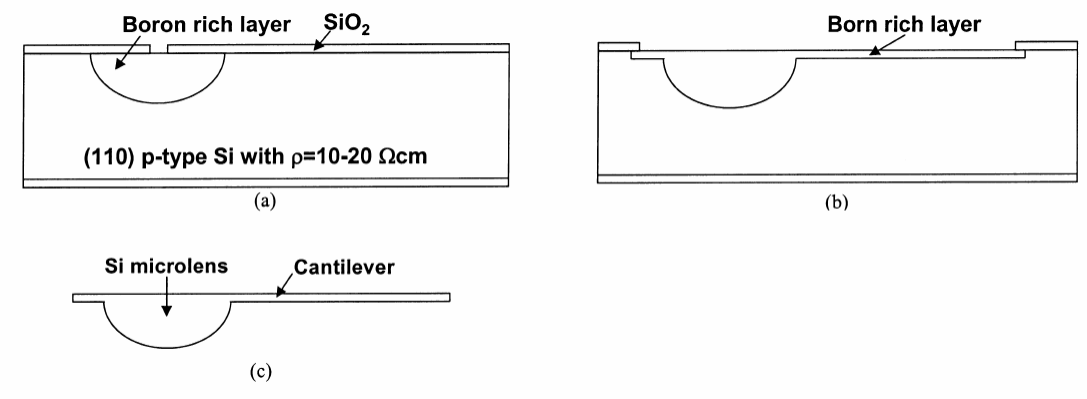

Fig.2.11 Fabrication procedures of Si microlens. A (110) silicon substrate with ρ=10-20Ωcm is used. (a) After SiO2 is patterned, boron diffusion is performed; (b) after SiO2 is patterned for a cantilever, then boron diffusion is performed; (c) the Si substrate is etched in EDP etchant. But boron rich-layer is selectively not etched. Thus, the remaining semi-circled shape of Si forms Si microlens. [43]

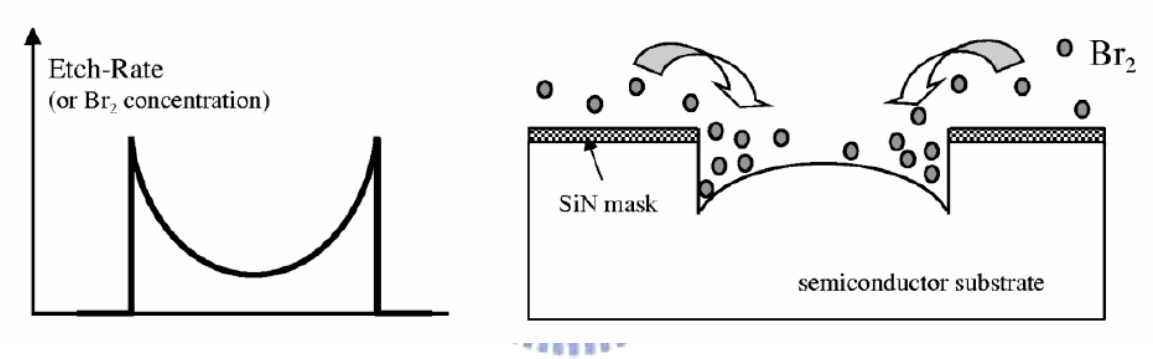

Fig.2.12 Schematic illustration of the semiconductor microlens fabrication process using Br_2-based diffusion-limited etching. The upper panel shows the distribution of the etch rate across the etch-window opening. [44]

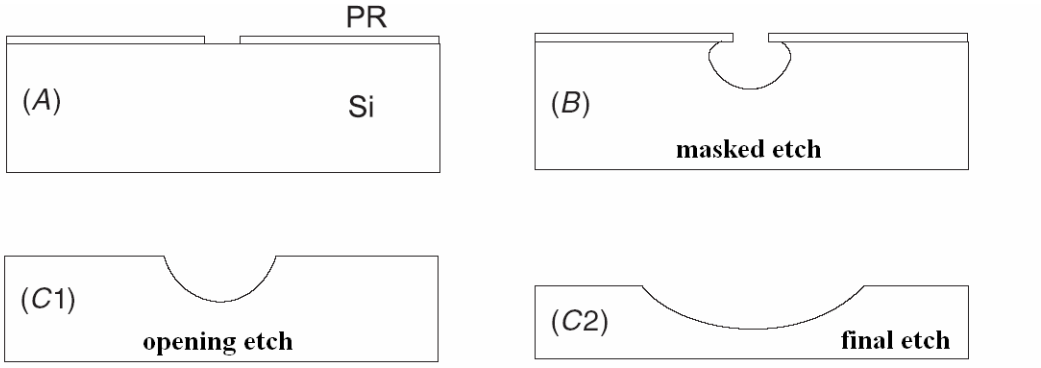

Fig.2.13 The process sequence for the silicon microlens mold. (A) Resist lithography. (B) A cavity is etched through the mask (masked etch). (C1) Intermediate maskless etch step used for the maskless etching tests (opening etch). (C2) Maskless etch until correct curvature is obtained for the cavities (final etch). [45]

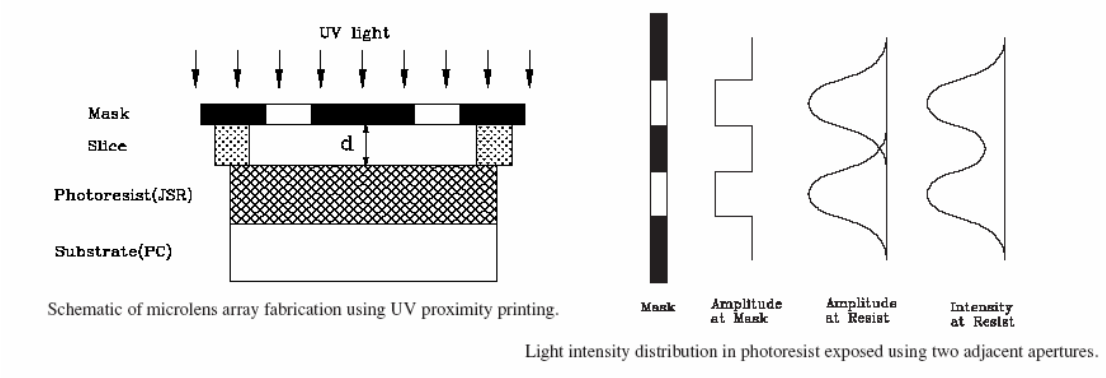

Fig. 2.14 On the left of Fig, light intensity distribution in photoresist exposed using two adjacent apertures. On the right of Fig, schematic of microlens array fabrication using UV proximity printing. [46]

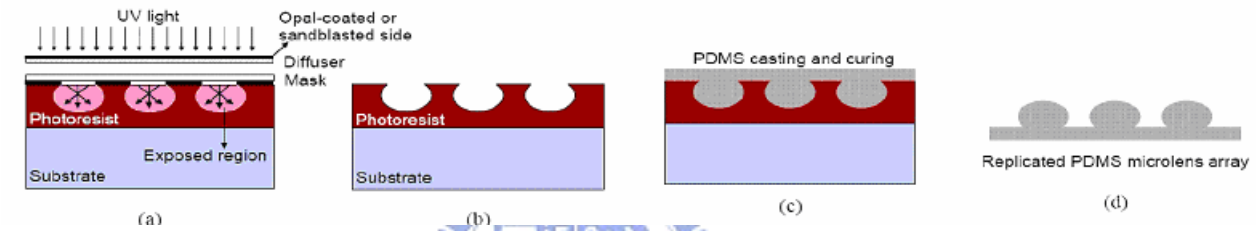

Fig.2.15 Process flow the proposed plastic microlens fabrication. (a) UV exposure through a diffuser and a mask (b) Development (c) Liquid PDMS casting and curing (d) Replicated PDMS microlens peel-off. [47]

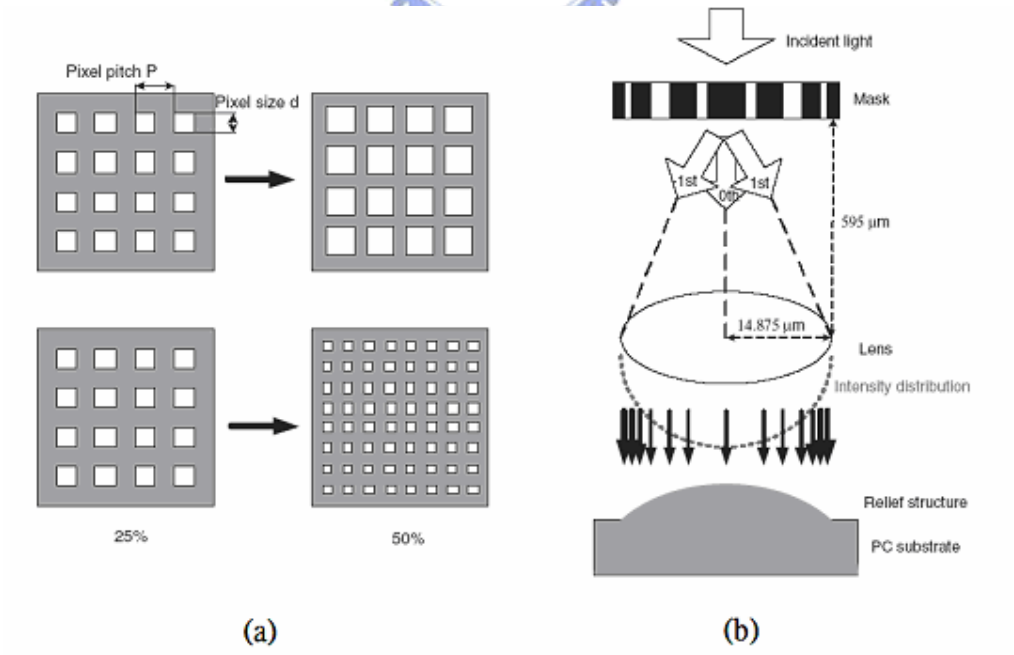

Fig.2.16 (a) Schemes of the coded gray-tone mask (b) Illustration of intensity modulation by gray-tone photolithography with different dot densities. [48]

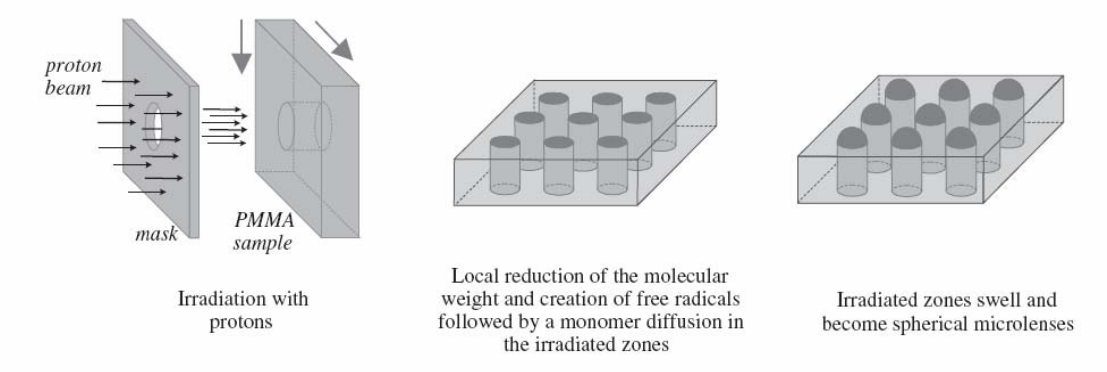

Fig.2.17 Basic fabrication process for arrays of spherical microlenses with deep lithography with protons: irradiating the PMMA layer through a mask and applying a vapor on one surface of the irradiated sample are the basic processing steps for the fabrication of 2D arrays of stable and uniform spherical microlenses. [49]

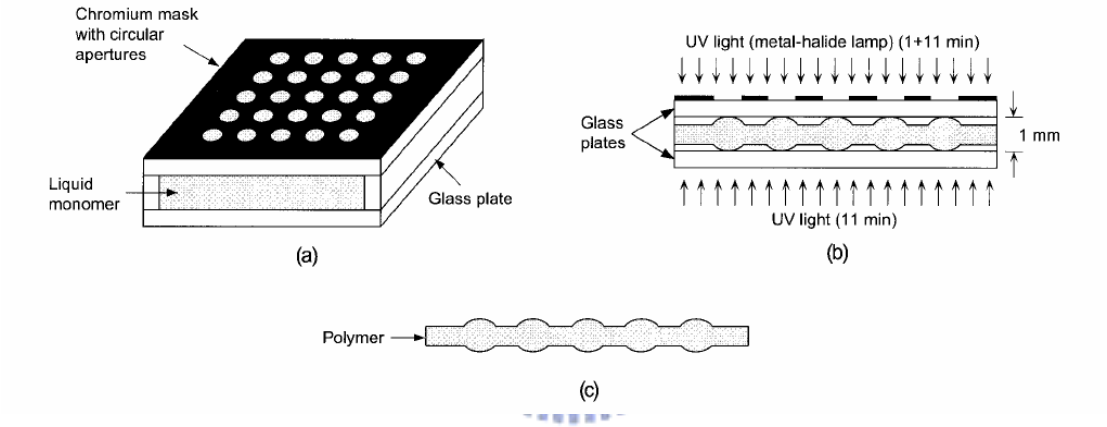

Fig.2.18 Fabrication process for microlens arrays: (a) The TEMA monomer is poured into a cell. (b)The liquid monomer is irradiated from above. (c) Annealing yields a convex microlens-array plate. [50]

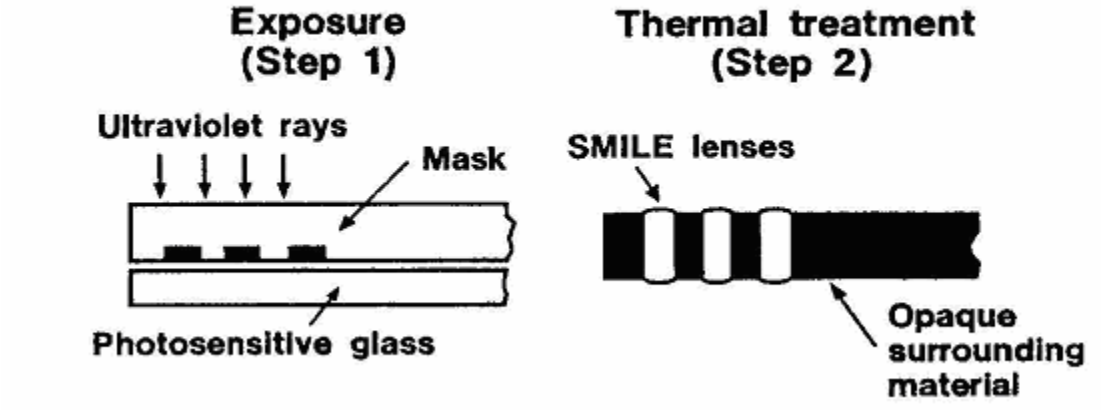

Fig.2.19 Special glass is exposed through a mask, then heated. Exposed area densifies and squeezes soft unexposed glass to form spherical protuberances. [51]

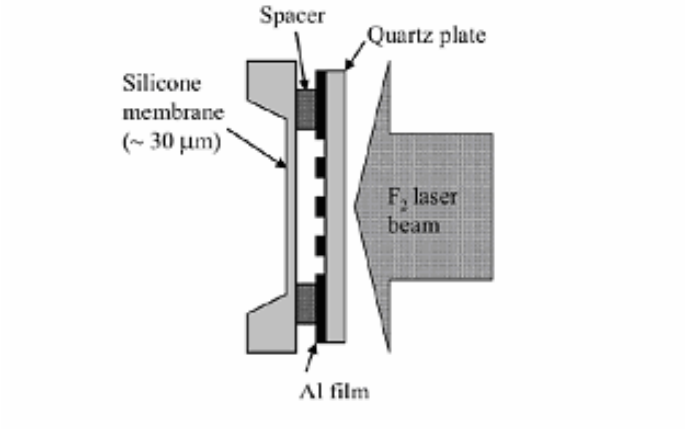

Fig.2.20 Experiment setup for fabrication of microlenses on silicone rubber. [52]

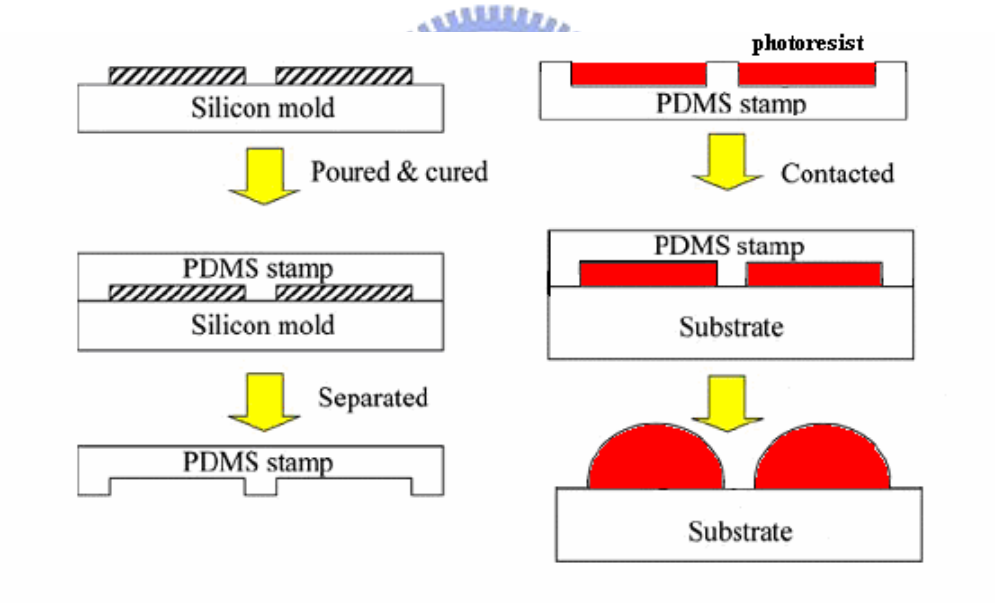

Fig.2.21 Process flow for micro-transfer molding with soft mold. [53]

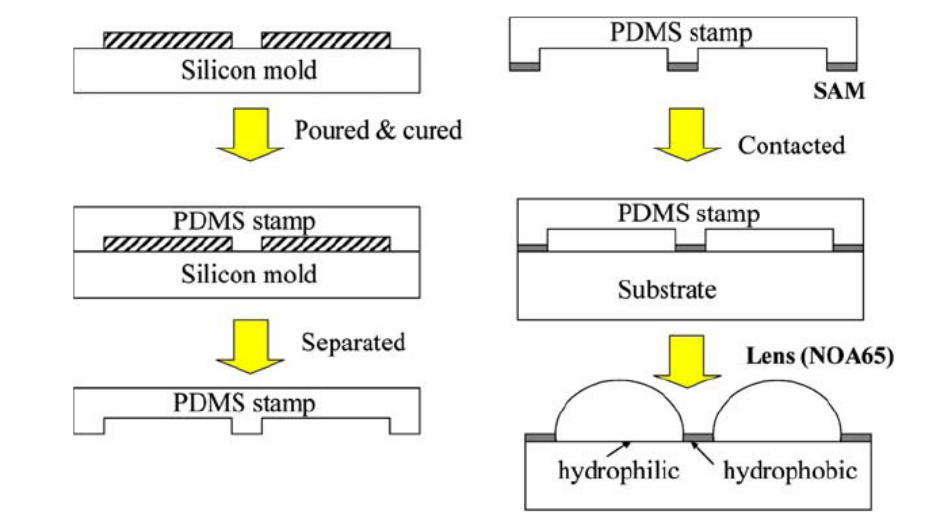

Fig.2.22 Fabrication processes of PDMS mold and microcontact printing. The pattern of the hydrophobic regions was defined by microcontactprinting of SAMs. After spin coating of the prepolymer (NOA65) on the substrate, the microlenses were self-organized on the hydrophilic regions. Finally, the microlenses were completed by UV curing. [54]

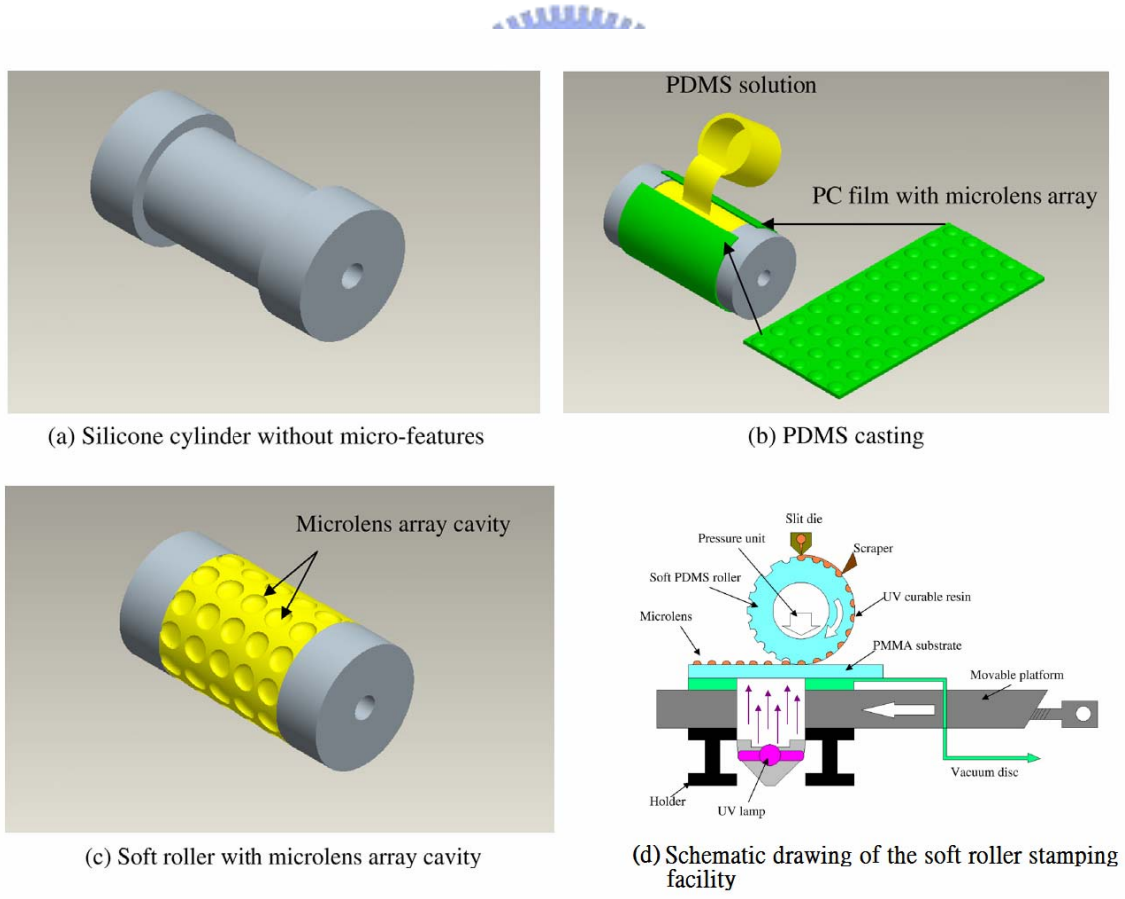

(a) Silicone cylinder without micro-features

(b) PDMS casting

(c) Soft roller with microlens array cavity

(d) Schematic drawing of the soft roller stamping facility

Fig.2.23 Procedures for fabricating soft roller with microlens array cavity. [55]

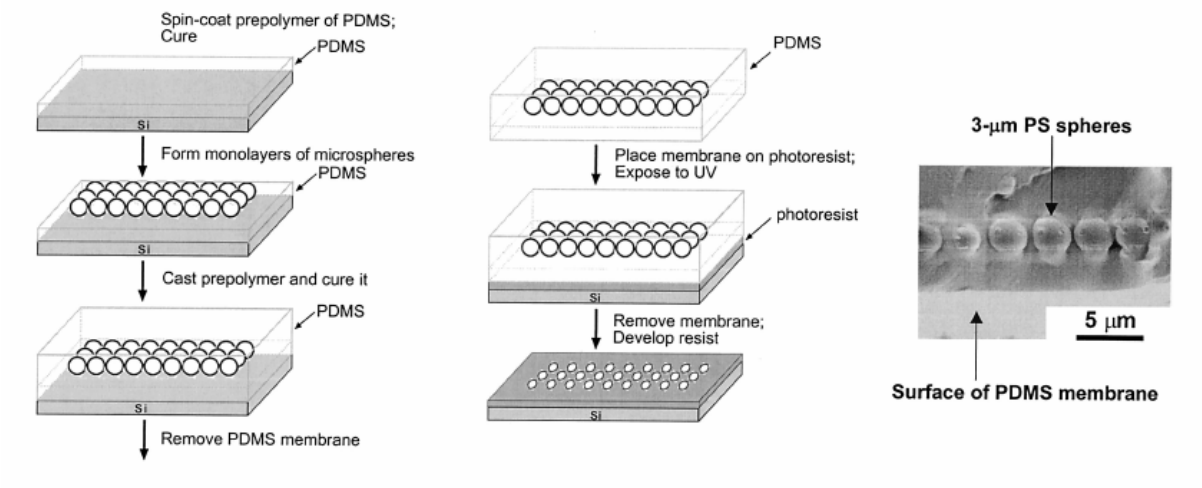

Fig.2.24 Illustration of the fabrication of a PDMS membrane with a 2-D crystalline array of embedded microspheres. The spheres are separated from the surface of the membrane by a distance *t*, equal to the thickness of the PDMS spacer. [56]

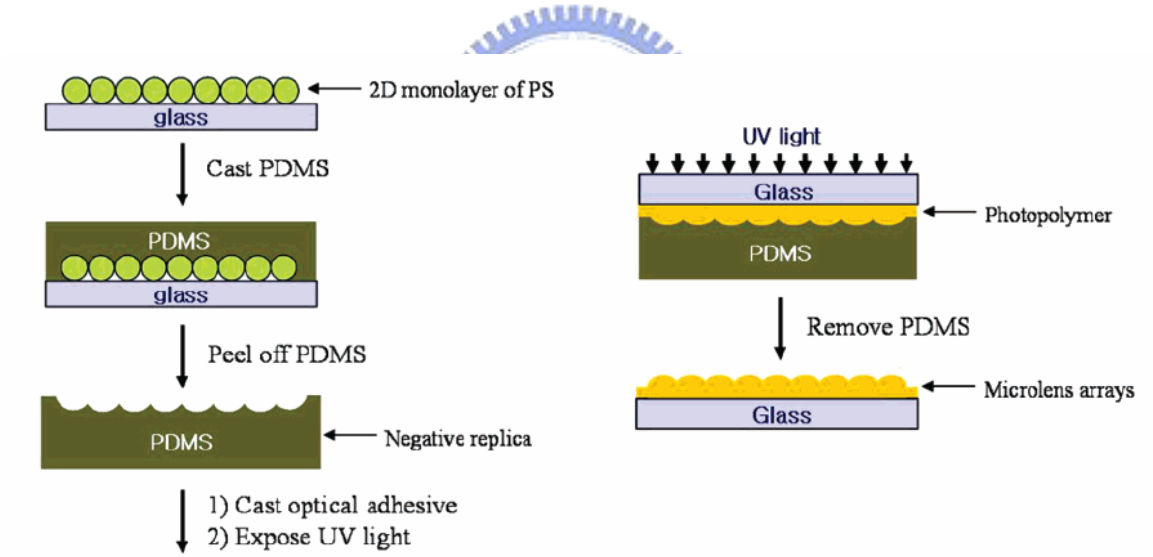

Fig.2.25 Schematic illustration for hemispherical polymer microlens arrays prepared by PS microspheres assembled on glass surface. [57]

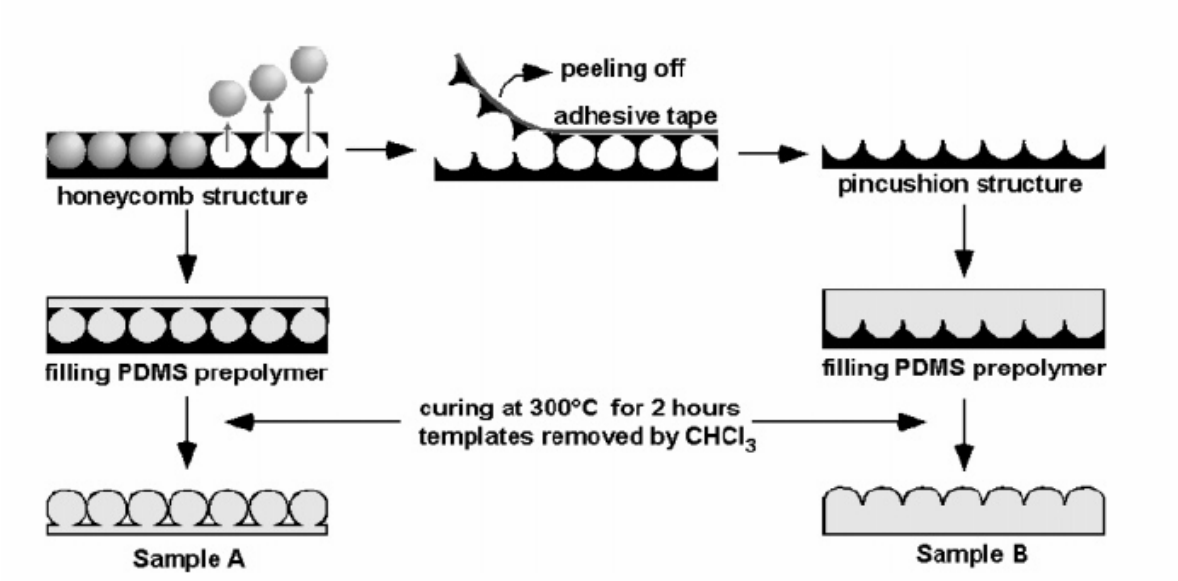

Fig.2.26 Shematic illustration of MLA preparation [58]

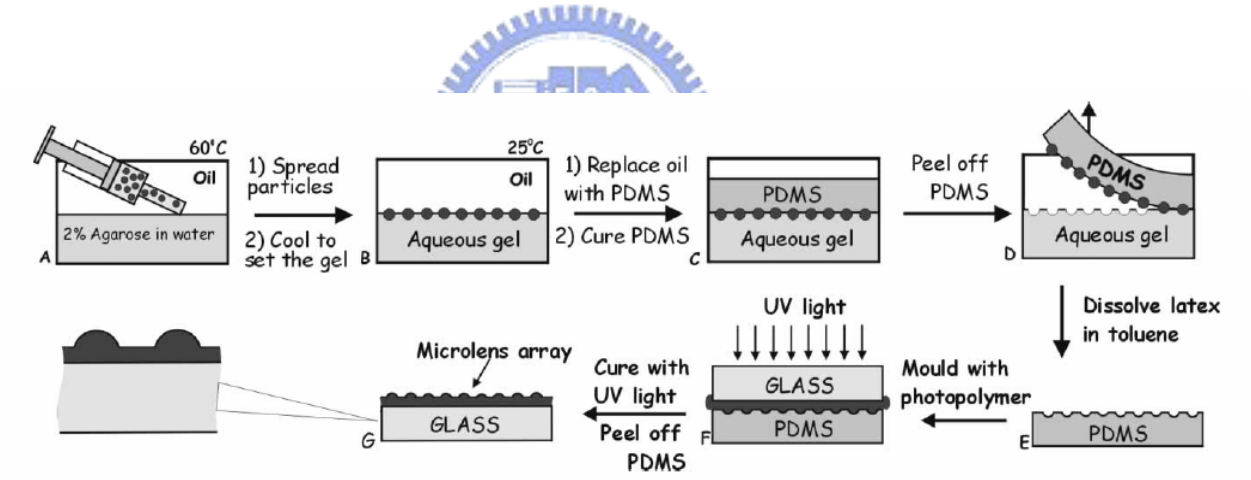

Fig.2.27 Scheme of the gel trapping technique (GTT) for fabrication of microlens arrays: (A) spreading of charged latex particles at the interface between an oil and a hot aqueous solution of agarose. After the gel sets the particle monolayer is trapped at the interface (B) and the oil phase is replaced with curable PDMS (C). By peeling the cured PDMS (D) and dissolving the latex particles in toluene, the PDMS template (E) is cast with a photopolymer (F) which produces a microlens array on a glass support (G). [59]

Chapter 3 Experimental Instruments

3.1 Experimental Instruments

3.1.1 Excimer laser

An excimer laser is a form of ultraviolet chemical laser which is commonly used in eye surgery and semiconductor manufacturing. An excimer laser typically uses a combination of an inert gas (Argon, krypton, or xenon) and a reactive gas (fluorine or chlorine). Under the appropriate conditions of electrical stimulation, a pseudo-molecule called a dimer is created, which can only exist in an energised state and can give rise to laser light in the ultraviolet range. This light is exceptionally well focussed and capable of very delicate control, and is well absorbed by biological matter and organic compounds. These properties make excimer lasers well suited to precision micromachining organic material (including certain polymers and plastics), or delicate surgeries such as eye surgery (LASIK). Kansas State University pioneered the study of the excimer laser which made LASIK surgery possible. Rather than burning or cutting material, the excimer laser adds enough energy to disrupt the molecular bonds of the surface tissue, which effectively disintegrates into the air in a tightly controlled manner through ablation rather than burning. Thus excimer lasers have the useful property that they can remove exceptionally fine layers of surface material with almost no heating or change to the remainder of the material which is left intact.

3.1.2 Sputtering

Sputtering is a physical process whereby atoms in a solid target material are ejected into the gas phase due to bombardment of the material by energetic ions. It is commonly used for thin-film deposition, as well as analytical techniques. Standard physical sputtering is driven by momentum exchange between the ions and atoms in the material, due to collisions. The process can be thought of as atomic billiards, with the ion striking a large cluster of close-packed atoms (billiard balls). Although the first collision pushes atoms deeper into the cluster, subsequent collisions between the atoms can result in some of the atoms near the surface being ejected away from the cluster. The number of atoms ejected from the surface per incident particle is called the sputter yield and is an

important measure of the efficiency of the sputtering process. Other things the sputter yield depends on are the energy of the incident ions, the masses of the ions and target atoms, and the binding energy of atoms in the solid. The ions for the sputtering process are supplied either by a plasma that is induced in the sputtering equipment, or an ion or electron accelerator. In the plasma sputtering devices, a variety of techniques are used to modify the plasma properties, especially ion density, to achieve the optimum sputtering conditions, including usage of RF (radio frequency) alternating current, utilization of magnetic fields, and application of a bias voltage to the target.

3.1.3 Spin coater

Spin coater is a procedure used to apply uniform thin films to flat substrates. In short, an excess amount of the solvent is placed on the substrate, which is then rotated at high speed in order to spread the fluid by centrifugal force. A machine used for spin coating is called a spin coater, or simply spinner.Rotation is continued while the fluid spins off the edges of the substrate, until the desired thickness of the film is achieved. The applied solvent is usually volatile, and simultaneously evaporates. So, the higher the angular speed of spinning, the thinner the film. The thickness of the film also depends on the concentration of the solution and the solvent. Spin coating is widely used in microfabrication, where it can be used to create thin films with thicknesses below 10 nm. It is used intensively in photolithography, to deposit layers of photoresist about 1 micron thick. Photoresist is typically spun at 20 to 80 Hz for 30 to 60 seconds.

3.2 Analysis Instruments

3.2.1 Optical Microscopy (OM)

The optical microscope is a type of microscope which uses visible light and a system of lenses to magnify images of small samples. Optical microscopes are the oldest and simplest of the microscopes. The optical components of a modern microscope are very complex and for a microscope to work well, the whole optical path has to be very accurately set up and controlled. Despite this, the basic optical principles of a microscope are quite simple.The objective lens is, at its simplest, a very high powered magnifying glass i.e. a lens with a very short focal length. This is brought very close to the specimen

being examined so that the light from the specimen comes to a focus about 160 mm inside the microscope tube. This creates an enlarged image of the subject. This image is inverted and can be seen by removing the eyepiece and placing a piece of tracing paper over the end of the tube. By careful focusing a rather dim image of the specimen, much enlarged can be seen. It is this real image that is viewed by the eyepiece lens that provides further enlargement. In many designs, the virtual image comes to a focus between the two lenses of the eyepiece, the first lens bringing the real image to a focus and the second lens enabling the eye to focus on the now virtual image (As shown in Fig.3.1). In all microscopes the image is viewed with the eyes focused at infinity.

3.2.2 Scanning Electron Microscopy (SEM)

Scanning electron microscopy is used to observe the surface morphology of wide range kinds of objects. It has the advantage of rather easy sample preparation, high image resolution, large depth of field and high magnification. A common SEM contains an electron gun to generate electron beams, which will be accelerated under 0.4-40kV voltage. By deflecting the incident beams with the focusing coils, a two dimensional image can be obtained by detect the reflected secondary electrons and the backscatter electrons. The model we use here is JEOL 6500, with field emission electron source and 15kV accelerate voltage.

3.2.3 Atomic force microscope (AFM)

The AFM consists of a microscale cantilever with a sharp tip (probe) at its end that is used to scan the specimen surface. The cantilever is typically silicon or silicon nitride with a tip radius of curvature on the order of nanometers. The diabram of AFM is shown as Fig.3.2. When the tip is brought into proximity of a sample surface, forces between the tip and the sample lead to a deflection of the cantilever according to Hooke's law. Depending on the situation, forces that are measured in AFM include mechanical contact force, Van der Waals forces, capillary forces, chemical bonding, electrostatic forces, magnetic forces (see Magnetic force microscope (MFM)), Casimir forces, solvation forces etc. Typically, the deflection is measured using a laser spot reflected from the top of the cantilever into an array of photodiodes. Other methods that are used include optical

interferometry, capacitive sensing or piezoresistive AFM cantilevers. These cantilevers are fabricated with piezoresistive elements that act as a strain gage. Using a Wheatstone bridge, strain in the AFM cantilever due to deflection can be measured, but this method is not as sensitive as laser deflection or interferometry.

If the tip were scanned at a constant height, there would be a risk that the tip would collide with the surface, causing damage. Hence, in most cases a feedback mechanism is employed to adjust the tip-to-sample distance to maintain a constant force between the tip and the sample. Traditionally, the sample is mounted on a piezoelectric tube, that can move the sample in the z direction for maintaining a constant force, and the x and y directions for scanning the sample. Alternately a 'tripod' configuration of three piezo crystals may be employed, with each responsible for scanning in the x,y and z directions. This eliminates some of the distortion effects seen with a tube scanner. The resulting map of the area s = f(x,y) represents the topography of the sample. The AFM can be operated in a number of modes, depending on the application. In general, possible imaging modes are divided into static (also called Contact) modes and a variety of dynamic modes.

3.2.4 UV-visible spectroscopy

The instrument used in ultraviolet-visible spectroscopy is called a UV/vis spectrophotometer. It measures the intensity of light passing through a sample (I), and compares it to the intensity of light before it passes through the sample (I_o). The ratio I / I_o is called the transmittance, and is usually expressed as a percentage (%T). The absorbance, A, is based on the transmittance:

$$A = -\log(\%T)$$

The diabram of UV-visible spectroscopy is shown as Fig.3.3. The basic parts of a spectrophotometer are a light source (often an incandescent bulb for the visible wavelengths, or a deuterium arc lamp in the ultraviolet), a holder for the sample, a diffraction grating or monochromator to separate the different wavelengths of light, and a detector. The detector is typically a photodiode or a CCD. Photodiodes are used with monochromators, which filter the light so that only light of a single wavelength reaches the detector. Diffraction gratings are used with CCDs, which collects light of different wavelengths on different pixels.

3.2.5 Fourier transform spectroscopy (FTIR)

Fourier transform spectroscopy is a measurement technique whereby spectra are collected based on measurements of the temporal coherence of a radiative source, using time-domain measurements of the electromagnetic radiation or other type of radiation. It can be applied to a variety of types of spectroscopy including optical spectroscopy, infrared spectroscopy (IR), nuclear magnetic resonance, and electron spin resonance spectroscopy. There are several methods for measuring the temporal coherence of the light, including the continuous wave Michelson or Fourier transform spectrometer and the pulsed Fourier transform spectrograph (which is more sensitive and has a much shorter sampling time than conventional spectroscopic techniques, but is only applicable in a laboratory environment). The diabram of FTIR is shown as Fig.3.3.

3.2.6 X-ray Photoelectron Spectroscopy (XPS)

X-ray Photoelectron Spectroscopy (XPS) is a quantitative spectroscopic technique that measures the empirical formula, chemical state and electronic state of the elements that exist within a material. Basic components of a monochromatic XPS system are shown in Fig.3.5. XPS spectra are obtained by irradiating a material with a beam of X-rays while simultaneously measuring the kinetic energy (KE) and number of electrons that escape from the top 1 to 10 nm of the material being analyzed. XPS requires ultra-high vacuum (UHV) conditions. XPS is also a surface chemical analysis technique that can be used to analyze the chemistry of the surface of a material in its "as received" state, or after some treatment such as: fracturing, cutting or scraping in air or UHV to expose the bulk chemistry, ion beam etching to clean off some of the surface contamination, exposure to heat to study the changes due to heating, exposure to reactive gases or solutions, exposure to ion beam implant, exposure to UV light, for example. XPS is routinely used to analyze inorganic compounds, metal alloys, semiconductors, polymers, pure elements, catalysts, glasses, ceramics, paints, papers, inks, woods, plant parts, make-up, teeth, bones, human implants, bio-materials, viscous oils, glues, ion modified materials and many others.

3.2.7 Contact Angle Measuring Device (CA)

Analysis of the shape of a sessile drop of test liquid or a air bubble in liquid placed on

a solid is the basis for optical contact angle (CA) / surface tension measurement or goniometry. The basic elements of a measuring device include a light source, sample stage, liquid/air bubble dispensing device, lens and image capture. Contact angle can be assessed directly by measuring the angle formed between the solid and the tangent to the drop surface. The contact angle is the angle at which a liquid/vapor interface meets the solid surface. The contact angle is specific for any given system and is determined by the interactions across the three interfaces. Most often the concept is illustrated with a small liquid droplet resting on a flat horizontal solid surface. The shape of the droplet is determined by the Young-Laplace equation. The contact angle plays the role of a boundary condition. Contact angle is measured using a contact angle goniometer. The contact angle is not limited to a liquid/vapour interface; it is equally applicable to the interface of two liquids or two vapours.

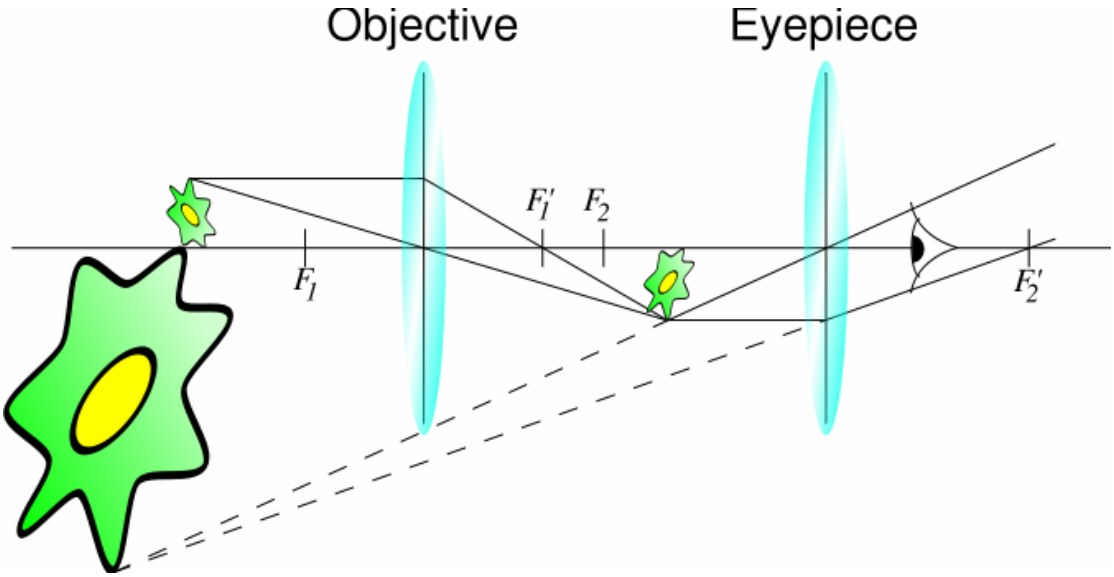

Fig.3.1 A diagram of a optical microscope

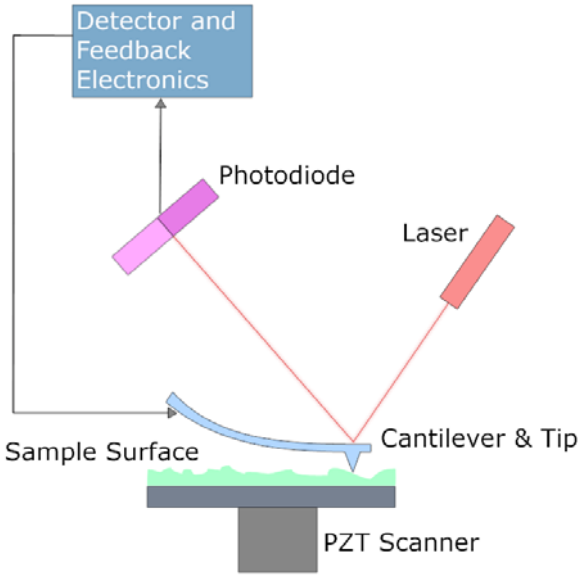

Fig.3.2 A diagram of atomic force microscope

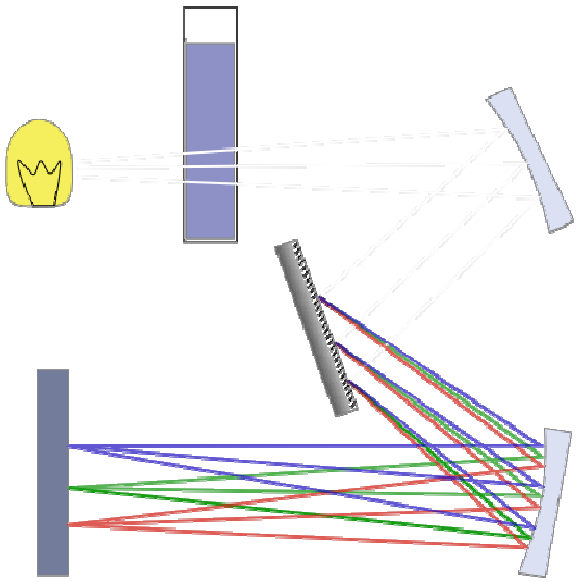

Fig.3.3 Diagram of a single-beam UV/vis spectrophotometer

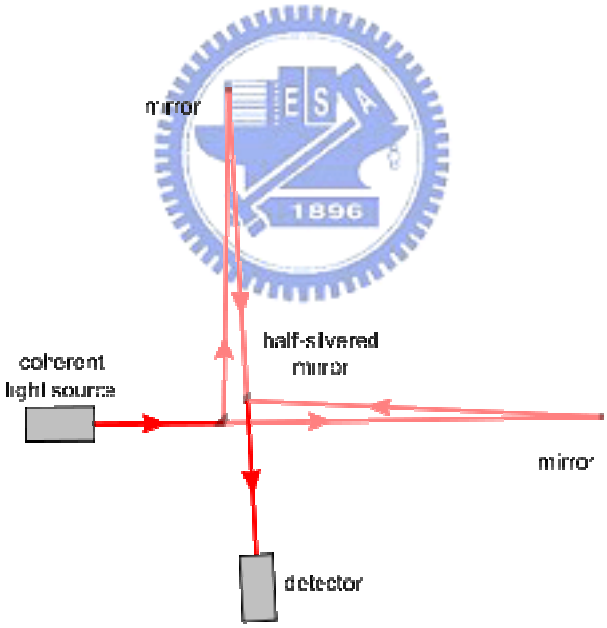

Fig.3.4 The Fourier transform spectrometer is just a Michelson interferometer but one of the two fully-reflecting mirrors is movable, allowing a variable delay (in the travel-time of the light) to be included in one of the beams.

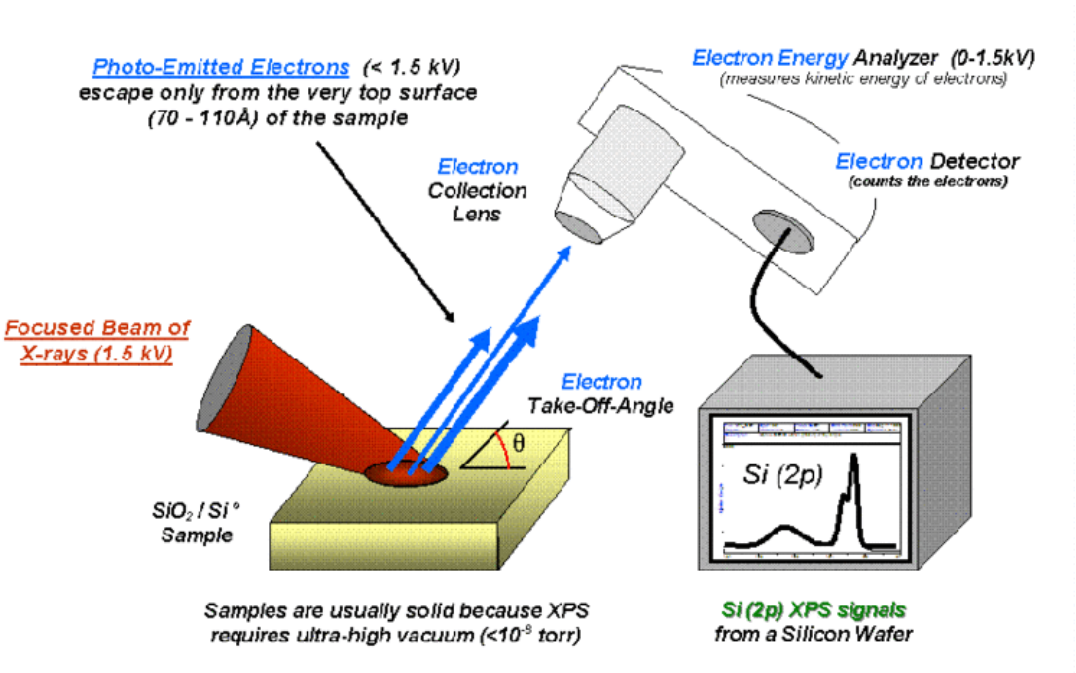

Fig.3.5 Basic components of a monochromatic XPS system

Chapter 4 The character and fabrication of Microlenses

4.1 Introduction of refractive microlens

In order to satisfy the needs of recent photoelectric systems, many researchers have been exploring various ways to fabricate refractive microlens arrays on different lens materials. Various lens materials and corresponding technologies have been presented, like polymer, silica, diamond and sol-gel. For the modern science and technology, most of fabrication technologies for these materials must involve the photolithography process, leading to the high-priced charges. With fast development of flexible devices, soft materials, PDMS, have been paid much attention and have been used to fabricate various components due to it's fascinating properties such as low surface energy, thermal curing property, it's refractive about 1.41 and soft nature.

We reported a great deal of the fabricated technologies for refractive microlenses in chapter 2 but the shapes of these fabricated microlenses were almost spherical surface due to the physical mechanism of fabricated technologies. However, a spherical surface would lead spherical aberration when light was concentrated on the focused spot. In order to eliminate spherical aberration, an aspherical surface has been demonstrated to be able to improve effectively this disadvantage. One of most direct methods to form an aspherical surface is the use of gray lithography technology but this technology is very expensive. Hence, one of our challenges is how to fabricate asperical surface structures using a simple and cheap technology. Here, we developed a new technology for microlens fabrication without the use of expensive equipment.

4.2 The novel way for refractive microlens fabrication

4.2.1 The fabrication of PDMS microlenses

Referring to the schematic depicted in Fig. 4.1, steps for fabricating PDMS microlens arrays are described as follows:

(1) The footprint with designed shape and size for a required structure was defined on a metallic mask through which the excimer laser wrote the footprint directly onto a polycarbonate (PC) plate. By monitoring the power intensity and number of laser shots, depth of the holes drilled by the excimer laser could be well controlled. Fig. 4.1(a) shows

the resultant PC plate with microholes that serves as the pedestal in the next step.

(2) A thin liquid polymethylmethacrylate (PMMA) film was then coated on the PC-based pedestal through spin-coating. As the liquid PMMA was rapidly spreading out, due to its own weight and viscosity, a film, suspended on the pedestals and with special curvature, was formed on the pedestal. The schematic is shown in Fig. 4.1(b). The effect of the liquid surface tension results in good surface uniformity, providing that the liquid PMMA is at reasonable thickness. After baking at 60℃ for 5 min, the liquid film was solidified and stuck fixedly on the pedestal.

(3) Soft PDMS microlens arrays were formed by the replica molding process. A liquid PDMS mixture (Sylgard 184, Dow Corning, the weight ratio of silicone elastomer to curing agent is 10 to 1) was cast onto the PMMA film obtained in Step 2 and then a glass or plastic substrate was covered on it. The schematic is shown in Fig. 4.1 (c). After baking at 70℃ for 30 min, the solidified PDMS microlens arrays could be easily stripped from the PMMA film. The resulting PDMS microlens arrays are shown in Fig. 4.1 (d).

4.2.2 The control of polymeric molds using spin-coater

Fig. 4.2 shows three continuous concave surface patterns, obtained by Step 2 and measured by the step, of the PMMA film suspended on the pedestal with a circle footprint of diameter 150μm. Our experiments revealed that except for patterns close to the boundary of the PC plate, the uniformity of the continuous concave surface patterns is very good.

A model for the formation mechanism of a film with special curvature was addressed here. First, we simplified the problem of the curved PMMA film and introduced four assumptions into it. As a PMMA film was spread and covered on the porous PC plate, four assumptions were described here (1) every microhole on the PC plate is individual and there was no any interaction between each other; (2) a liquid film is immediately solidified and has no any ductility; (3) a PMMA film sticks strongly on the surface of the PC plate without slippage; (4) a three-dimensional condition is simplified to a two-dimensional one. Hence, the formation mechanism of a curve PMMA film should be similar to the model of a flexible cable with its weight suspended on fixed points [65]. In Step 2, the mass of a PMMA film itself was uniformly distributed on it and this film

suspended on two points located on the same horizontal line. According to the cable model, the curved orbit of the PMMA film can be expressed through the following equation： $y = wx^2 / 2T$

Parameters such as a distance between the lowest point and the horizontal roof of a curve (y), a diameter of a microhole (x), the mass of a film itself (w), and a inner tension of a film (T). Following this formula, the curve of a PMMA film, obtained in Step 2, depended mainly on the diameter of a microhole and the mass of a film itself. Table 4.1 shows the measured height of a suspended PMMA film obtained from different thickness of a PMMA film based on three diameters, with three kinds of different diameters, x= 50, 100 and 150 μm. This model verified this proposed tendency that the suspended depth of a PMMA film increased with increasing the diameter of a microhole and the thickness of a PMMA film. Fig.4.3 presents that the surface profile of a suspended PMMA film, measured by α-stepper, can be closely fitted a parabolic shape and the fitting equation was expressed as： $y=ax^2+bx+c$, where a=0.0076, b =-1.3807, and c=44.6349. However, the fitting equation was incompletely matched with the cable model. We suggested that the formation process of a curve film involved some rebellious problems. For instance, we did not know whether a liquid PMMA film would stretch during a cured process and the evaporation influence of a solvent existed in PMMA liquids. But this model still provided advancing information to understand the effect of controllable parameters and the explanation of a film with parabolic orbit.

4.2.3 The character of PDMS microlenses

Because the coefficient of thermal expansion of PDMS is quite small, replication structures cast against a suspended PMMA mold is faithfully replicated in Step 4. Fig.4.4 reveals that surface relief of PDMS microlenses with different diameters have different heights at spinning coating rotating speed of 5000 rpm. Then, the optical character of PDMS was measured by UV-visible spectrophotometer. Fig. 4.5 shows a transmittance curve of PDMS as a function of incident wavelength. The PDMS transmittance is of approximately 85% at the wavelength range of 290 nm to 1100nm. This wavelength range contains ultraviolet rays, visible light, and a part of infrared rays. To compared with

poly(methyl methacrylate) (PMMA)(~90%), the transmittance of PDMS seems to be adopted. Hence, PDMS is surely a suitable material for lenses. Next, focusing properties of a 3 by 3 PDMS microlens arrays, of which each has diameters of 100 μm were examined through a optical setup consisted of a He–Ne laser diode as a light source, beam focusing and expanding lenses, filter, microscope objective, CCD camera, and imagine display and recording system. A schematic of the experimental setup is shown in Fig. 4.6. Fig. 4.7 shows a portion of the spot pattern produced by a 3 by 3 microlens array. The imagine reveals strong focusing function of the microlens arrays. The theoretical diffraction-limited spot size of these microlenses is 2.68 μm. Measurement shows the focused spots have the size of 2.88 μm. Finally, Fig. 4.8 shows that the root mean square surface roughness was about 1 nm in areas of 5*5 μm^2 by AFM. The RMS values of the scanned surfaces were all within 8 nm, corresponding to a total integrated scattering within 5% for visible light. This is because the spin-coated PMMA film should be stayed in the liquid state for a reasonable time and with a certain film thickness so that the effect of the surface tension can modify the surface uniformity. Hence, PDMS microlens arrays with a high-quality surface could be obtained.

Parameters such as height h, radius of curvature R, focal length f, and F numbers are all usually employed to characterize the microlenses. For an axial symmetrical planoconvex lens, focal length, height, radius of curvature, diameter and the number are related through the following formulas expressed as [66]:

$$R = \frac{(K+1)h^2 + (\frac{\phi}{2})^2}{2h}, \quad f = \frac{R}{n-1}, F\# = \frac{f}{\phi}$$

where is the diameter of the microlens ϕ, K is the aspherical constant, and n is the refractive index of the material of the microlens. To estimate characteristics of the microlenses, we approximate the profile as parabolic the parabolic fit in Fig. 4.3, and thus, K take to be 1. The corresponding focal lengths of the microlenses as a function of the thickness of the PMMA film is presented in Fig. 4.9. In these calculations, the refractive index is taken to be 1.41 for the PDMS mircolenses. These results demonstrate that the geometrical configuration of the microlenses can be regulated by suitable arrangement of the diameter of the microdrilled hole and spin-coating parameters. The $F\#$ of the

fabricated microlens is between 0.8 to 1.5.

4.2.4 The diffusers plate using PDMS microlenses

With the fast development of flexible display, PDMS microlens arrays could be attached to a flexible plastic substrate and be used in the flexible display. Due to the soft nature of PDMS, these microlenses would be not damaged by stresses which existed in deformable devices. However, it would be difficult for general microlenses to bend the underlay substrate, due to stress destruction. In addition, In order to increase this fill factor, adding another microlens array with the original microlens shifted halfway along the diagonal. This process can not only enhance the fill-factor in an underlay substrate but also be used as diffusers. A schematic diagram of diffusers plate using PDMS microlenses is shown in Fig.4.10. To understand how efficiency for the made diffuser is, a schematic diagram of the experimental setup for measuring efficiency of components is shown in Fig. 4.11 (a). The setup consisted of a laser diode as a light source, samples, screen and CCD camera, imagine display and recording system. As a laser beam propagated through the sample, an expended beam would be projected finally on the screen. A CCD camera can be acted as a detector and capture the image of intensity distribution of a laser beam. Therefore, optical intensity distributions can be clearly analyzed through commercial optical software called beam profile. Three kinds of cases, including a laser beam without any elements, with microlens arrays attached to one side of an underlay substrate, and with the made diffuser, were respectively examined. Three kinds of resulting images are shown in Fig. 4.11 (b)-(d), respectively. The intensity distribution for a high-intensity laser without any component is shown in Fig. 4.11 (b). In Fig. 4.11 (c), the original shape of the laser beam started to expand through the underlay substrate with microlens arrays, but the center of the expanded beam still kept a high intensity. However, the laser beam passed through the made diffuser, a uniform intensity could be clearly observed in Fig. 4.11 (d) and the center of the expanded beam was almost similar to other area. Hence, the fabricated diffuser can effectively expand a high-intensity laser beam.

4.2.5 The fabrication of polymeric microlenses using soft replica molding

In most photoelectric systems, microlenses are made of inorganic material, such as

silica, diamond and sol–gel, due to its environment stability and a long life cycle. A simple approach to transfer polymeric microlens into inorganic ones is the technology of reactive ion etching technology. After etching, PDMS has a rugged and rough surface. Hence, PDMS is not a good material for reactive ion etching process. In order to improve this problem, the best way is the use of commercial polymer. Therefore, PDMS is often served as materials for molds, due to low surface energy. Here we developed a novel technology to generate positive and negative PDMS molds which can be used to replica polymeric structures by following our earlier works.

Based on the excimer laser microdrilling and the spin coating scheme, polymeric molds on a thin plastic pedestal sheet was proposed. A soft PDMS mold with microlens patterns is formed by a casting process. Specifically, a liquid PDMS mixture was cast onto the PMMA film obtained in Step 2. After baking at 70℃ for 30 min, the solidified PDMS mold can be easily stripped from the PMMA film. Then, a concave soft mold can be fabricated by a second replica molding using the convex PDMS mold. To make sure both the concave and convex PDMS molds can be separated after baking, the weight ratio of the silicone elastomer and the curing agent for the concave mold should be different from that for the convex mold. Here, the ratio for the concave mold is set at 5 to 1. Finally, both concave and convex polymer microlens arrays can be fabricated by another replica molding by casting the desired polymeric liquid, for example PMMA, SU-8 and other photoresists, in the corresponding convex and concave molds, respectively. For the replica process of PDMS molds which are reproduce from another PDMS molds, we called this technology soft replica molding. Fig 4.12 shows the fabrication of polymeric microlens by soft replica molding.

4.2.6 The fabrication of various surface relief structures

Compared to photography lithography, pulsed eximer laser through metallic mask is flexible to create a corresponding microhole severed as a plastic pedestal and the depth of the pedestal also can be controlled by the number of laser shots or the power intensity. As the depth of a pedestal is deeper than the drooping depth of a liquid film, a parabolic shape is not restricted by the bottom of PC plate. Hence, microlenses can be fabricated. However, the depth of the pedestal is shallower than the drooping depth of a liquid film.

The bottom of the spin-coated liquid film is able to touch the bottom of the pedestal during the spin-coating step. Instead of shaping a curved film, a flat bottom curved film is formed. After the process of soft replica molding, microlens array with flat top surface was fabricated. Fig. 4.13(a) shows a 4 by 4 microlens array with flat top surface. The height of this structure is about 8 lm and the width of a platform is about 100 lm that is shown in Fig. 4.13(b). With decreasing the depth of a pedestal, the width of a flat-top structure increases gradually. Hence, the size of a focused spot can be easily determined by changing the width of the platform. Such structures have been used in improving the external quantum efficiency of organic light emitting diodes [67].

Besides, a lens-on-lens structure can be also created by this technology. A concentric pedestal composed of an outer square and an inter square on the PC plate is considered. Under our fabricated processes, the lens-on-lens structure is, for example, consisted of a smaller lens with a width of 200μm and the bigger lens with a width of 400μm and the smaller lens is stacked on the bigger one. Fig.4.14 shows a stacked structure of smaller lens on bigger lens. Based on this fact that the size of microholes can determine the curvature of a liquid film, both lenses have different focal lengths. Hence, the element can generate two focus spots but the spots have different focal length. Such an element has been applied in focusing laser light onto two separate planes on dual-layer disks or for multiple-layer optical tweezers configurations [68].

Although an eximer laser can easily create desired microholes through desired metallic masks, whereas the sidewall of microholes is not vertical under a high aspect ratio condition. The depth of microholes is more and more deep, leading the focused plane of the laser to go away from a suitable position. Hence, a cone-like microhole is fabricated, due to energy scatter. Therefore, the slanting angle for cone-like microholes is smaller than the curved face of a liquid film, leading to have no influences on the formation of the curved face. However, a pedestal combined two adjacent microholes, fabricated by laser microdrilling, have obviously influences. The middle of this pedestal has a support, due to a cone-like shape of microholes. A schematic diagram of the pedestal structure with the support formed through laser microdrilling is shown in Fig. 4.15(a). After coating a liquid film and soft replica molding, a double-peak structure is fabricated (shown in Fig. 4.15(b)). The double-peak structure consists of two single microlenses, of

which each has the diameter of 100μm. Due to the meddle support, two microlenses are independent.

For the function of the middle support, it can support a liquid film to form a complicated surface. For example, the special pedestal was created through a mask with a circular pattern. First, a circular hole was randomly fabricated on the PC plate. Then, moved the distance within a quarter of the diameter of a circular pattern from the original location, laser was again bombarded the PC plate until a suitable depth was achieved. After coating a liquid film, an asymmetry structure can be fabricated. Fig.4.16 shows SEM image for the asymmetry structure. This structure consists of a lens-like pattern and a meniscus pattern. The lens-like pattern has the diameter of 100μm and a meniscus pattern has the width of 25μm. Such asymmetric structure is very difficult to fabricate by the use of traditional photolithography.

4.3 The fabrication of reflective microlens

4.3.1 Introduction of reflective microlens

Micro-optical elements with their own scale of a few to several hundred micrometers are extensively applied to optical devices using MEMS technology to collect, distribute and modify optical radiation. In general, micro-optical elements can be roughly grouped into three generic areas; one is refractive, another is diffractive and the other is reflective. Refractive elements used in photoelectric systems are usually more popular than reflective ones. But reflective optics is useful for packaging an optical system into a smaller space than that which can be currently used for refractive optical elements [69]. Therefore, the optical characteristics of refractive elements depend mainly on the spectroscopic characteristics of photopolymerized resin used for its fabrication [69]. In order to eliminate this dependency, a reflective element could substitute for a reflective one and its optical performance was as good as that of a refractive element.

Generally speaking, reflective elements are essentially consisted of surface relief structures and metallic reflective coating. The focused ability of reflective elements mainly depends on surface relief structures and surface metal coatings. Therefore, various metal coatings could reflect light with a special region of wavelength. For example, Silver films have a good reflectance in the whole visible spectrum and in the

near-ultraviolet; Gold films have a good reflectance in the infrared region [70] Therefore, we hope to develop additionally a reflective function under analogous fabrication processes. Although one of most direct approaches is that a metallic film deposited on the PDMS surface, a PDMS layer covered a metallic film would form spontaneously wavy structures on the PDMS surface due to the different contraction rates of cooling between the metal film and the PDMS layer. Fig.4.17 shows the SEM image of wavy structures on the patterned surface of PDMS covered a metallic film with 100 nm thickness. These wavy structures on PDMS surface would cause the diffusion of light as light irradiated this surface. Therefore, metal films would easily crack under a small physical deformation due to the different ductility between the metal film and the PDMS layer.

4.3.2 The preparation of soft reflective materials

Because most of photoelectric systems have a light source with a visible-light wavelength ranged between 350 and 700 nm, we hoped to get a high-reflectance material in the visible-light region. PDMS mixtures mixed with various kinds of nanoscale powder, including silica (SiO_2), titania (TiO_2), calcium carbonate ($CaCO_3$), zirconia (ZrO), zinc oxide (ZnO), and alumina (Al_2O_3)were respectively characterized by UV-VIS spectrophotometer. Fig. 4.18 shows a reflectance curve of PDMS mixture polymers as a function of incident wavelength ranged between 200nm and 1100nm. Consequently, we found that the reflectance of TiO_2/ PDMS, which achieved 98%, was the most suitable candidate in these PDMS mixtures. The TiO_2/ PDMS mixtures could reflect most of visible light and its reflectance value was better than the value of traditional aluminum coatings (90%) using as reflective films. Hence, the PDMS/TiO_2 mixtures could substitute for metal coatings to reflect visible light.

It has been known that the processes of absorption, refraction, scattering and other interactions would occur as light illuminated on any matter. In this study, light can be reflected by PDMS mixtures, which is due to light scattering phenomenon. As PDMS mixtures in which nanoscale particles distributed uniformly were illuminated by light, particles would absorb light with a special energy and then excited electrons in particles released other types of radiation such as ultraviolet rays, visible light and infrared rays in all directions when excited electrons returned ground state. Hence, scattering processes

can be simply expressed as: Scattering = excitation + reradiation [71]. In fact, light scattering processes involved many factors, such as the size and shape of particles, the type and property of materials and other corresponding factors etc. Additionally, the surface color of powders was also an important factor. For example, as the color of powders is close to white, it means that most of visible light is reflected; On the contrary, as the color of powders is black, it means most of light is absorbed.

Here, we adopted a simple model to explain experimental results. According to Rayleigh scattering formula, the intensity of light scattering can be roughly expressed as [71]:

$$I = \frac{8\pi^4 r^6}{\lambda^4}\left(\frac{n^2-1}{n^2+2}\right)^2\left(1+\cos^2\theta\right)$$

where r, n, λ, θ are the radius and refractive index of powders, wavelength and incident angle of light. The intensity of light scattering depended strongly on the size and refractive index of powders. Table 4.2 shows the refractive index and color of various powders. White TiO_2 powders have a larger refractive index than other materials in Table 4.2, causing to have the best reflectance for TiO_2/PDMS mixtures in Fig. 4.18. Then, the size influence of TiO_2 powders was also considered. Fig4.19 shows a reflectance curve of TiO_2 with three sizes, r=40nm, 400nm, and 45μm, /PDMS mixtures as a function of incident wavelength ranged between 200nm to 1100nm. We found that the intensity of light scattering decreased slightly with the increase of particle size. Experimental results were contradicted with Rayleigh formula in which the intensity of light scattering was proportional to the six power of particle size. We observed that bigger particles in high-viscosity polymers would aggregate easily to form a bulk and such bulk would deposit on the bottom of PDMS. This aggregate phenomenon led the non-uniform distribution of particles and lowered the intensity of light scattering. Hence, the best fillers should be nanosize powders with a high refractive index.

4.3.3 The fabrication and optical performance of soft reflective microlenses

Instead of PDMS without filler, PDMS with TiO_2 powders was used as the mold's material. It has been demonstrated that both of positive and negative molds can be fabricated through soft replica molding. Here, these molds can be directly acted as soft

reflective microlenses without a metal coating, avoided the problem of wavy structures generation on PDMS surface.

Then, the focusing property of the fabricated concave elements was examined experimentally. A schematic diagram of the experimental setup is shown in Fig. 4.20 (a). This setup consisted of a lamp as a white light source, microscope, CCD camera, image display and a micrometer scale resolution Z-stage. A 2*2 concave element with 100 μm diameter array was placed on the Z-stage and a lamp with a small inclined angle illuminated the surface of the concave element. The light would be focused on a spot by the reflection of concave surface structures. When the bright spot was arrived a minimal scale along the move of Z direction, this minimal spot was the focused spot of the concave element. The focused spots shown in Fig.4.20 (b) were about 4.2 μm. The other spots in Fig.4.20 (b) were due to the light reflected form the edge of the concave element. Hence, experiment results demonstrated fabricated concave elements are capable of generating spot arrays.

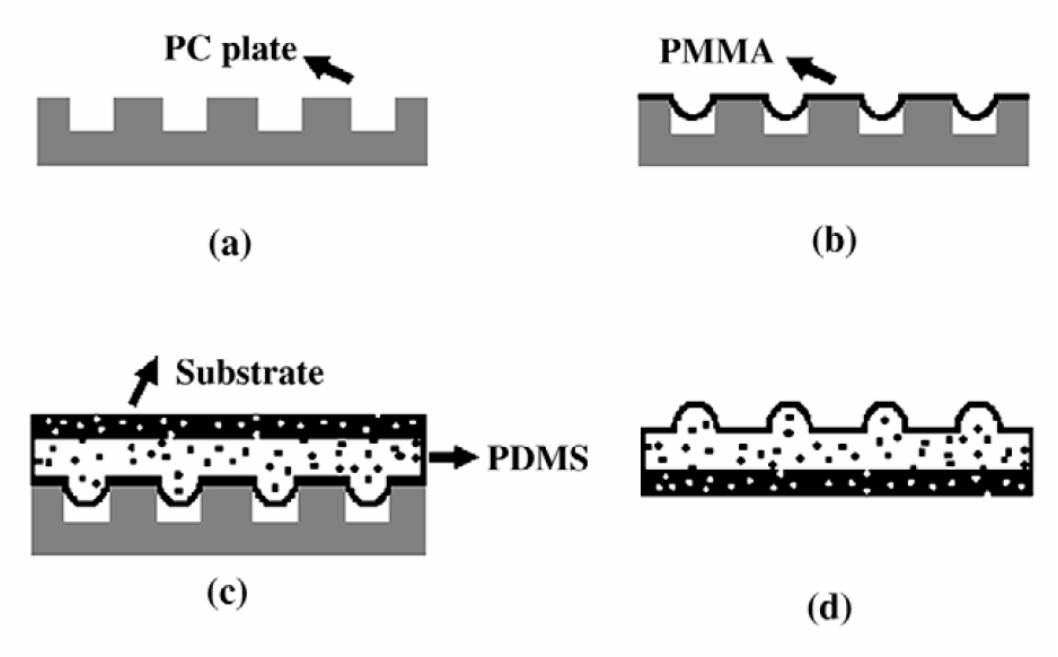

Fig.4.1 Schematic for fabrication of PDMS arrays by replica molding

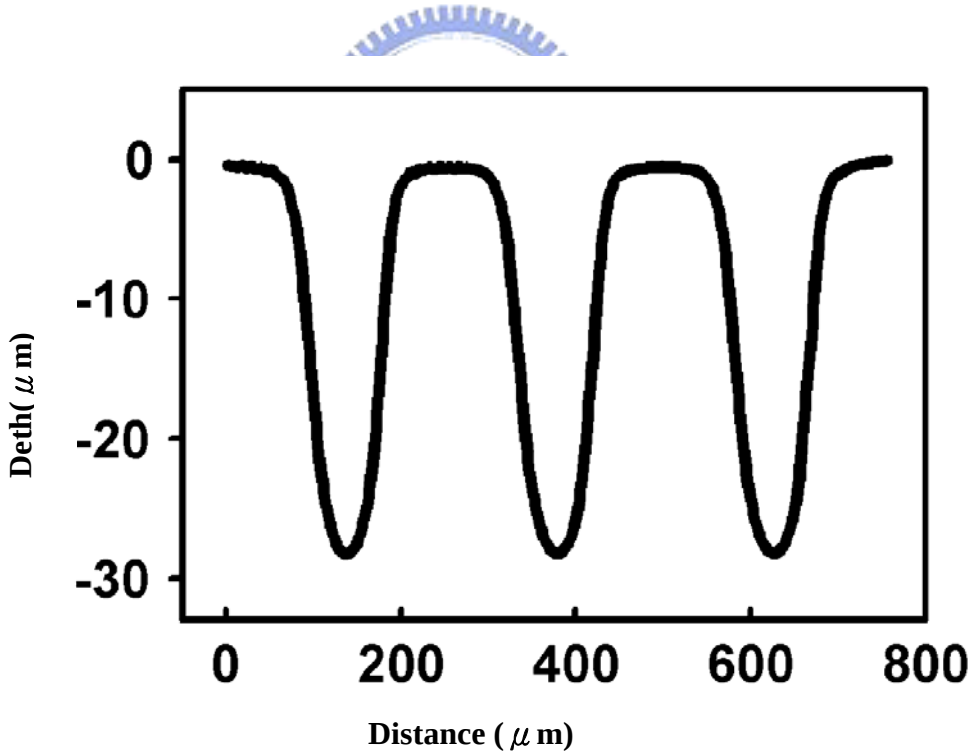

Fig.4.2 Surface profile of the PMMA film scanned by the α-step

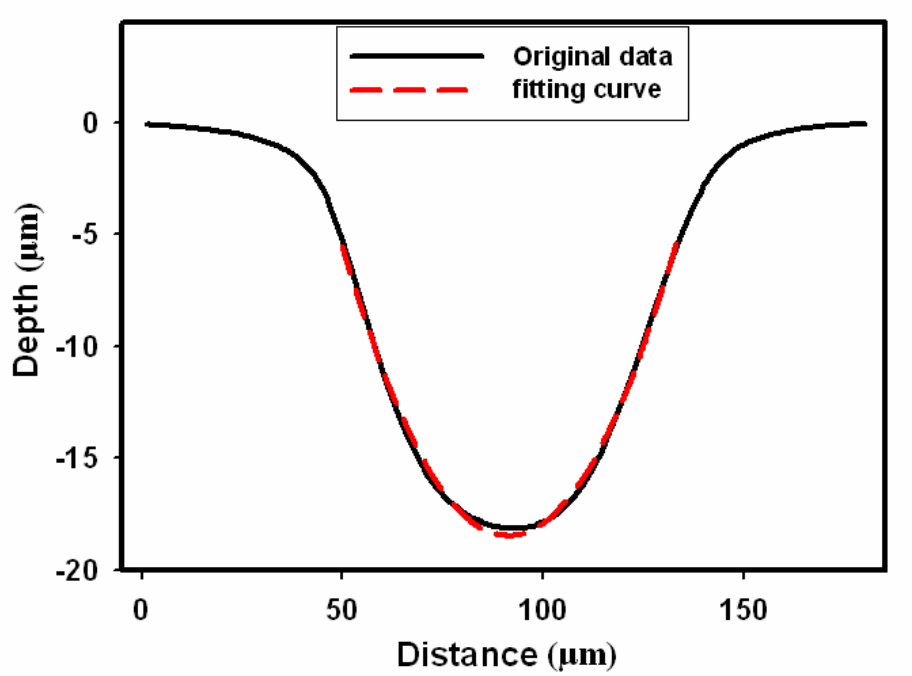

Fig.4.3 The scanned profile of a suspended PMMA film through the measure of α stepper

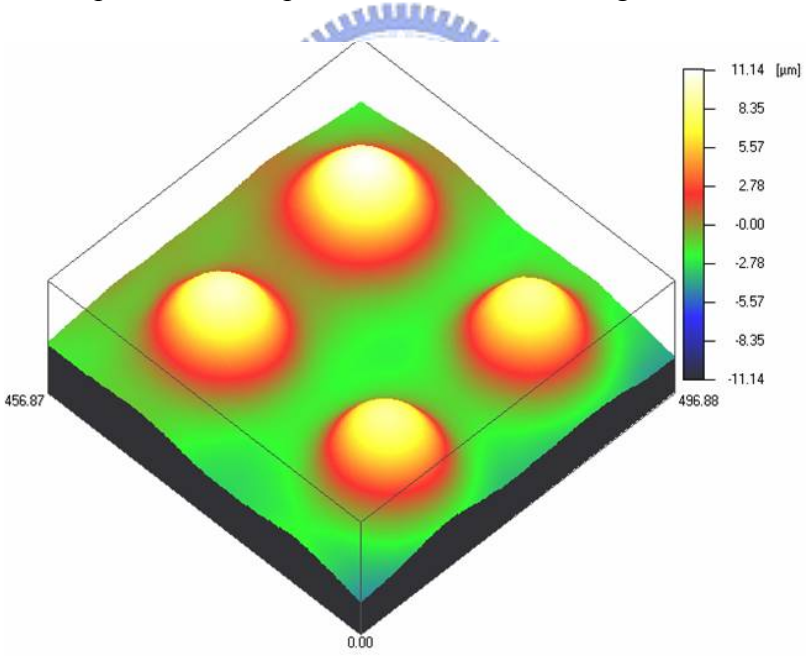

Fig.4.4 3-D images of microlens arrays by confocal microscope

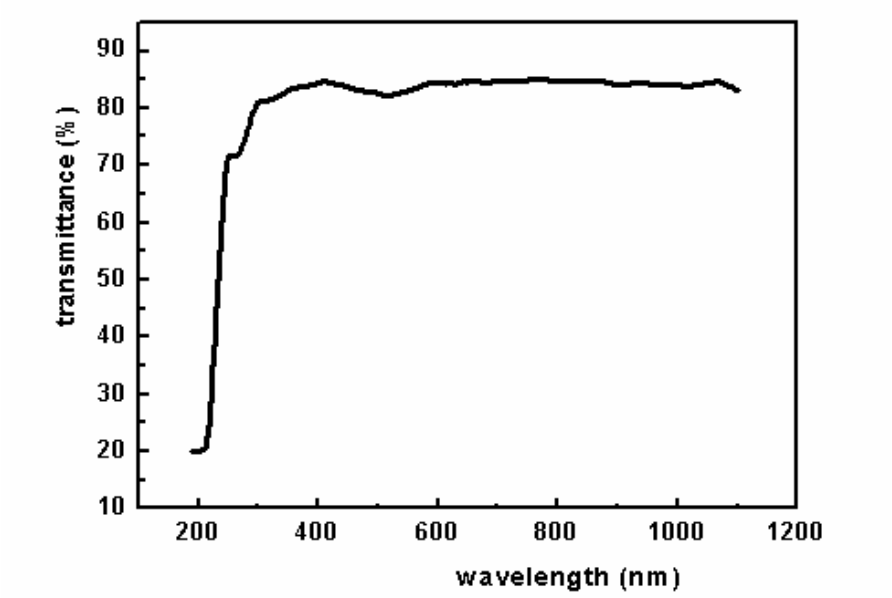

Fig.4.5 A transmittance curve of PDMS as a function of incident wavelength

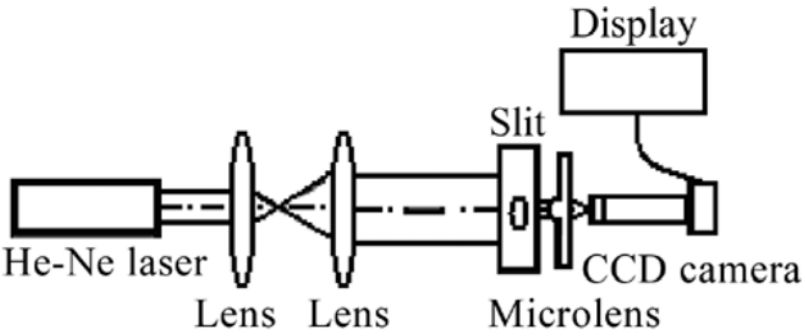

Fig.4.6 Schematic showing the experimental setup for measuring focused spots

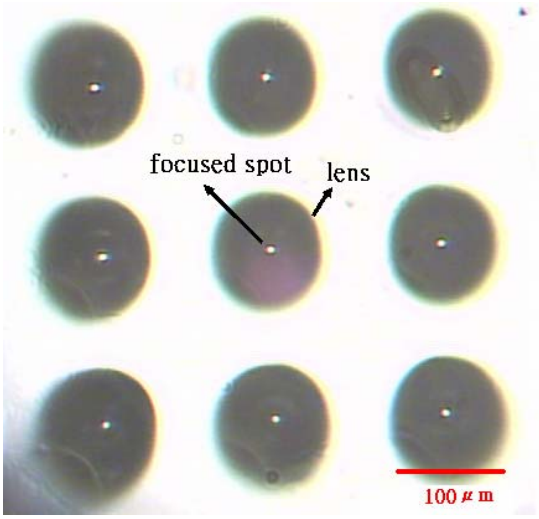

Fig.4.7 The optical image of focused spots of microlens

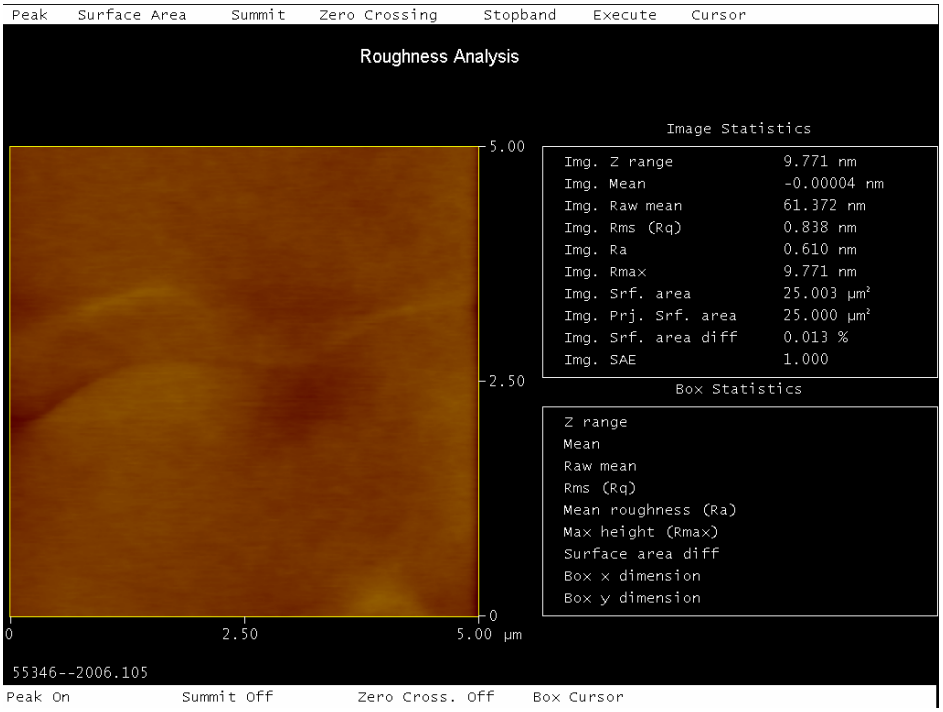

Fig.4.8 Images of surface roughness by AFM

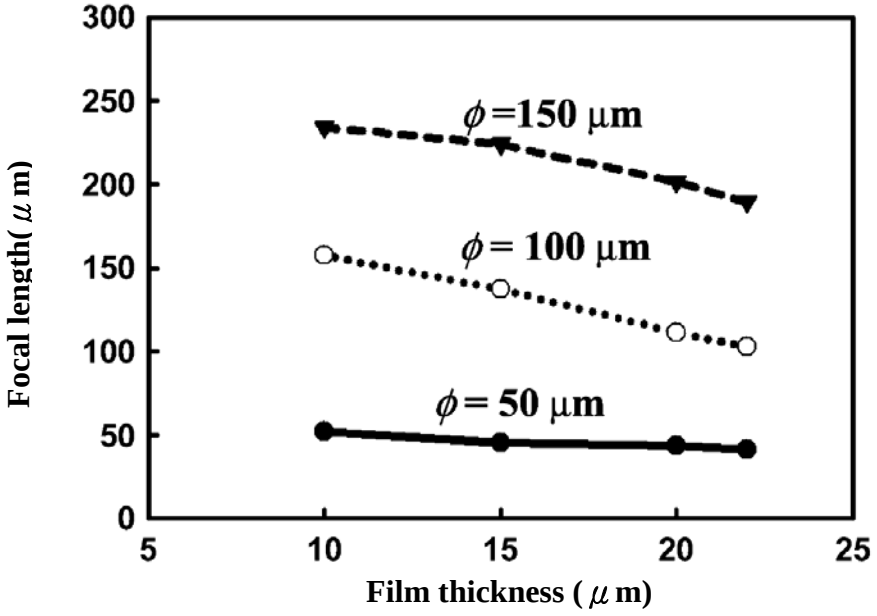

Fig.4.9 Focal length of microlens as a function of film thickness

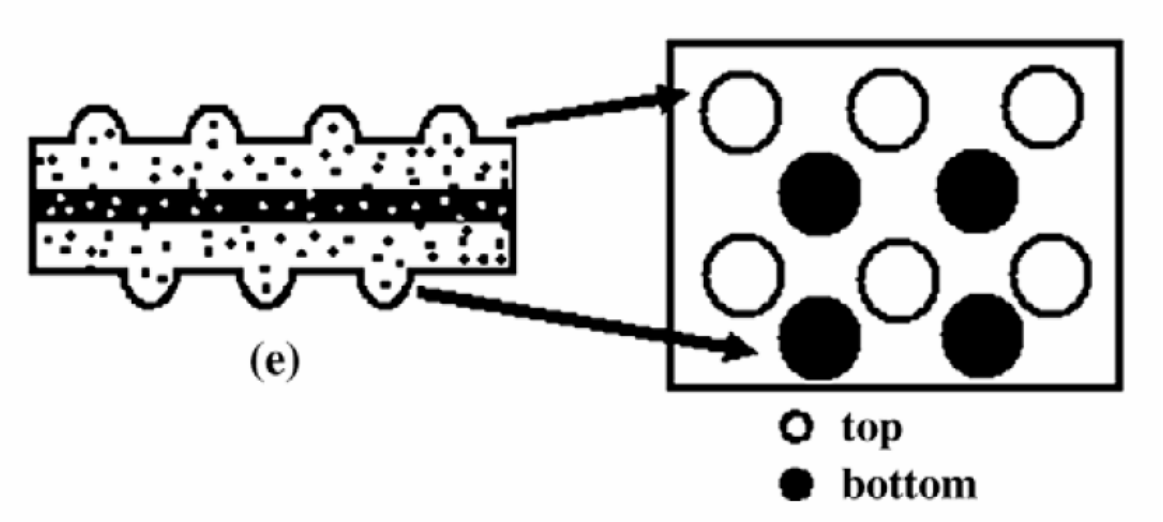

Fig.4.10 A schematic diagram of diffusers plate using PDMS microlenses

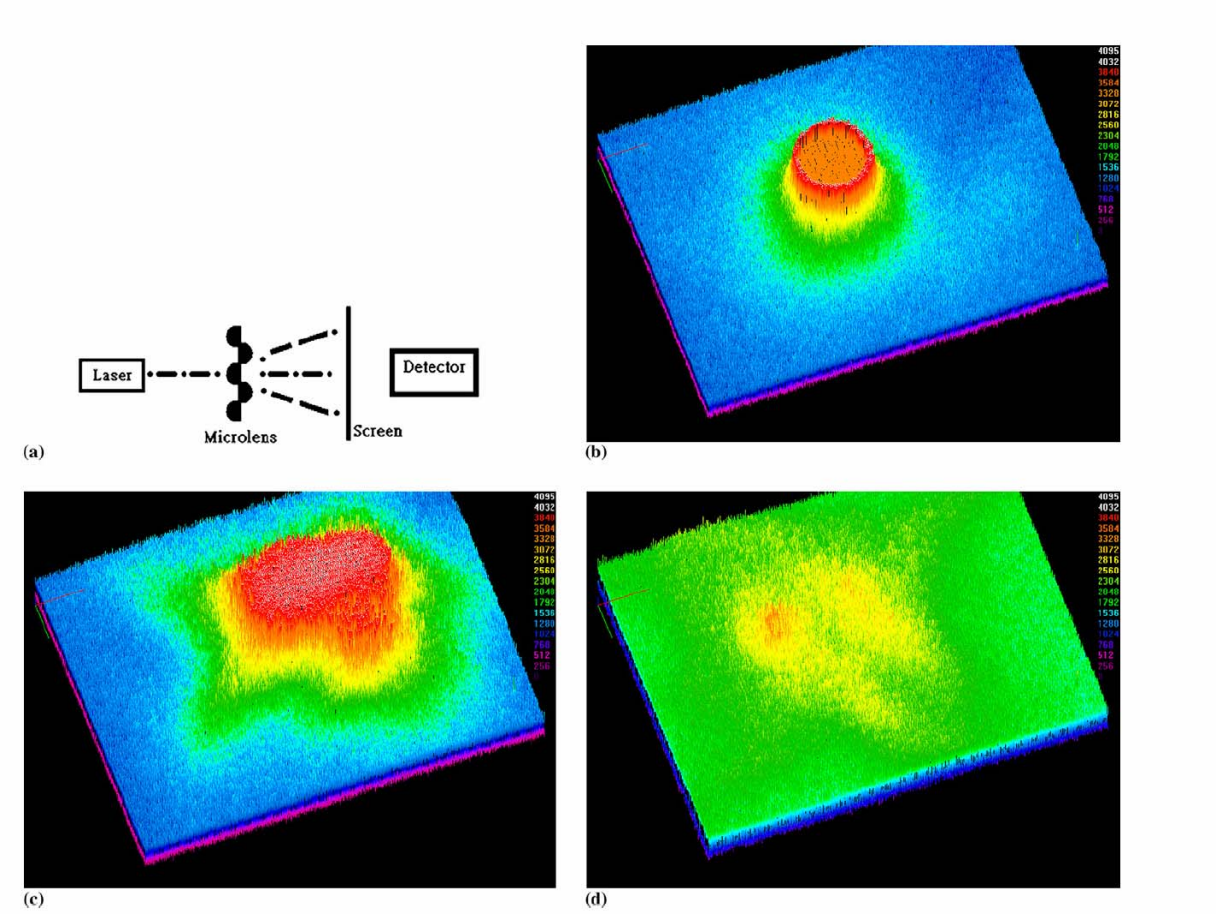

Fig.4.11 Diffuser spot measurement: (a) schematic showing the experimental setup, (b) optical intensity of a laser beam without any component, (c) optical intensity of a laser beam with microlens arrays, and (d) optical intensity of a laser beam with diffusers

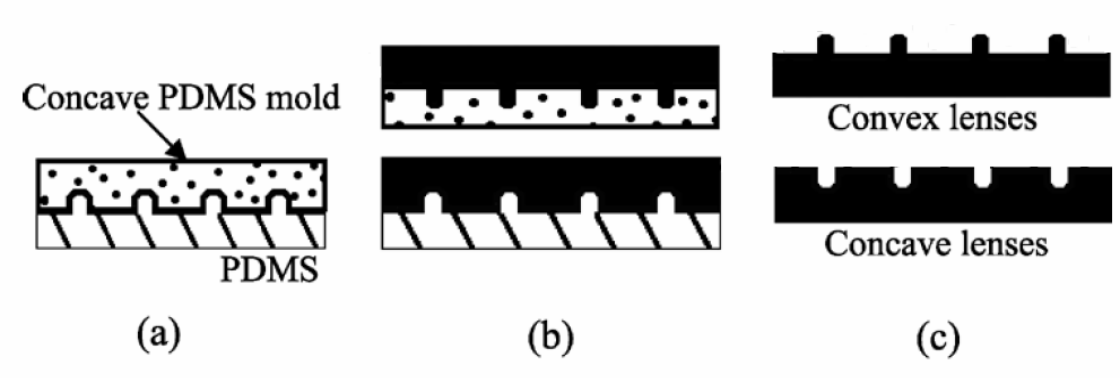

Fig.4.12 Schematic for fabrication of polymeric microlens by soft replica molding

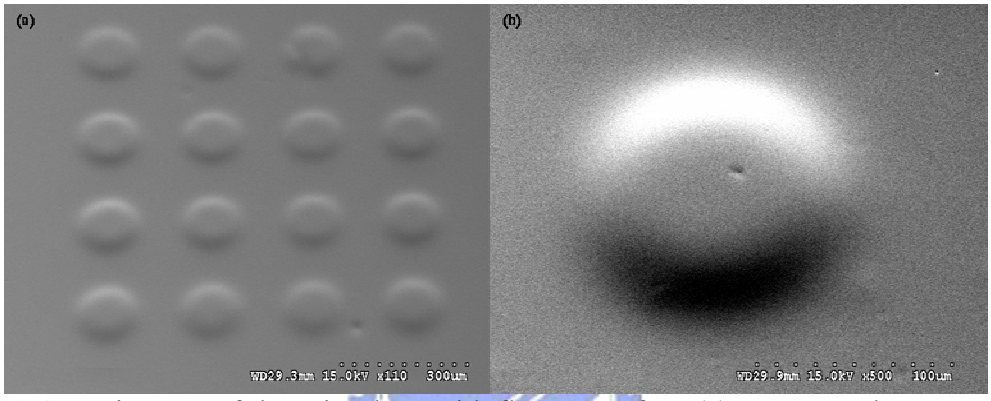

Fig.4.13 SEM images of the microlens with flat top surface (a) a patterned array and (b) a single pattern

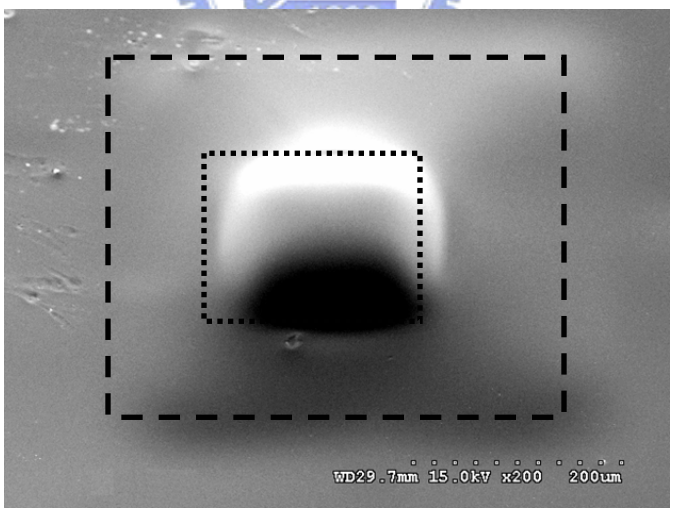

Fig.4.14 The SEM image for a bifocal structure of smaller lens stacked on bigger lens

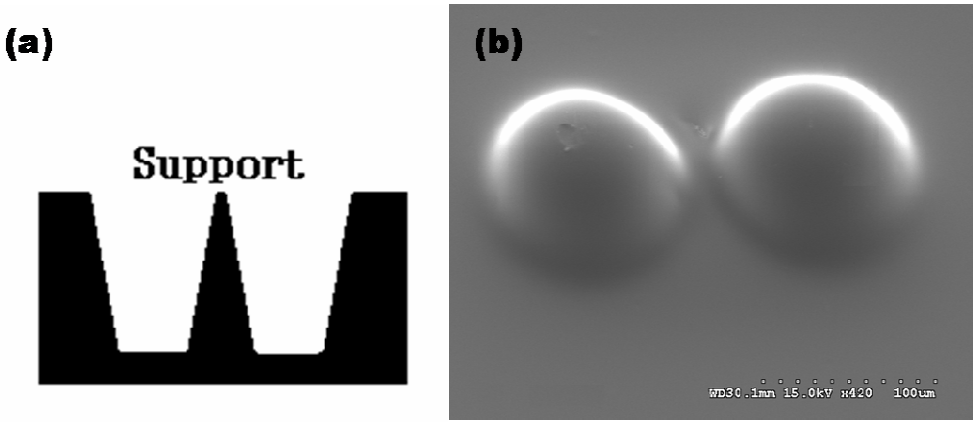

Fig.4.15 (a) Schematic diagram of the pedestal structure with the support formed through laser microdrilling (b) the SEM image for a double-peak structure

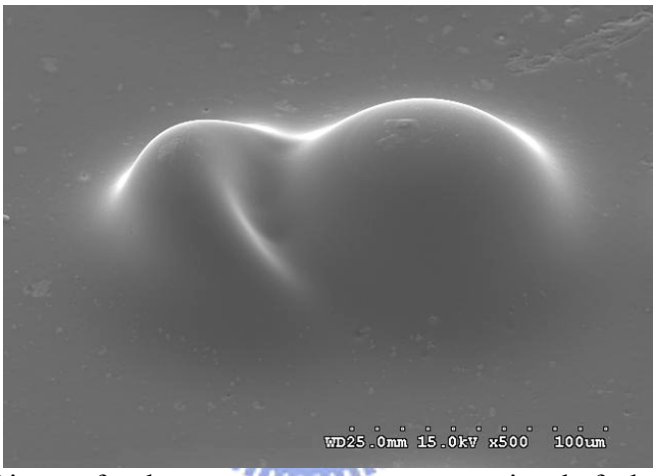

Fig.4.16 shows SEM image for the asymmetry structure consisted of a lens-like pattern and a meniscus pattern

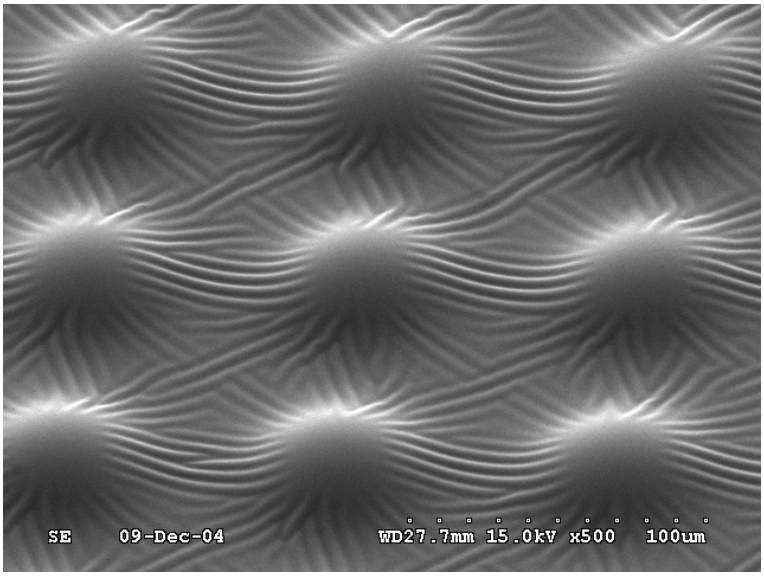

Fig4.17 The SEM image of wavy structures on the patterned surface of PDMS covered a metallic film with 100 nm thickness.

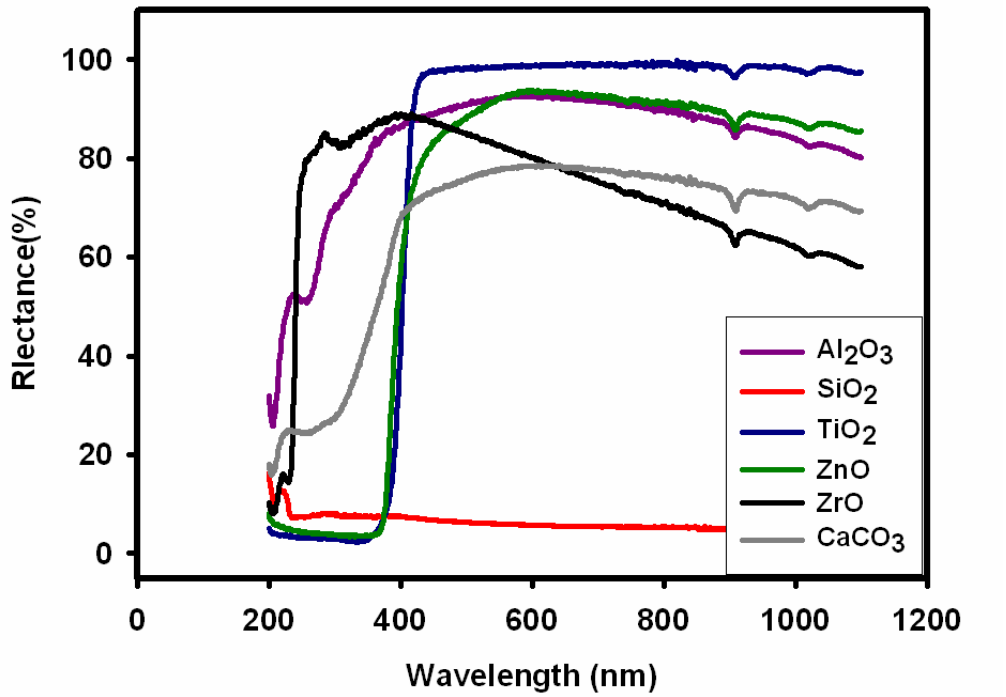

Fig 4.18 A reflectance curve of PDMS mixture polymers as a function of incident wavelength ranged between 200nm and 1100nm

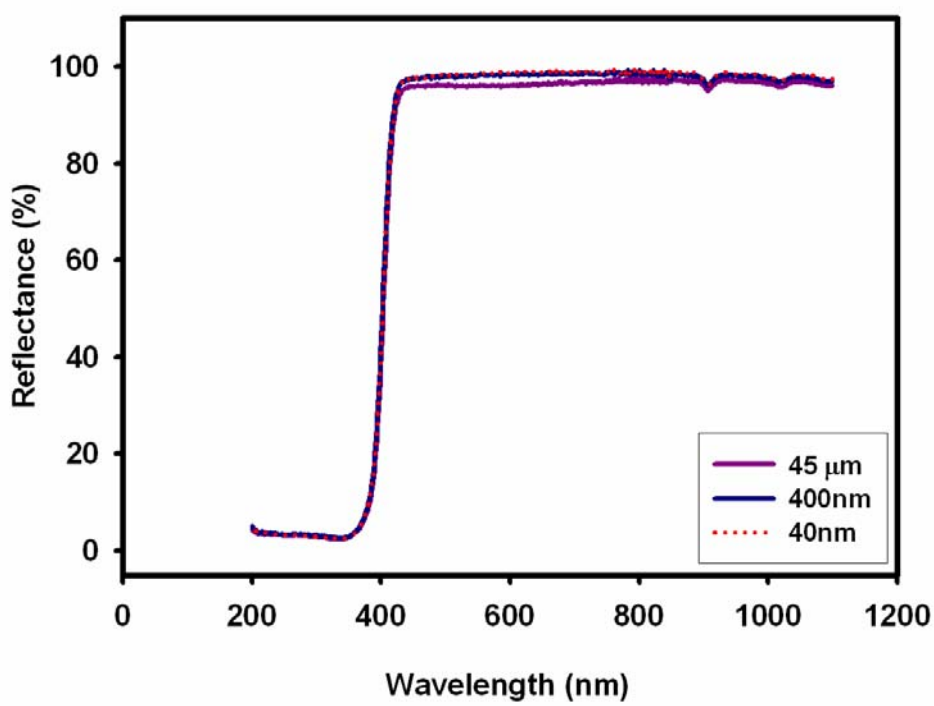

Fig4.19 A reflectance curve of TiO_2 with three sizes, r=40nm, 400nm, and 45μm, /PDMS mixtures as a function of incident wavelength ranged between 200nm to 1100nm

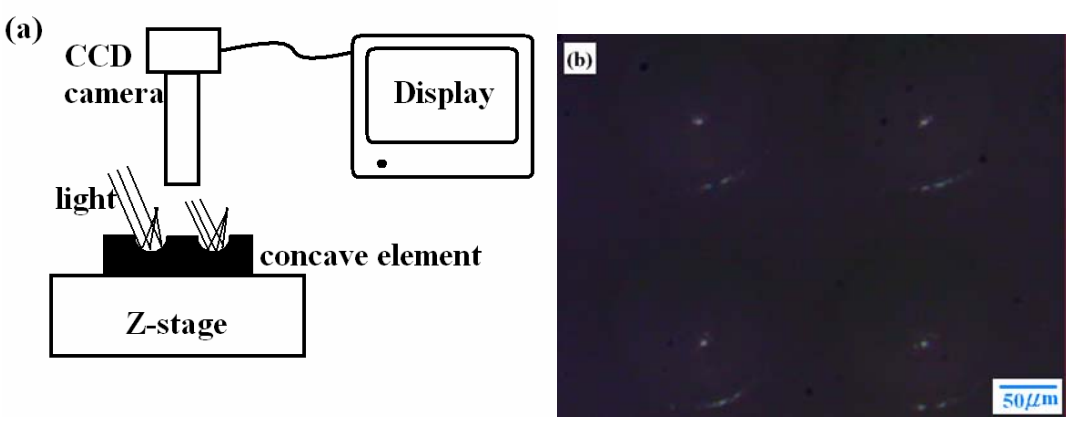

Fig.4.20 Focused spot measurement (a) Schematic showing the experimental setup (b) focused spot image

Table 4.1 Fabrication parameter for film thickness and microlens height

The thickness of a PMMA films (μm)	The height of a microlens		
	Φ=50μm	Φ=100μm	Φ=150μm
22	15.4	24.8	30.3
20	14.7	22.9	28.5
15	14.0	18.6	25.6
12	12.3	16.2	24.5

Table 4.2 The refractive index and color of various powders

Type of powderes	TiO_2	ZnO	ZrO	$CaCO_3$	Al_2O_3	SiO_2
Refractive index of powders	2.76	2.02	2.17	1.58	1.7	1.55
Color of powders	White	Light yellow	White	Off-white	White	Translucent

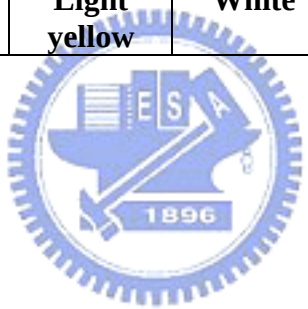

Chapter 5 Self-organization wrinkles on PDMS surface

A special phenomenon that wavy structures were spontaneously generated at this process of golden films covered on PDMS surface was observed in section 4.3. In this Chapter, we will have a detail discussion about this interesting phenomenon and apply it to fabricate optical gratings.

5.1 Introduction of wavy structures on PDMS surface

Virtually all work reported to date utilized a two-layer system comprising a thick foundation made of PDMS, a highly elastic material having the Young's modulus of ~1 M Pa, decorated with a thin rigid layer made of either metal or a silicon oxide. Bowden and coworkers reported several strategies of forming wrinkles/buckles on top of PDMS [72]. One of them [73] involved increasing the volume of the PDMS block by heating, exposing it to oxygen plasma for controlled periods of time, and finally cooling the sample down to room temperature. The plasma oxidation converted the topmost part of the PDMS into a silica-like layer. The wavelength and the amplitude of the wrinkles increased with increasing plasma treatment time. This behavior was caused by increasing the thickness and/or the Young's modulus of the silica-like layer. Bowden and coworkers also reported that the buckle wavelength (λ) was independent of the magnitude of the compressive stress, regulated by pre-heating the PDMS block to various temperatures. In the same paper, the researchers showed that while wrinkles were generally disordered in plane when formed on a flat PDMS sheet (shown in Fig. 5.1a), they oriented when generated on PDMS substrates comprising 3D posts. Specifically, at the posts in PDMS substrate, the stress perpendicular to the post was relieved by expansion, causing the wrinkles to orient in the direction perpendicular to the post (shown in Fig. 5.1b). In a subsequent paper, Chua and coworkers reported on the formation of complex surface structures with tailored sizes created by exposing PDMS substrates with holes (rather than protrusions) to oxygen plasma.[74] These morphologies were associated with the disruption of equibiaxial stresses during the plasma treatment of PDMS (shown in Fig. 5.2).

Several groups studied the formation of buckled structures on elastomeric foundations

by vapor deposition of thin metal films onto thick PDMS substrates. Bowden and coworkers prepared buckles by depositing thin layers of gold onto thick PDMS at elevated temperatures [72]. Subsequent cooling of the substrate developed compressive stresses in the specimens that were relieved via the formation of buckles having periodicity of 20–50 μ m. While wrinkles generated on flat PDMS sheets were organized randomly in plane (see Fig.5.3 a), they formed oriented morphologies extending over large areas (shown in Fig.5.3b and c) when deposited on PDMS substrates containing 3D protrusions.

Huck and coworkers extended the work of Bowden et al. by first stiffening selected areas on the substrate via crosslinking and subsequent metal deposition at elevated temperatures [75]. After cooling the sample, the surface exhibited a complex arrangement of buckled structures. Specifically, while the buckles were found to be aligned perpendicular to the boundaries between the strips on pre-crosslinked areas on the sample, they oriented parallel to the boundaries on the ‘‘bare’’ PDMS loci (shown in Fig.5.4).

Another very recent example of modulating wrinkling patterns in thin sheets has been presented by Ohzono and coworkers, who deposited thin films of platinum onto hexagonally organized arrays of holes in PDMS [76] and showed that the directional order of buckles was induced by the underlying substrate when the periodicity of the substrate pattern matched the intrinsic wavelength of the wrinkles (shown in Fig.5.5). Ozhono and coworkers also studied response of wrinkles to applied stress [77]. They first evaporated a thin film of platinum onto a thick PDMS slab, which resulted in a disordered array of wrinkles (shown in Fig. 5.6). By applying a small uniaxial stress to the samples, they showed that the wrinkles aligned perpendicularly to the direction of the stress; only 7% strain was needed to achieve almost perfect wrinkle alignment. Ozhono et al. determined that ordered domains of wrinkles grew via rearrangement of the stripe orientation of neighbors, merged with one another, and finally covered a large area on the surface. Upon releasing the stress, the wrinkles returned to their original disordered morphology, albeit with a small hysteresis (shown in Fig. 5.6). In a subsequent publication, Ohzono et al. were able to reproduce their earlier experimental observations using computer simulation models [78]. Their study confirmed that the strong memory of the initial wrinkling pattern was responsible for the recovery of the sample to the initial

morphology after the strain, which was used to align the wrinkles, was removed. In all the examples discussed thus far, the strain imposed on the PDMS foundation was relatively small, only a few percent.

In addition, the oxygen plasma treatment of PDMS typically leads to silicon-oxide-like layers, whose thicknesses are on the order of a few tens to several hundreds of nanometers [79]. Efimenko and coworkers recently reported on fabrication of wrinkles by uniaxially stretching PDMS network sheets (thickness ~0.5 mm) in a custom-designed stretching apparatus [80] and exposing them to ultraviolet/ozone (UVO) radiation for extended periods of time (30–60 min) [81]. Previous studies established that the UVO treatment of PDMS converts the first ~5 nm of the PDMS surface into a stiff skin, [82] whose density is approximately half that of silica. [83] Optical microscopy and scanning force microscopy (SFM) experiments confirmed that the surfaces were originally flat in the presence of strain. After the UVO treatment, the strain was removed from the specimen and the skin buckled perpendicularly to the direction of the strain. A detailed analysis of the buckled surface with SFM and profilometry uncovered the presence of hierarchical buckling patterns (shown in Fig. 5.7). Buckles with smaller wavelengths (and amplitude) rested parallel to and within larger buckles, forming a nested structure. Further release of the applied strain led to additional effective compression; the composite skin buckled on a much larger length scale. The formation of higher generation buckles continued until the strain was completely removed from the substrate hence creating a hierarchical buckled pattern, where each buckle generation was a scaled-up version of the primary buckle.

5.2 Study of leading factors in formation of wrinkles on a metal/rubber bilayer system

Here, the periodicity and orientation of wavy structures on a metal/rubber bilayer system are modified from two major effects: shape of pattern on the PDMS substrate; and, thickness of the surface metallic film. To understand the effect of the pattern shape on the wavy structure, convex patterns with both circular and square shapes and concave patterns with circle shapes were created on the PDMS substrate. Orientations of structures around a single pattern and among patterns in array were also presented and

discussed. With changing the thickness of the deposited metallic film, the compressive stress, induced by different volumetric contraction rates between the metallic film and the PDMS substrate, could be varied that resulted in formations of different wavy structures.

5.2.1 Effect of pattern shape

First, the surface with the 100 nm thick Au film covered on a flat PDMS substrate without any patterns was examined. Wavy structures were formed randomly on the surface that is shown in Fig.5.8 (a). Disordered structures were driven by the unbalanced compressive stresses that were induced by the large difference in volumetric contraction rates between the PDMS substrate and the Au film. Because there were no constraints on the PDMS surface, these unbalance compressive stresses led to disordered wavy surface structures. The surface topography of these disordered wavy structures was shown in Fig.5.8 (g) that was scanned by an atomic force microscopy (AFM). The height of the wavy structures (distance from the crest to the trough, the peak-to-peak distance) was roughly within 500 nm.

To study the effect of the pattern on the substrate fabricated by casting against the PC plate microdrilled by excimer laser through a desired mask, a single step-like, bumped pattern was first examined. The corresponding surface wavy structures for a square pattern and a circle pattern were shown in Fig. 5.8(b) and Fig. 5.8(c), respectively. It was shown, instead of growing randomly, the wavy surface structures became more orderly nearby the pattern. These ordered wavy structures stretched radically out from the boundaries of the pattern and were arranged in directions that were perpendicular to the sidewalls of the pattern. These ordered structures could, however, sustained only within a certain region close to the pattern boundary. Beyond that region, the randomly structures reappeared. The circular pattern shown in Fig. 5.8 (c) was with a diameter of 750 μm and height of 10 μm. The range of the region for the ordered wavy surface structures in Fig. 5.8(c) was relatively larger than that in Fig. 5.8 (b) where the square pattern was with side length of 450 μm and height of 10 μm. The heights for the wavy structures nearby circular pattern and square pattern were about 4 μm and 2 μm, respectively. The range of the region for the ordered structures depended, on the other hand, more strongly upon the size of the pattern. With the continuous increase of the pattern size, the constraint to the

growth of the random wavy structures was enhanced that resulted in increasing both the range of the ordered region and the height of the wavy structure.

The wavy structures on the PDMS substrate with patterns in array were also considered. An array with 5 by 5 square patterns, each having a length of 100 μm, height of 10 μm, and pitch of 100 μm, was studied. According to the general rules for generating the surface wavy structure discussed in the previous paragraph, orientations of the surface wavy structures were affected by the nearby bumped patterns. The resultant SEM image is shown in Fig. 5.8 (d). These wavy structures in the middle of patterns presented certain orders and two groups of structures were observed. The first group is for the structures between parallel sidewalls of any two adjacent patterns. Their orientations were perpendicular to the sidewalls and thus presented either in horizontal or vertical directions on the SEM image. The second group was for the structures in regions in the midst of any four closest patterns. Their orientations were roughly aligned in the diagonal direction on the image, from the up-left to the bottom-right. Based on these observations, a compound grating, combining the vertical patterned grating and transverse wavy structures, could be fabricated by forming strip patterns on the PDMS substrate. The resultant SEM image for the wavy surface structures between two rectangular strip patterns is shown in Fig. 5.8 (e). The width for each rectangular strip pattern was about 80 μm and the distance between the two strips was about 150 μm. The resulting periodicity of the wavy structures was about 4 μm. Finally, the structures on the top surface of a bumped pattern was also examined and shown in Fig. 5.8 (f). Instead of the wavy structure, a porous structure, with pore size around 2 μm, was formed on the top surface of the bump pattern. It was conjectured that the rough exterior was transformed from the PC plate where the unevenness was formed during the excimer laser micro-drilling process.

The PDMS substrate with patterns of lens-like bump was also discussed. Fig. 5.9(a) shows an array with 3 x 3 patterns. Each circular pattern was with a diameter of 50 μm and height of 15 μm. Like the results presented in Fig. 5.8, the orientations of the wavy structures among patterns were affected by the existence of the patterns and showed particular regularities. The wavy structures close to the pattern boundaries, however,

showed a different trend. In Fig. 5.8, they stopped at, or stretched out from, the pattern boundaries. In Fig. 5.9(a), they were, however, not bounded by the pattern boundaries and could extend to the surface of the patterns. This is because the boundary for the lens-like bumped pattern was relatively smooth and indistinct. The wavy structures could thus extend up onto the surfaces of the patterned regions. Fig. 5.9(b) shows the surface wavy structures around a single lens-like, circular bumped pattern that was with a diameter of 100 μm and a height of 20 μm. Because the slope of the bump in Fig. 5.9(b) was steeper and the height of pattern was higher than those in Fig. 5.9(a), the extent of the wavy structures on the bump surface was relatively smaller. Hence, besides the slope, the height of the pattern affected the extent of the wavy structure that can propagate from the substrate onto the pattern surface.

In addition to the convex patterns, the wavy structures on the PDMS substrate with concave patterns were also examined. Fig. 5.9(c) shows the distribution of wavy structures on the PDMS substrate with an array of 2 by 3 concave circular patterns, each having a diameter of 50 μm. These concave patterns were formed by replica molding from the convex patterns and the pattern boundaries were thus sharp and step-like. Fig. 5.9 (c) shows that the effect of concave pattern on the wavy structure was similar to the effect from the convex pattern.

5.2.2 Effect of thickness of metallic film

To understand the effect of the thickness of metallic film on the surface structures, the PDMS substrates deposited with different thicknesses of metallic films were examined. Our experiments showed that the thickness was below 30 nm, wavy structures were hardly to be observed. However, as the thickness was larger than 30 nm, wavy structures became gradually clearer. Hence, the thickness of the metallic film can affect the development of the wavy structures. Fig. 5.10 (a)–(d) show four surface images of the PDMS substrates that respectively covered by an Au film with film thickness of 50 nm, 100 nm, 150 nm, and 200 nm. There was a circular, step-like bumped pattern that was with the diameter of 100 μm and height of 10 μm on each substrate. The observed periodicities of the wavy structures for Fig. 5.10 (a)-(d) were given by 5.38, 6.25, 7.39, and 8.33 μm, respectively. These results demonstrated the

periodicity of the wavy structures increased with the increase of the film thickness. Experimental data further revealed that as the film thickness was increased by 50 nm, the periodicity of wavy structures was increased roughly by 1 μm. Hence, the periodicity of wavy structures could be adjusted, to some extent, by the film thickness. The AFM images showing the surface topographies for Fig. 5.10(a)-(d) are presented correspondingly in Fig. 5.11 (a)-(d). The heights of wavy structures were within the ranges of 150 to 200 nm, 450 to 500 nm, 550 to 600 nm, and 950 to 1100 nm for the Au films with thicknesses of 50 nm, 100 nm, 150 nm, and 200 nm, respectively. In addition to those on the PDMS substrate, structures on the top surface of the bumped pattern were also examined. As the film thickness was increased from 50 nm to 200 nm, the surface structures went from a porous structure, 5.10 (a), to a random wavy structure, 5.10 (d). Thus, the wavy structures are more likely to form on a flat surface without geometrical constraints or on a surface deposited with a relatively thick metallic film.

5.3 Fabrication of optical gratings by shrinkage of a rubber material

Following the above experiment, we can understand that compressive stress is a key role for wavy structures formation. In this section, we will introduce an external compressive force with a uniaxial direction to align wavy structures on PDMS substrate. The ordered wavy structures will be acted as optical gratings in the future.

5.3.1 The approaches of optical gratings fabrication

Steps for fabricating diffraction gratings on the surface of PDMS substrate are described as follows.

(a) The liquid silicone pre-polymer, Sylgard 184 from Dow Corning, was mixed in a weight ratio of 10:1 with the curing agent. After mixing, the pre-polymer was poured into a respective mold and cured for 1 hour at a temperature of 70℃. The solidified PDMS plate with 1 mm thick could be easily fabricated. Then, the PDMS plate was stretched by an external, uniaxial tension load and it was extended in the specified direction prescribed by the tension load. The resulting PDMS substrate is shown in Fig. 5.12(a).

(b) A thin gold film with a reasonable thickness was then deposited on the surface of the

pre-stretched PDMS substrate in a sputter. The schematic is shown in Fig. 5.12(b).

(c) After the thin metal film was deposited, the pre-stretching load on the substrate was released. The elasticity in the PDMS intended to draw the pre-stretched substrate back to its original dimension that resulted in the formation of the wavy structures on the PDMS surface. The schematic is shown in Fig. 5.12 (c).

(d) In order to promote the optical transmittance of the substrate, the surface Au film should be removed. It could be done by dipping the PDMS substrate with the surface Au film, obtained in Step (c), into a chemical solution with the mixture of hydrochloric acid and nitric acid at a volume ratio of 3 to 1 for 30 seconds. The resulting single-layer gratings are shown in Fig. 5.12 (d).

(e) Repeating Step (a), (b) and (c), the second wavy structures could be formed on the other side of the PDMS substrate. After removing the Au films on both sides of the substrate using the same recipe depicted at Step (d), the resulting substrate with double-layer wavy structures, shown in Fig. 5.12 (e), was obtained.

5.3.2 The control of periodicity on optical gratings

In order to guide the generated wavy structures to arrange regularly, a preloaded tension stress with designated direction and magnitude was considered to be introduced into the PDMS substrate before the Au film was deposited. One of the most straightforwardly employable preload was the uniaxial tension. In fabrication Step (b), we observed that there were no wavy structures formed until the preload was released. This was because the magnitude of the compressive stress due to the substrate contraction was smaller than the stretched tension stress introduced by the preload and the substrate was unable to shrink to form any surface wavy structure. Once the preload was released, the elasticity in the rubber PDMS tended to draw the stretched substrate back to its original dimension and led to a uniaxial compression of the substrate. Due to its smaller thermal-expansion coefficient, the surface Au film, however, was not able to contract to the same degree as the substrate did and could only form the wavy structures in order to release the compressive stress from the beneath. These wavy structures were ordered and their orientations were perpendicular to the prestretched direction along which the substrate was contracted. Fig. 5.13 shows the SEM image of the formed surface

structures after the uniaxial preload tension was released. Each wavy structure there was placed side by side and arranged nearly in parallel. This result demonstrated that a highly ordered surface wavy structure could be achieved by the present method.

An optical grating can be composed of parallel slits with a reasonable distance. As an incident light propagates through a grating, diffraction patterns can be formed. Parameters such as the slit separation (d), the order number of the diffraction pattern *(m)*, the observation angle corresponding to the m^{th} order number of the diffraction pattern (θ_m), and the wavelength of incident light (λ) are usually employed to characterize the diffraction gratings and they are related through the grating equation given by $d \sin\theta_m = m\lambda$ [84]. Therefore, the resolving power of the grating increases with the increase of the order number and the number of illuminated slits [84]. Hence, the parameter, the pitch of the wavy structures, is very important for determining the resolving power. In order to adjust the pitch, two controllable experimental parameters, the magnitude of the pre-stretched strain and the thickness of the Au film, were illustrated in this study. The effect of the stretched strain on the pitch of the structure was first examined and the influence from the thickness of the Au film was then investigated.

A PDMS substrate covered with an Au film with thickness fixed at 100 nm and under a stretched strain ranging from 5% to 30% was investigate. The corresponding pitch of the ordered structure as a function of stretched strain was presented in Fig. 5.14(a). It indicted that an enhancement of the stretched strain would result in a reduction in the pitch. Generally speaking, an increase of the stretched strain led to an increase of the recovering uniaxial compressive stress as the preload was released. That would generate more surface wrinkles, corresponding to smaller pitch, and vice versa. After measuring by an atomic force microscope (AFM), the cross-section image of the ordered wavy structures with stains of 5% and 30% were respectively presented in Fig. 5.14 (b)- (1) and (2). Both cross-section profiles were close to the sinusoidal function. As the stretched strain was increased form 5% to 30%, the depth of wavy structures was changed form 195 nm to 262 nm.

The influence of the thickness of the surface Au film on the pitch was investigated based on a PDMS substrate with the stretched strain fixed at 30% but varying the film thickness from 50 nm to 200 nm. The corresponding pitches of the wavy structures as a

function of the film thickness were presented in Fig. 5.15(a). Experiment results demonstrated an increase of the film thickness would result in an increment of the pitch. The increase of the film thickness gave rise to the enhancement of the mechanical strength of the Au film to defend against the substrate contraction. Consequently, the thicker the metal film the larger the periodicity was formed, and vice versa. The AFM cross-section images for the ordered wavy structures covered with an Au film with thicknesses of 50 nm and 200 nm were presented in Fig. 5.15(b)- (1) and (2), respectively. As the thickness of the Au film was increased form 50 to 200 nm, the change in the depth of wavy structure was not obvious.

5.3.3 Optical performance of optical gratings

To investigate the optical performance of these wavy structures, an experimental apparatus consisting of a laser diode as the light source, a PDMS plate with the generated wavy structures as the test grating, a screen and CCD camera as the imagine display and recording system was set up. As the laser beam passed through the grating, the generated diffraction patterns were projected on the screen, then they were captured and recorded by the CCD camera.

By this apparatus, two gratings with different periodicities in the wavy structures were examined. Grating 1 was the PDMS plate with the stretched strain of 5% and the thickness of the Au film of 100 nm. For Grating 2, the stretched strain and the thickness of the Au film were 30% and 50 nm, respectively. The diffractive patterns based on Grating 1 and Grating 2 are shown in Fig.5.16 (a) and (b), respectively. These results showed that only the diffraction patterns to the second-order, $m = 2$, could be produced when Grating 1 was examined and the patterns up to the fourth-order, $m = 4$, were still observable if Grating 2 was the test sample. These results clearly demonstrated that gratings with different resolving power could be fabricated by adjusting the stretched strain and the thickness of the deposited Au film.

Because the orientation and periodicity of the wavy structures could be controlled by the direction and the strength of the preloaded strain, following the fabrication steps introduced in Section 2, two gratings with different orientations and periodicities could be fabricated respectively on both sides of a PDMS plate, a double-sided grating plate.

Fig. 5.16 (c) shows the SEM image for part of the diffractive patterns from a double-sided grating plate where the orientations of the two-sided gratings were perpendicular to each other. Compared with the diffractive patterns from the single-sided grating, the patterns here were arranged in a two-dimensional array that was the pattern type a traditional two-dimensional grating generated.

5.4 A novel way to generate wrinkles using a chemical oxidization method

Although the periodicity and orientation of waves can be effectively controlled by the above-mentioned technologies such as the surface of PDMS covered a thin metallic films and exposed to oxygen plasma or ultraviolet/ozone (UVO) radiation, low-cost methods for generating well-controlled and high-quality surface wavy structures are still very much expectable.

For the molecular structure of a PDMS polymer, it consisted of ($-SiO(CH_3)_2$) repeated units is a helical structure, where the inner part of the helices is composed of siloxane units and out part is composed of methyl groups [85]. Some literatures regarding the surface modification of carbon nanotubes have been reported that a strong acid solution was often used to attack or modify carbon atoms and then -OH and -OOH groups could be grafted onto carbon atoms [86-89]. Hence, we tried a chemical approach to modify the surface state of PDMS and to oxidize the carbon atoms in PDMS chains by dipping into a strong acid solution during few seconds to several minutes.

5.4.1 The experimental steps for chemical oxidization method

The liquid PDMS polymer that mixed PDMS silicone elastomer (Sylgard 184) and curing agent with the weight ratio of 10:1 was prepared. PDMS films with 100 μm thickness were deposited onto clean glass plates through a spin-coating process or coated with glass tubes by dipping into the PDMS liquids. In addition, PDMS films with step-like patterns were also prepared by casting against a PC-based mold fabricated by the micro-drill technology of excimer laser. These PDMS films were subsequently cured in an oven at 70 ℃ for 20 min. Simultaneously, a strong acid that mixed sulfuric acid solutions (H_2SO_4, content 95%) and nitric acid solutions (HNO_3, content 66-71%) with the volume ratio of 3:1 was prepared. Then, solidified PDMS films were immersed into

H_2SO_4/ HNO_3 solutions during few seconds to several minutes. Finally, the acid-modified PDMS films was dipped into clean water to remove the residual acid liquids and then dried by an air gun or an oven. Wrinkles could be found on the surface of PDMS.

5.4.2 The surface character of the modification PDMS

PDMS silicone polymers have a strongly chemical stability to resist various acid solutions, such as hydrochloric acid (HCl), sulfuric acid (H_2SO_4), and nitric acid (HNO_3). Surprisingly, H_2SO_4/ HNO_3 solutions seem to can react with PDMS polymers. After dipping H_2SO_4/ HNO_3 solutions during few seconds, PDMS polymers started to change from transparent to white. An unknown white material which generated on the surface of PDMS polymers was supposed to be the product of chemical reaction after dipping in HNO_3/H_2SO_4 solutions. In order to verify what the white material was, FTIR, which is a useful instrument for the investigation of changes in the chemical structure of polymers, was utilized to analyze the difference between the pristine and the modified PDMS. Fig. 5.17 (a) and (b) shows respectively the FTIR spectra of the pristine and modified PDMS and every characteristic peak is assigned corresponding groups on it. We found that absorption peaks of C-H groups changed obviously from a shape peak to a broad band and other absorption bands of C=C, C-O, C=O groups strengthened strongly after chemical modification. It suggested that hydrogen atoms in methyl groups were abstracted from the polymer chains to generate radical within the polymer chains located at the surface. Some of carbon radicals in the polymer chain combined with oxygenic radicals formed in the acid-modified process.

The other evidence for the modification of the methyl groups was the change of contact angle. The pristine PDMS surface has a low surface energy to cause the hydrophobic nature, which is due to methyl groups located on the out part of a PDMS chain (water drop contact angle is 110°). As a contact angle changed from 110° to 75°, we believed that parts of methyl groups in PDMS chains should be fractured after chemical modification. The contact angle image for a pristine and modified PDMS surface is respectively shown in Fig.5.18 (a) and (b). In addition, the IR spectra of treated PDMS polymers exhibited an OH absorption broad band from 3250 to 3900 cm^{-1} and a

characteristic peak corresponding to OH groups of silanol moeties was also found at around 3750cm^{-1}[90].

Besides, the element quantification of an oxidized PDMS was determined by x-ray photoelectron spectroscopy (XPS). The composition of the surface was $Si_1O_{1.493}C_{1.58}$ before oxidation and was $Si_1O_{1.763}C_{1.6}$ after oxidation. The oxygen content in PDMS polymer only increased but carbon content was almost invariable. It implied that carbon atoms in PDMS chain were merely grafted other oxygenic groups. However, the composition of the oxidized surface in chemical treatment was obviously different from that in oxygen plasma treatment. After oxygen plasma treatment, oxygen content in PDMS polymer increased but carbon content decreased, resulting in the formation of silica-like structures on the surface of PDMS [73].

On the other hand, a diluted H_2SO_4/ HNO_3 solution (H_2SO_4/ HNO_3 mixtures with three volumes of water) was also examined through the following experimental steps. Under the same experiment condition, we found no any change in the appearance of PDMS. It indicated that the acid concentration was an important factor for the generation of an oxidized PDMS.

5.4.3 The surface topography of the modification PDMS

A stiff film (oxidized PDMS polymers) was capped on the soft foundation (pristine PDMS polymers) that was confirmed in the study. Such bilayer systems such as Al/PS films [91], Au/PDMS films [72] and SiO_x/PDMS films [73] have been demonstrated the formation mechanism of wrinkles by several research groups. The young's modulus of a stiff layer mismatched greatly with that of an underlayer elastical materials. The mismatched young's modulus would lead to the generation of compress stress. In order to release the compress stress, the surface would form wrinkles and remain eventually the incompressible status. Because one of formation methods for wrinkles is a thin metallic film covered with an elastomer, we used only optical microscopy (OM) to observe the modified surface of PDMS in order to avoid the influence of a metal/elastomer system. Fig.5.19 (a) shows that OM image of disordered wrinkles formed by dipping into H_2SO_4/ HNO_3 solutions during five seconds. Fig. 5.19 (b) shows that the dipped time as a function of the periodicity of wavy structures. The periodicity ranged from 11 to 165 μm

during one second to three minutes was increased very rapidly with increasing the dipped time. Wrinkles generated in a wet process were discontinuous and bug-like in initial stages, but were continuous in later stages, which is because growing wrinkles would merge smaller ones. However, wrinkles generated in metal/elastomer systems were continuous in initial stages and these wrinkles grow hardly into several ten micrometers. For wrinkles on bilayer systems, the periodicity (λ) of the buckles can be expressed as Eq.,

$$\lambda = 4.36t\left(\frac{E_s(1-v_p{}^2)}{E_p(1-v_s{}^2)}\right)^{1/3}$$

where t, E_s, v_s E_p and v_p are the thickness of stiff layer, the elastic modulus and Poisson's of the stiff layer and the soft foundation layer and the thickness[72]. Because we had only a very limited knowledge about the oxidized PDMS layer, we could not judge whether this Eq. described wrinkles on the surface exactly. However, this equation could explain the reason for the increase of wavelength with the increase of dipping time. In this Eq., the wavelength of wrinkles depended mainly on the thickness of the capped layer. In other words, the thickness of oxidized PDMS layer grew rapidly with the increase of dipping time.

5.4.4 The control for the arrangement of wavy structures

Some reports have been verified that the arrangement of waves formed on the bilayers system could be effectively controlled. There are mainly three approaches to align waves: (1) the arrangement of waves was always perpendicular to the surface of bas-relief patterns; (2) waves were ordered on a cylindrical surface; (3) waves are ordered after releasing a prestretched substrate. In this study, we tried these approaches to arrange wrinkles on the modified PDMS surface.

To study the effect of the pattern on the orientation of the wrinkles, a single circular step-like pattern was first examined. The circular pattern shown in Fig. 5.20(a) was with a diameter of 750 μm and height of 10 μm and disordered wrinkles were respectively found on the top and bottom of the step-like pattern on PDMS plates. Then, wrinkles on the PDMS plate with patterns in array were also considered. An array with two-by-two

square patterns, each pattern having a side length of 100 μm, height of 10 μm, and pitch of 100 μm, was studied. Disordered wrinkles were still found in this array. These wrinkles would not be regularly arranged along the sides of step-like patterns regardless of the change of the size and shape of step-like patterns. The resultant image is shown in Fig. 5.20(b). Therefore, as the scale of wrinkles grew with dipped time was bigger than that of step patterns, the patterns would be devoured by wrinkles.

Then, to study the effect of the curved surface on the orientation of the wrinkles, curved surface with different curvatures were respectively examined. Wrinkles which were still found on different curved surfaces arranged randomly with the change of curvatures. The resultant image is shown in Fig. 5.20(c). Although disordered wrinkles was formed on curved faces, the ring-like wrinkles, which were different form the bug-like wrinkles on non-curved surfaces, were first found on it.

Finally, the effect of uniaxial forces applied to stretch a PDMS substrate before oxidization was studied. No wrinkles were found before releasing the oxidized substrate. But, ordered wrinkles, shown in Fig. 5.20(d), were found after releasing the oxidized substrate. Each of wrinkles faced almost a single direction which was perpendicular to the stretched direction of a PDMS plate. The magnitude of the compressive stress on the oxidized PDMS/PDMS due to the substrate contraction was smaller than the stretched tension stress introduced by the preload, leading to be able to arrange regularly wrinkles on the surface.

Experiment results revealed that wrinkles formed by a wet process were merely ordered through the guidance of external forces. These results were corresponding incompletely with previous literature regarding the arrangement of wrinkles formed through metal deposition or plasma treatments. We considered that metallic particles or plasma radicals merely deposited or implanted the surface of PDMS vertically by physical processes, which are unable to modify the sidewalls of steps on PDMS substrate. The generated compress stress, due to the surface contraction, in the sidewalls of steps was zero but was rapidly increased beyond the edge of steps. The gradient of stress would force to arrange regularly wrinkles. But, the orientation of wrinkles formed by a wet process were easily random because the foundation shrank homogeneously, included the surface of PDMS and the sidewalls of steps. Each part of PDMS surfaces in wet

processes was uniformly oxidized regardless of the sidewall of pattered steps or curved surfaces, leading PDMS surfaces were simultaneously contracted without the generation of the gradient of stress. Hence, a wet process to modify PDMS surfaces can be regarded as an isotropy modification.

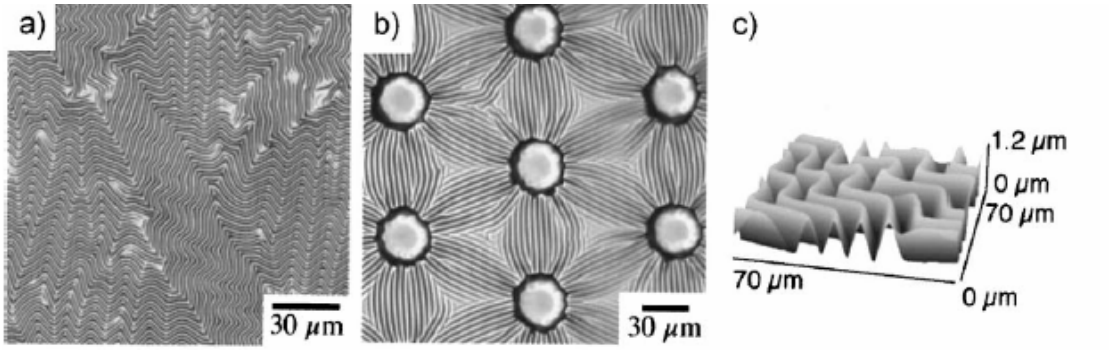

Fig.5.1 Optical micrographs of buckled surfaces prepared by plasma oxidation of heated poly(dimethylsiloxane) (PDMS) sheet comprising (a)homogeneous PDMS layer and (b) PDMS substrate with posts (height: 5 mm high, diameter: 30 mm) separated by 70 mm. The buckles were formed upon cooling the sample to room temperature. (c) Scanning force microscopy image of disordered buckling waves. [72]

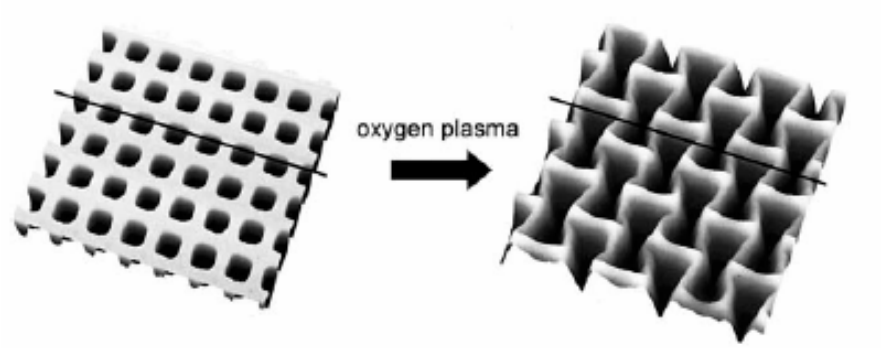

Fig.5.2 Scanning force microscopy images (20 6 20 mm2) of a poly(dimethylsiloxane) substrate with relief patterns prior to and after oxygen plasma modification. [73]

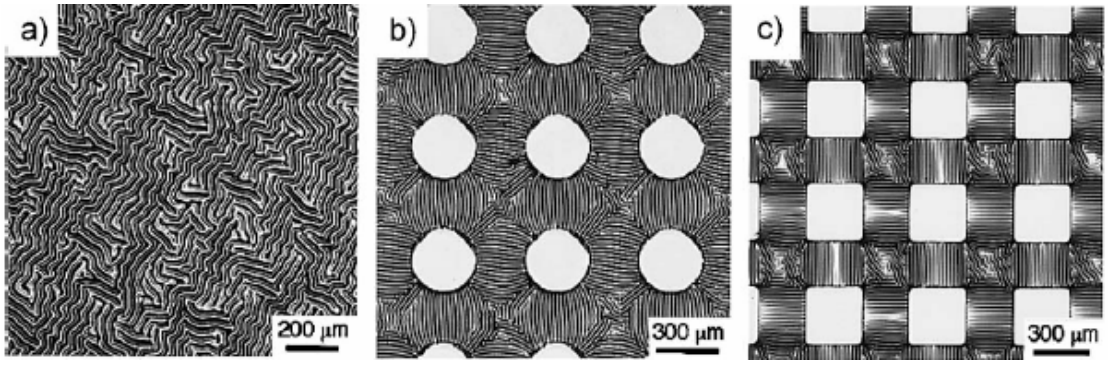

Fig.5.3 Optical micrographs of patterns formed when a thin layer of gold was deposited onto warm PDMS and the sample was cooled to room temperature. (a) Disordered patterns, (b) circles (radius: 150 μm), and (c) flat squares (side: 300 μm) elevated by 10–20 μm relative to the surface showed ordered patterns of waves on the recessed regions and no buckling on the plateaus. [74]

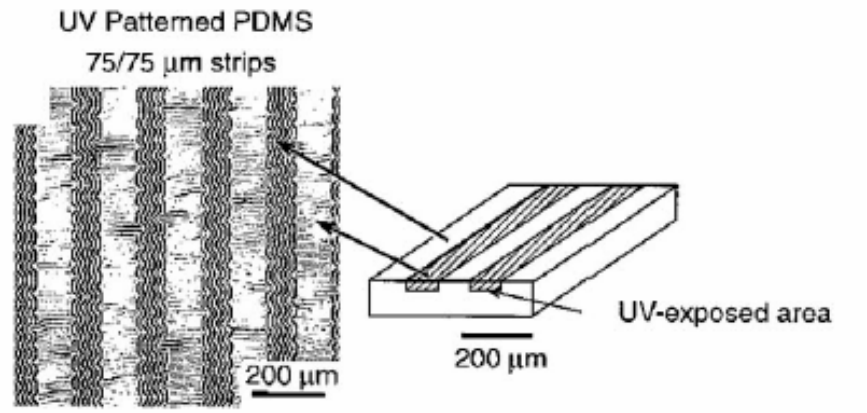

Fig.5.4 Alignment of buckles in thin films on PDMS patterned onto regions differing in Young's modulus and coefficient of thermal expansion. [75]

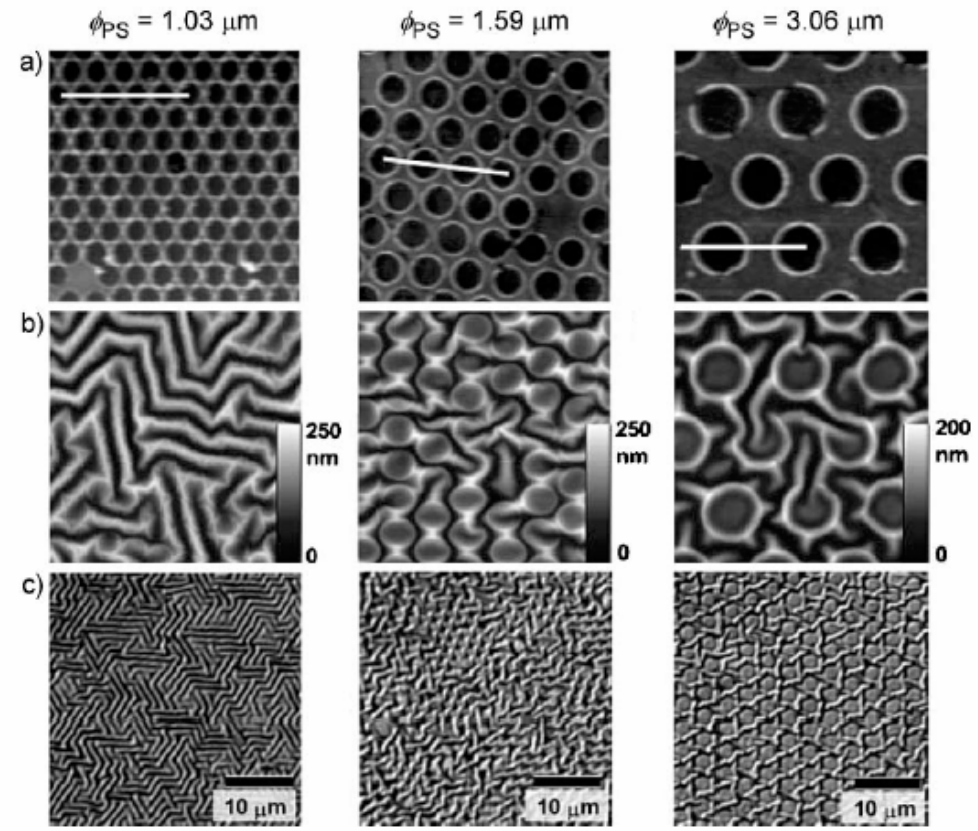

Fig.5.5 (a) Scanning force microscopy (SFM) images of the lithographic pattern produced by oxygen plasma treatment of PDMS after removing polystyrene (PS) latex microspheres. (a) SFM images and (c) optical microscopy images of wrinkle patterns coupled to lithographically patterned substrates. The left, middle, and right columns indicate the results for PS spheres having diameters (w) of 1.03, 1.59 and 3.06 μm, respectively. [76]

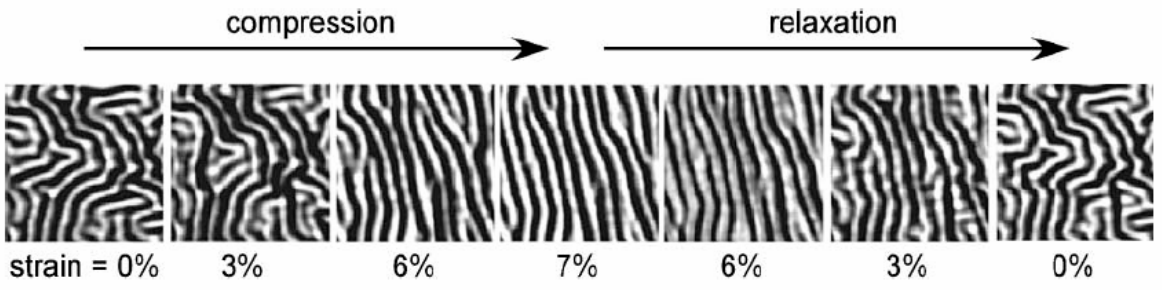

Fig.5.6 Scanning force microscopy images of wrinkled samples prepared by evaporating a thin layer of platinum onto a thick PDMS substrate. The images illustrate the rearrangement of the original disordered wrinkling pattern upon imposing a small uniaxial stress (the corresponding strains are indicated below each image) and a subsequent return to the original pattern upon stress removal. [78]

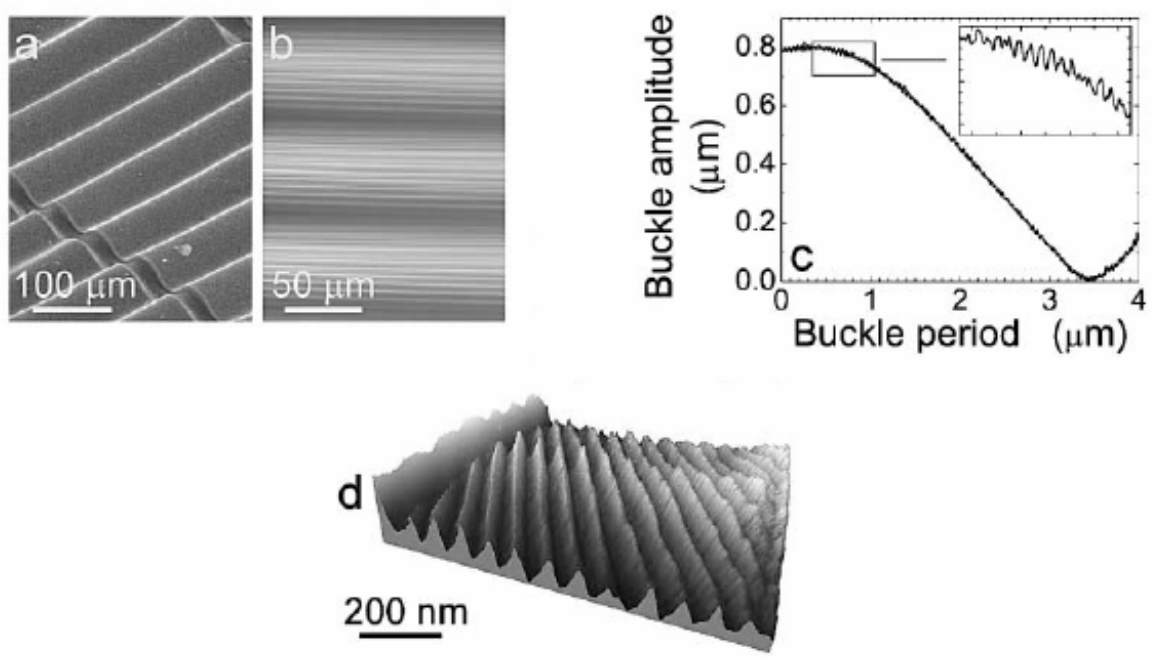

Fig.5.7 Characterization of the nested hierarchy of buckles (a) Scanning electron microscopy image of a buckle on PDMS substrate (b) Optical microscopy image in the transmission mode of generations of buckles (c) Topography profile collected with profilometry on generations of buckles. (d) Scanning force microscopy image revealing the structure of buckles. [81]

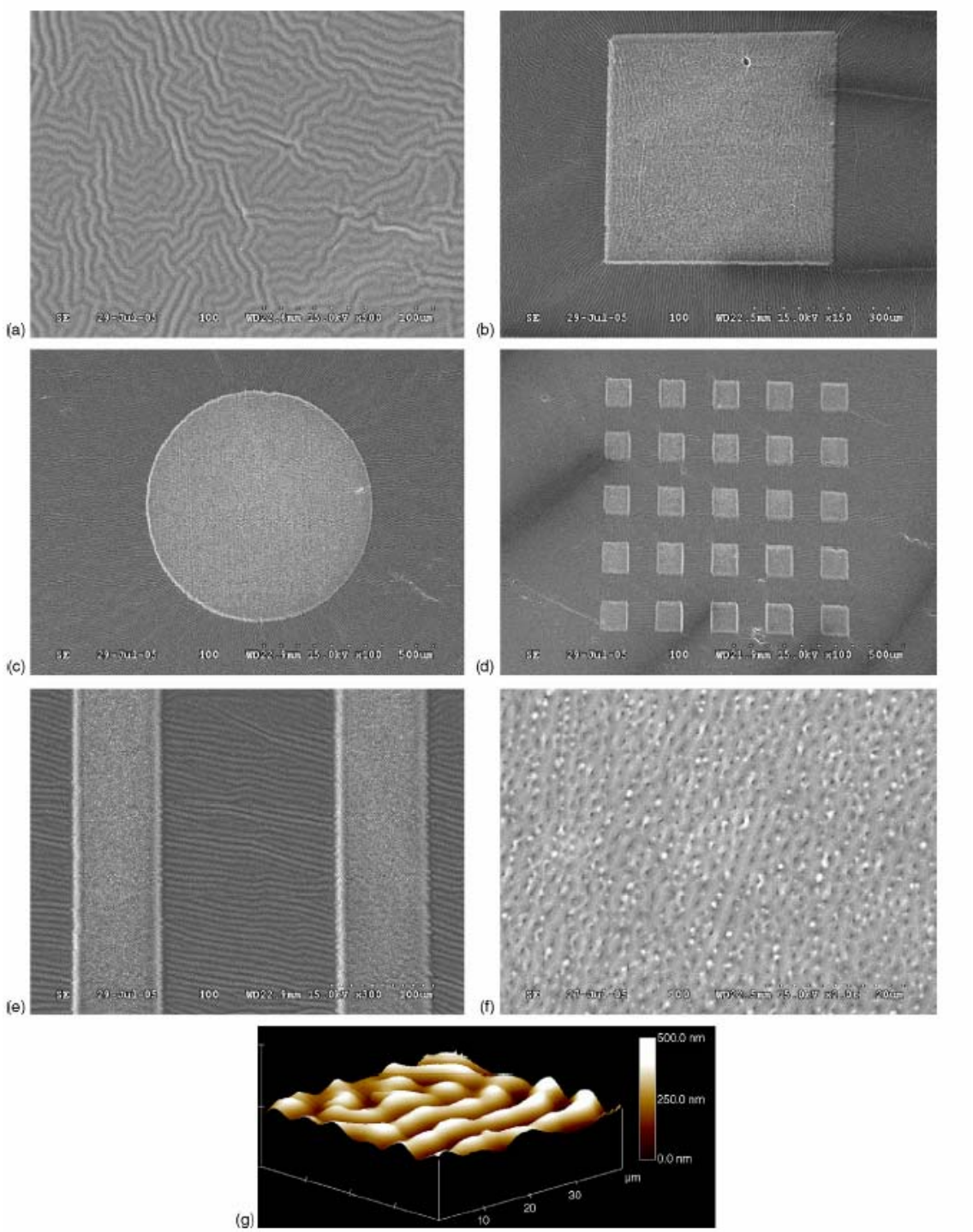

Fig.5.8. (a–f) Showing the SEM images for the surface structures of the PDMS substrates covered with a thin gold film at different surface configurations: (a) on a flat substrate; (b) on a substrate with a square, step-like bumped pattern; (c) on a substrate with a circular, step-like bumped pattern; (d) on a substrate with 5 by 5 square, step-like bumped patterns; (e) a compound structures combing longitudinal slender patterns and transverse wavy structures; and (f) porous structures on the top surface of patterns; (g) the AFM image showing the surface topography for (a).

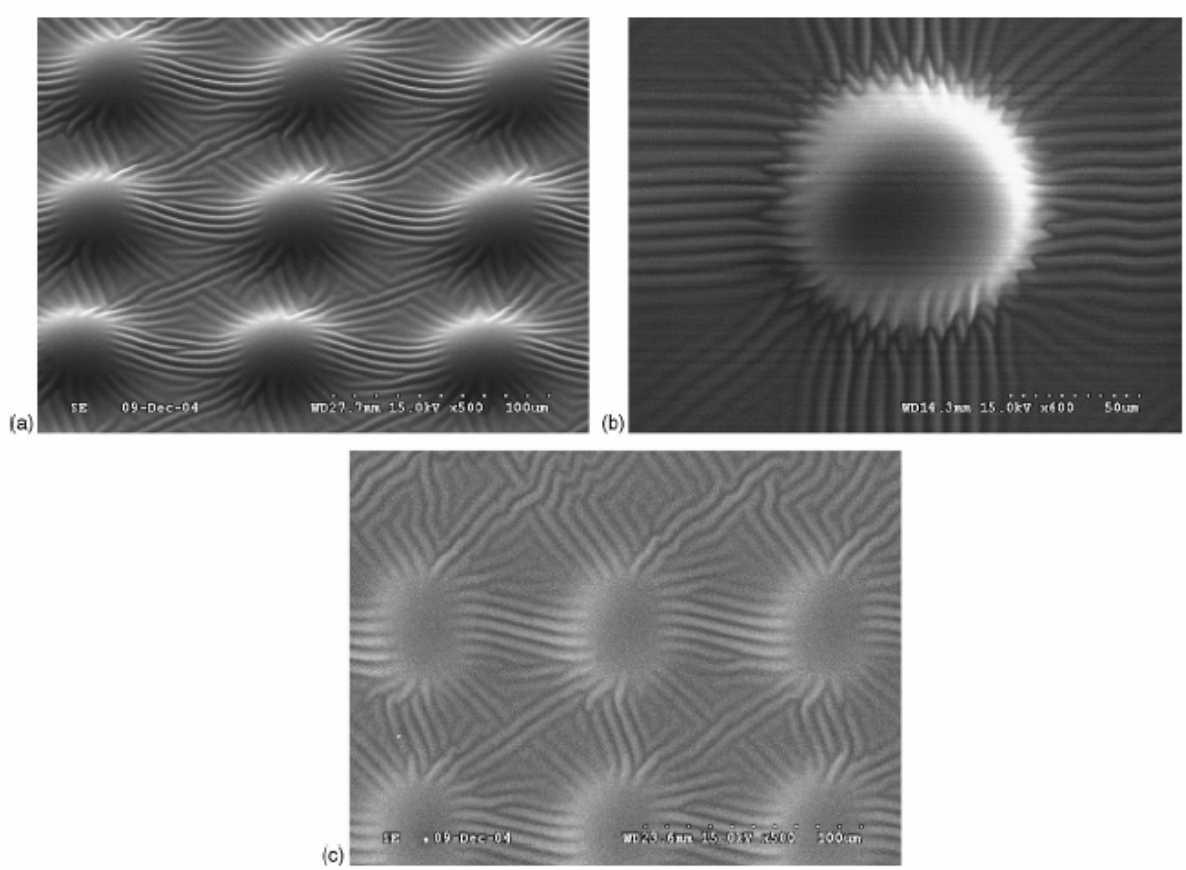

Fig.5.9 SEM images showing the surface structures of the PDMS substrates covered with a thin gold film and having different surface patterns: (a) an array of 3 by 3 lens-like bumped patterns; (b) a single lens-like bumped patterns; and (c) an array of 3 by 2 circular, concaved patterns.

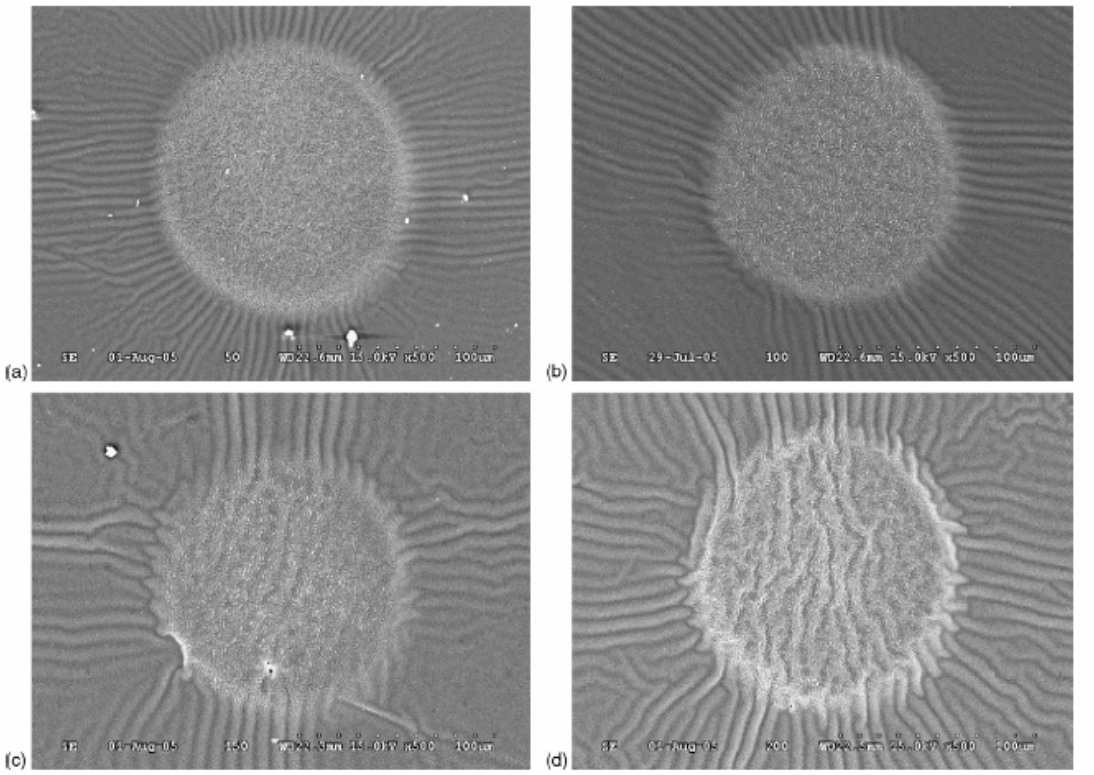

Fig.5.10 SEM images showing the surface structures of the PDMS substrates with a circular, step-like bumped pattern covered with a gold thin film with different thicknesses. (a) 50 nm; (b) 100 nm; (c) 150 nm; and (d) 200 nm.

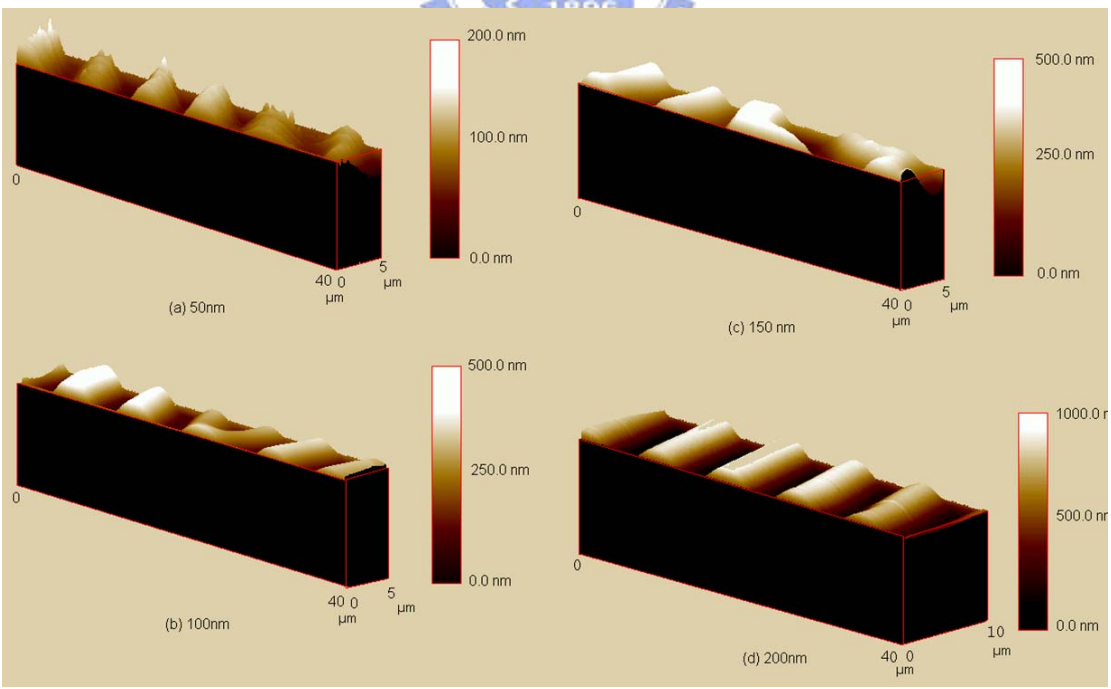

Fig.5.11 AFM images showing heights of the surface structures. (a), (b), (c), and (d) correspond to figures (a), (b), (c), and (d) in Fig. 5.10, respectively.

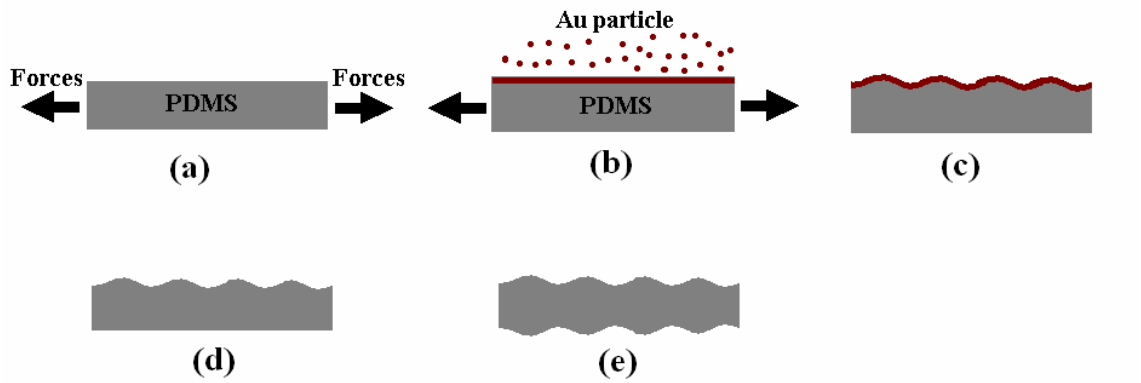

Fig.5.12 Schematic diagrams showing the fabrication process of optical gratings on a PDMS substrate.

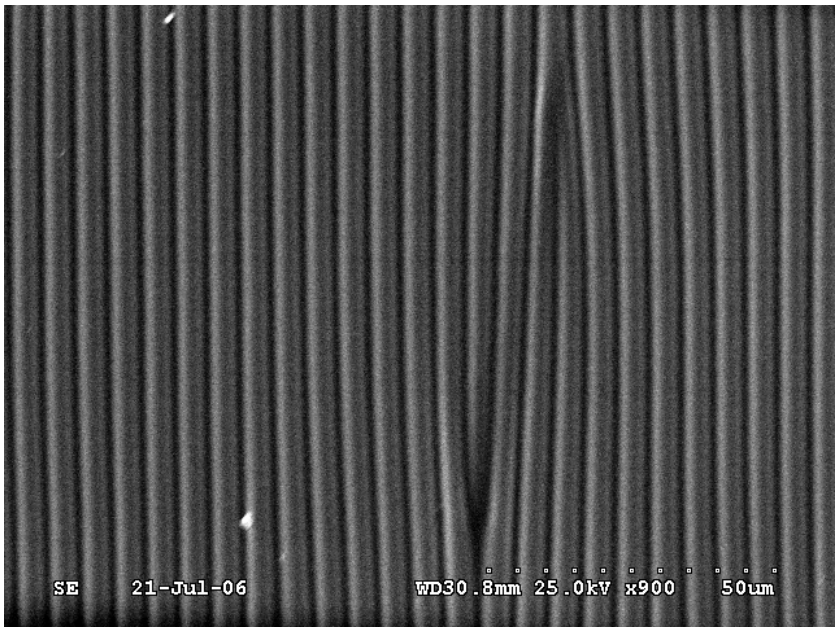

Fig.5.13 SEM surface images showing the ordered structures from a pre-stretched substrate

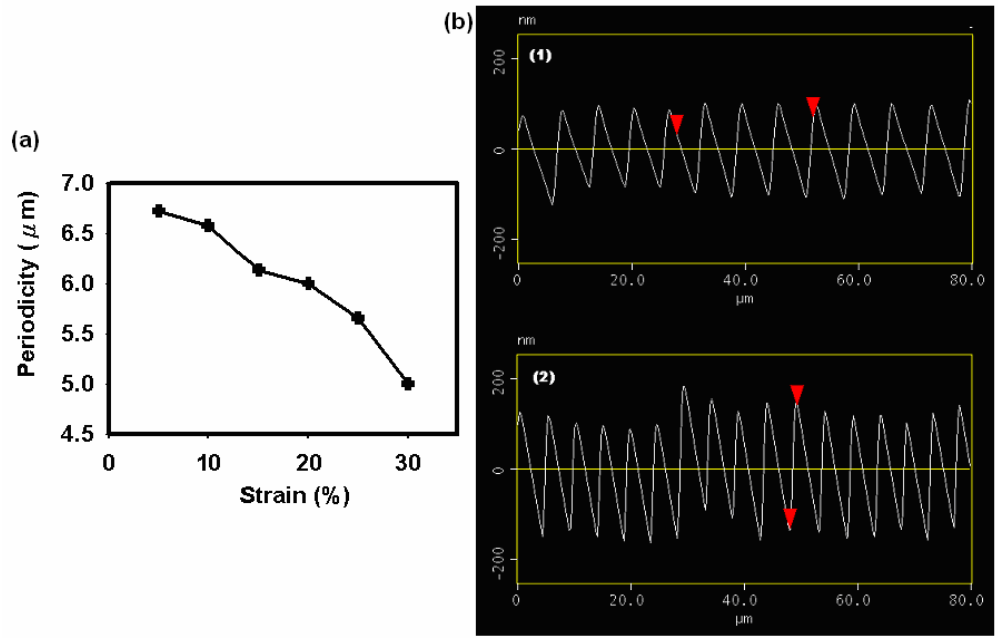

Fig.5.14 Effects of strength of the stretched strain and thickness of the metal film on the pitch and the depth of resulting surface wavy structures. (a) The pitch as a function of the strain when film thickness was fixed at 100 nm; (b) The corresponding AFM cross-section images for (a) showing the depths of the wavy structures at strains of 5% (upper) and 30% (lower), respectively

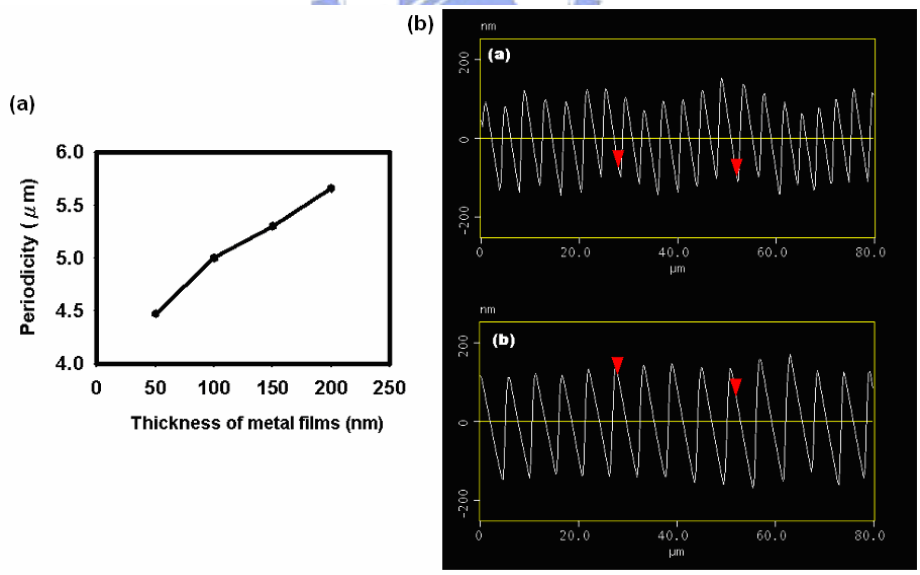

Fig.5.15 Effects of strength of the stretched strain and thickness of the metal film on the pitch and the depth of resulting surface wavy structures. (a) The pitch as a function of the thickness of metal film when the stretched strain was kept at 30%; (b) The corresponding AFM cross-section images for (a) showing the depth of the wavy structures for the film thickness of 50 nm (upper) and 200 nm (lower), respectively.

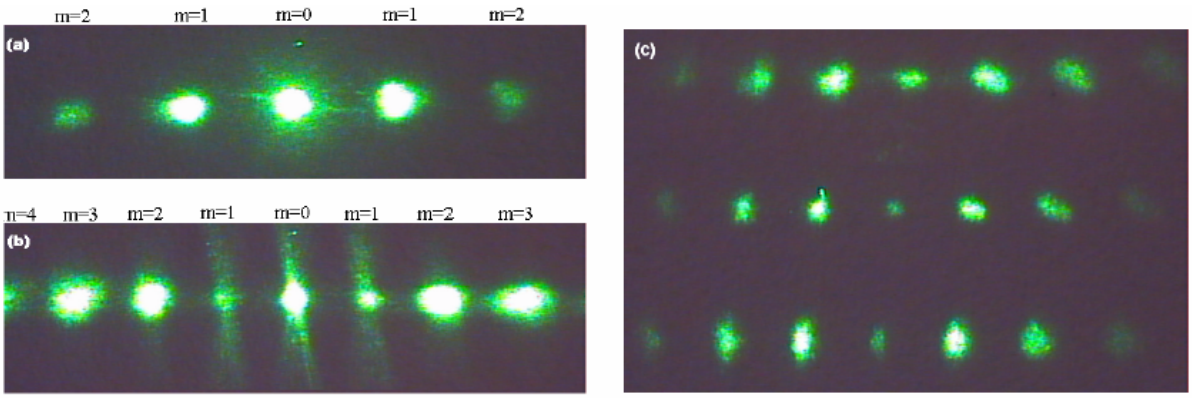

Fig.5.16 CCD images showing the diffractive patterns from the single-sided optical grating at differential fabrication conditions, (a) and (b), and from the double-sided optical gratings, (c).

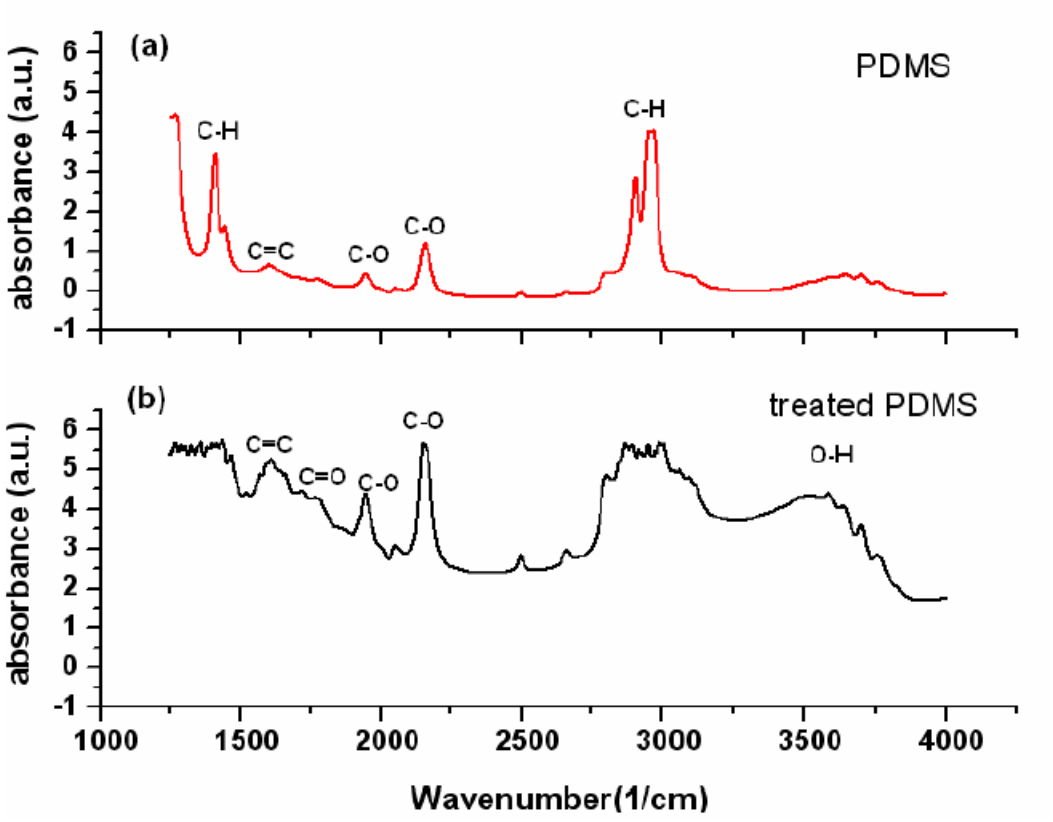

Fig.5.17 FTIR spectra of (a) the oxidized PDMS surface modified by dipped H_2SO_4/ HNO_3 liquids (b) the pristine PDMS surface

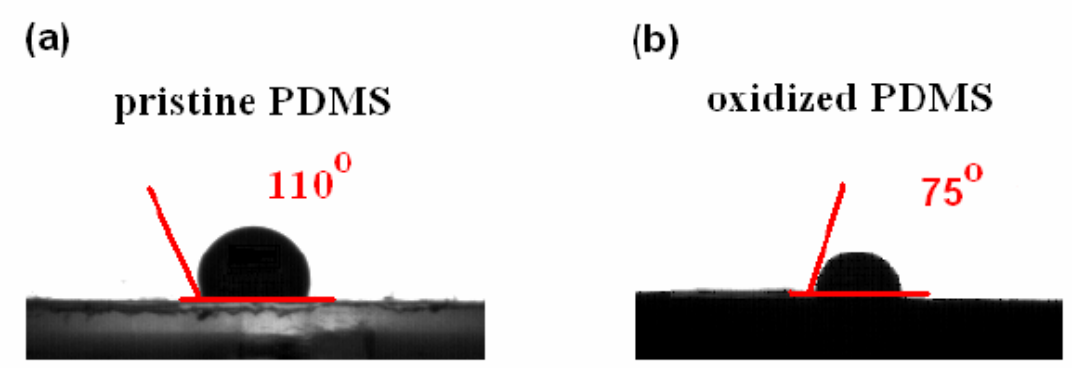

Fig.5.18 Photo of water drop on (a) the pristine PDMS surface (b) the oxidized PDMS surface

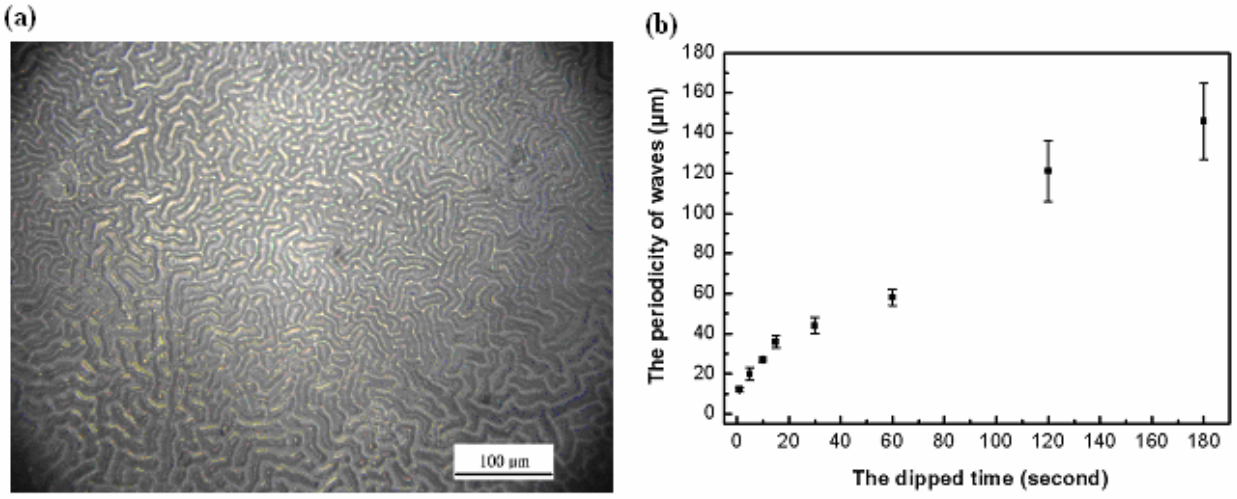

Fig.5.19 (a) OM image showing wrinkles formed by dipped into H_2SO_4/ HNO_3 liquids during five seconds on the PDMS surface (b) The dipped time as a function of the periodicity of wavy structures

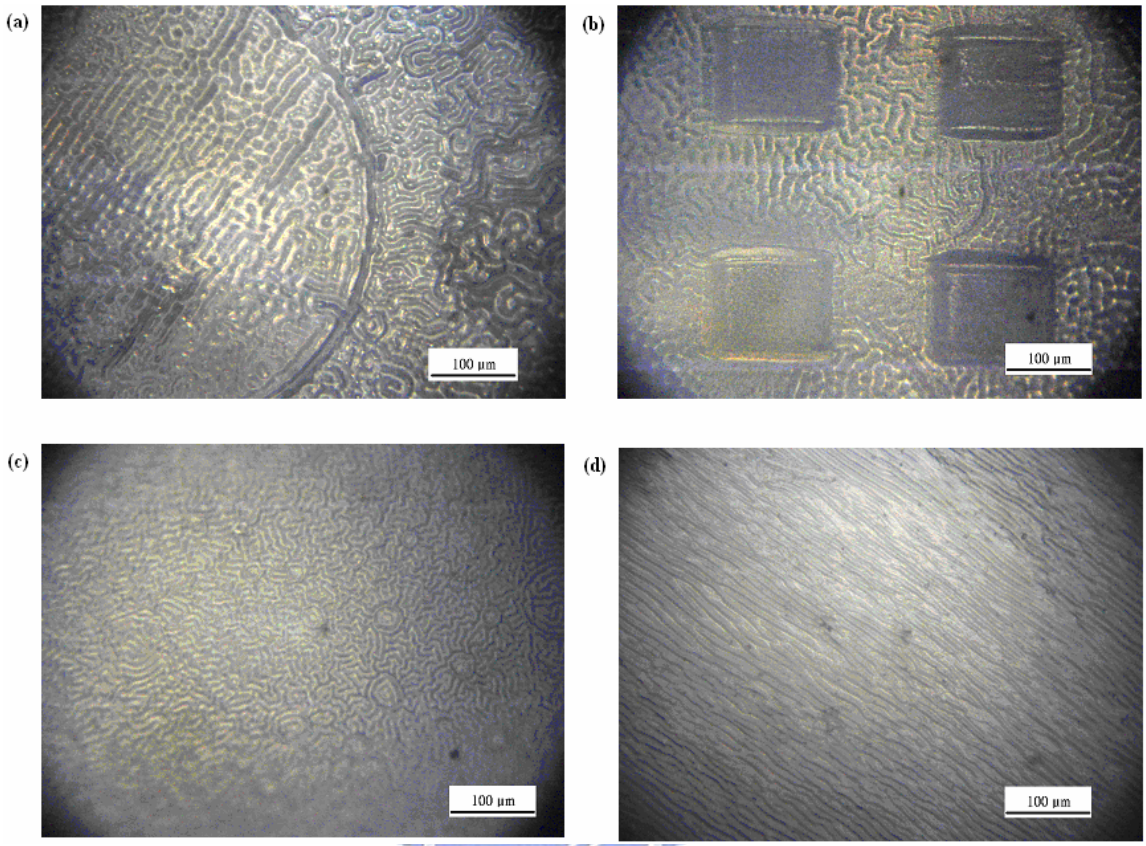

Fig.5.20 OM image showing wrinkles (a) on a two by two square step-like patterns array (b) on a circular step-like pattern (c) on the surface of a glass tube covered a layer of PDMS films (d) on the surface of a prestretched PDMS substrate

Chapter 6 Conclusion

Based on the unique characters of silicone polymers (PDMS), three kinds of microoptical elements, refractive/reflective microlenses and diffractive gratings, were achieved without the use of expensive instruments in this thesis. Some important conclusions for the fabrications and applications of microoptical elements by the use of PDMS polymer were demonstrated below.

In Chapter 4, a new fabrication method of nonspherical microlens arrays was here presented. Based on excimer laser microdrilling and spin coating processes, a PMMA film suspended on microdrilled holes was used as a concave mold. Then, the special patterns of PMMA molds could be easily replicated by the use of PDMS polymer, due to its low surface energy. In addition, PDMS polymers have a good transmittance in visible-light region (~85%) could be used as the optical material. By changing the shape of microdrilled holes, various curved microstructures could be fabricated, such as Gaussian-like, bifocal asymmetric microstructures and Gaussian-like structures with flat top surface. Therefore, the heights of these elements with the increase of the diameters of microholes and the thicknesses of PMMA films were increased. However, PDMS polymers are not suitable material for plasma treatment, leading to be not able to transfer microstructures' material from organic to in organic one. To overcome this problem, a new technology, soft replica molding, was developed. The original microstructures made of PDMS polymers were then replicated by another PDMS replica molding process. Under twice PDMS replication process, both convex and concave elastomeric molds can be fabricated.

Besides, based on light scattering phenomenon, a high-reflectance material, mixed PDMS rubber polymers with TiO_2 nanoscale powders, could be also achieved by the use of PDMS polymers. Both of concave and convex reflective elements could be fabricated through soft replica molding processes and these elements could directly reflect light without the deposition of metal coatings. Finally, the optical performances of these elements made of PDMS have been experimentally confirmed through optical examination.

In Chapter 5, surface contraction phenomenon of PDMS covered with metal films was here discussed. Because bilayer stacked structures, a stiff layer was capped on the

elastic PDMS substrate, was easily introduced compressive stresses into the mismatch interface and led to form wrinkles on the surface. First, some factors such as the thickness of metal films and the shape of patterns located on the surface of PDMS were examined. Some rules for the generated wavy structures could be tracked, such as the heights orientations and distribution of wavy structures. Then, wavy structures could be oriented by the guidance of external forces (This is the most effective way to orient orderly wavy structures). The orientation of the generated structures was always perpendicular to the pre-stretched direction and the pitch of the structure could be adjusted by controlling the strength of the prestretched strain and the thickness of surface metal film. Surprisingly, ordered wavy structures generated by the guidance of external forces were still found after removing the surface Au films. We extended this phenomenon to fabricate 1-/2-D optical gratings.

Besides, we presented a new technology to developed wavy structures using H_2SO_4/ HNO_3 solutions. A wet process can modify the surface of PDMS to form the oxidation on it. The hydrophobic surface of pristine PDMS was not only changed to hydrophilic but also formed wrinkles on it after chemical modification. The periodicity of wrinkles was controllable by controlling the duration of oxidation. Therefore, wrinkles were merely arranged orderly through a prestretched process before oxidization, which is different from bilayer metal/PDMS systems.

Reference

Chapter1

[1] M. Born and E. Wolf, Principles of Optics, 6th ed. Cambridge, MA: Cambridge Univ. Press, (1980).
[2] C. Palmer, Diffraction Grating Handbook. Rochester,NY: Milton Roy, (1994).
[3] B. Guenther, in Proc. Conf. Binary Optics: An Opportunity for Technical Exchange, 3227 (1993), 1–17.
[4] J. R. Meyers-Arendt, Introduction to Classical and Modern Optics, 4th ed. Upper Saddle River, NJ: Prentice-Hall, 1995.
[5] B. R. Brown and A.W. Lohmann, Appl. Opt., 5 (1966) 967–969.
[6] A. W. Lohmann and D. P. Paris, Appl. Opt., 6 (1967)1739-1748.
[7] L. Lesem, P. Hirsch and J. Jordan, IBM J. Res. Dev., 13(1969)150.
[8] J. A. Jordan, P. M. Hirsch, L. B. Lesem, and D. L. Van Rooy, Appl. Opt., 9(1970)1883–1887.
[9] W. H. Lee, in Progress in Optics Vol. XVI, E. Wolf, Ed. Amsterdam, The Netherlands: North-Holland, (1978) 121–232.
[10] L. d'Auria, J. P. Huignard, A. M. Roy, and E. Spitz, Opt. Comm., 5 (1972) 232–235,.
[11] J. J. Clair and C. I. Abitbol, in Progress in Optics Vol. XVI, E. Wolf, Ed. Amsterdam, The Netherlands: North-Holland, (1978)73–117.
[12] O. K. Ersoy, Optik, 46 (1976) 61–66.
[13] T. Fujita, H. Nishihara, and J. Koyama, Opt. Lett., 6 (1981) 613–615,.
[14] M. T. Gale and K. Knop, in Proc. SPIE Industrial Applications of Laser Technology, 398 (1983) 347–353.
[15] W. B. Veldkamp and G. J. Swanson, in Proc. Int. Conf. Computer Generated Holography, 437, (1983), 54–59.
[16] G. J. Swanson, MIT, Cambridge, MA, MIT Lincoln Lab. Rep. 854 (1989).
[17] M. B. Stern, "Binary optics fabrication," in Micro-Optics: Elements, Systems, and Applications, H. P. Herzig, Ed. London, U.K.: Taylor Francis, (1997) 53–85.
[18] P. P. Clark and C. Londoño, "Production of kinoforms by single-point diamond machining," Opt. News, 1989, 39–40.
[19] Z. D. Popovic, R. A. Sprague, and G. A. Neville Connell, Appl. Opt., 27 (1988) 1281–1284.
[20] D. Daly, R. F. Stevens, M. C. Hutley, and N. Davies, Meas. Sci. Technol., 1 (1990)759–766.
[21] R.H. Anderson, Appl. Opt. 18 (1979) 477–484
[22] R. Volkel, H.P. Herzig, P. Nussbaum, R.D. ndliker, Opt. Eng. 35 (1996) 3323–3330
[23] R.F. Stevens, N. Davies, Jour. Photographic Science 39 (1991) 199–208
[24] N. Lindlein, J. Pfund, J. Schwider, Opt. Eng. 40 (2001) 837–840
[25] G. Artzner, Opt. Eng. 31 (1992) 1311–1321,
[26] P. Arquint, P. D. van der Wal, B. H. van der Schoot and N. F. de Rooij, Proc. Transducers '95 (1995) 263–266
[27] J. C. L¨otters, W. Olthuis, P. H. Veltink and P. Bergveld, J. Micromech. Microeng. 6

(1996) 52–54
[28] Z. Chu, Proc. National Sensor Conf. (1996)121–4
[29] R. E. G. van Hal Advanced packaging of ISFETs, design, encapsulation and bonding PhD Thesis University of Twente (1994)
[30] S. J. Clarson and J. A. Semlyen, Siloxane Polymers (1993)
[31] ABCR Research Chemicals and Metals Catalogue Karlsruhe, Germany (1994)
[32] D. W. van Krevelen and P. J. Hoftyzer, Properties of Polymers (1976)
[33] Y. Xia and G. M. Whitesides, Soft Lithography, Angew. Chem. Int. Ed. 37, (1998) 550-575

Chapter2

[34] R. Hooke, Micrographia. The Royal Society of London,1665
[35] Z.D. Popovic and R.A. Sprague, G.A.N. Connell, Appl. Opt. 27(1988) 1281–1288
[36] H. Yang, C.-K. Chao, M.-K. Wei and C.-P. Lin, J. Micromech. Microeng. 14 (2004) 1197-1204
[37] H. Yang, C.-K. Chao, C.-P. Lin and S.-C. Shen, J. Micromech. Microeng. 14 (2004) 277-282
[38] C.-C. Yang, Y.-H. Huang, T.-C. Peng, M.-C.Wu, C.-L. Ho, C.-C. Hong, I.-M. Liu and Y.-T. Tsai, Sens. and Actuators A 136 (2007) 398-402
[39] D.L. MacFarlane, V. Narayan, J.A. Tatum, W.R. Cox, T. Chen and D.J. Hayes, Photon. Tech. Lett. 6 (1994) 1112-1114
[40] C.-C. Yang, T.-C. Peng, Y.-H. Huang, M.-C. Wu, C.-L. Ho and W.-J. Hong, Photon. Tech. Lett. 17(2005) 603 – 605
[41] D.M. Hartmann, O. Kibar and S.C. Esener, Opt. Lett. 25 (2000) 975-977.
[42] M. Wakaki, Y. Komachi, and G. Kanai, 37(1998) appl. opt.627 –631
[43]C.-S. Lee, and C.-H. Han, Sens. Actuators A 88(2001) 87-90
[44]Y.-S. Kim; J. Kim; J.-S. Choe, Y.-G. Rob, H. Jeon and J.C.Woo, Photon. Tech. Lett. 12(2000) 507 – 509
[45]K. P. Larsen, J. T. Ravnkilde, and O.Hansen, J. Micromech. Microeng. 15 (2005) 873-882
[46]C.-P. Lin, H. Yang , and C.-K. Chao, J. Micromech. Microeng. 13 (2003) 748-757
[47]S.-I. Chang , and J.-B. Yoon,Optics express12(2004)6366-6371
[48]C.-H. Tien, Y.-E. Chien, Y.Chiu , and H.-P. D. Shieh, Jpn. J. Appl. Phys. 42 (2003) 1280-1283
[49]H. Ottevaere, B. Volckaerts, M.Vervaeke, P. Vynck, A. Hermanne and Hugo Thienpont, Jpn. J. Appl. Phys. 43 (2003) 5832-5839
[50]T. Okamoto, M. Mori, T. Karasawa, S. Hayakawa, I. Seo, and H. Sato, Appl. Optics 38 (1999) 2991-2996
[51] N.F.Borrelli,D.L.Morse,R.H. Bellman, and W.L.Morgan, Appl.Optics 24 (1985) 2520-2525
[52]H. Takao, M. Okoshi, and Narumi Inoue, Jpn. J. Appl. Phys. 44(2005)241-242
[53]C.-Y. Chang, S.-Y. Yang, L.-S. Huang, and T.-M. Jeng, J. Micromech. Microeng. 16 (2006) 999-1005
[54]W.-K. Huang, C.-J. Ko and F.-C. Chen, Microelectron. Eng.83 (2006)1333-1335
[55]C.-Y. Chang, S.-Y. Yang, and M.-H. Chu, Microelectron. Eng.84 (2007) 355-361

[56]M.-H Wu and G.M. Whitesides, J. Micromech. Microeng.12(2002)747-758
[57]H.J.Nam, D.-Y. Jung, G.-R. Yi, and H. Choi, Langmuir, 22 (2006) 7358-7363
[58]H. Yabu, M. Shimomura, Langmuir, **21**, (2005)1709-1711
[59]O.J.Cayre and V.N.Pauuov, J.Mater.Chem.14(2004)3300-3302
[60]T. Dresel and J. Schwider, Appl. Surf. Sci., 106 (1996) 379-382
[61]A. Kowalik, K. Góra, Z. Jaroszewicz and A. Kołodziejczyk, Microelectron. Eng.77 (2005)347-357
[62]H. H. Solak, C. David, J. Gobrecht, V. Golovkina, F. Cerrina, S. O. Kim and P. F. Nealey, Microelectron. Eng. 67-68 (2003) 56-62
[63]J.J. Dubowski, A. Compaan and M. Prasad, Appl. Surf. Sci., 86(1995) 548-553
[64]S. Pissadakis, A. Ikiades, C. Y. Tai, N. P. Sessions and J. S. Wilkinson,Thin Solid Films 453-454 (2004) 458-461

Chapter 4

[65] J. L. Meriam, and L. G. Kraige, Engineering mechanics. Statics (1993) John Wiley & Sons
[66] P. Nussbaum, R. Völkel, H. P. Herzig, M. Eisner, and S. Haselbeck, Pure Appl. Opt. 6 (1997) 617–636
[67] S.Moller, and S.R.Forrest, J. Appl. Phys. 91 (2002) 3324-3327.
[68] H.W. Choi, E. Gu, C. Liu, J.M. Girkin, M.D. Dawson, J. Appl. Phys. 97 (2005) 063101.
[69] Y. Awatsuji, M. Sasada, N. Kawano, and T. Kubota, Jpn. J. Appl. Phys. 43 (2004) 5845-5849
[70] M. Daniel, and B. J. Thompson, Handbook of optical engineering (2001) New York :Marcel Dekker
[71] C.F. Bohren and D.R. Huffman, Absorption and Scattering of light by Small Particles (1983) Wiley

Chapter 5

[72] N. Bowden, S. Brittain, A.G. Evans, J.W. Hutchinson, G.M. Whitesides, Nature 393 (1998) 146–149.
[73] N. Bowden, W. T. S. Huck, K. E. Paul and G. M. Whitesides, Appl. Phys. Lett., 1999, 75, 2557–2559.
[74] D. B. H. Chua, H. T. Ng and S. F. Y. Li, Appl. Phys. Lett., 2000, 76, 721–723.
[75] W. T. S. Huck, N. Bowden, P. Onck, T. Pardoen, J. W. Hutchinson and G. M. Whitesides, Langmuir, 2000, 16, 3497–3501.
[76] T. Ohzono, S. I. Matsushita and M. Shimomura, Soft Matter, 2005, 1, 227–230.
[77] T. Ohzono and M. Shimomura, Phys. Rev. B: Condens. Matter, 2004, 69, Art. No. 132202.
[78] T. Ohzono and M. Shimomura, Simulation of strain-induced microwrinkle pattern dynamics with memory effect, Jpn. J. Appl. Phys., 2005, 44, 1055–1061.
[79]H. Hillborg, J. F. Anker, U. W. Gedde, G. D. Smith, H. K. Yasuda and K. Wilstro¨m, Polymer, 2000, 41, 6851–6863.
[80]J. Genzer, D. A. Fischer and K. Efimenko, Adv. Mater., 2003, 15, 1545–1547.

[81]K. Efimenko, M. Rackaitis, E. Manias, A. Vaziri, L. Mahadevan and J. Genzer, Nat. Mater., 2005, 4, 293–297.
[82]M. Ouyang, C. Yuan, R. J. Muisener, A. Boulares and J. F. Koberstein, Chem. Mater., 2000, 12, 1591–1596.
[83]K. Efimenko, W. E. Wallace and J. Genzer, J. Colloid Interface Sci., 2002, 254, 306–315.
[84] D. Halliday, R. Resnick and J. Walker, Fundamentals of Physics, New York: Wiley, 1993
[85] M.T. khorasani, H. Mirzadeh, and Z. Kermani, Appl. Surf. Sci. 242 (2005) 339-345
[86] S. Porro, S. Musso, M. Vinante, L. Vanzetti, M. Anderle, F. Trotta and A. Tagliaferro, Physica E, In Press
[87] Y. Zhang, Z. Shi, Z. Gu and S. Iijima, Carbon 38 (2000) 2055-2059
[88] M. T. Martínez, M. A. Callejas, A. M. Benito, M. Cochet, T. Seeger, A. Ansón, J. Schreiber, C. Gordon, C. Marhic, and O. Chauvet, Carbon 41(2003) 2247-2256
[89] C.-C. Chen, C.-F. Chen, C.-M. Chen and F.-T. Chuang, Electrochem. Commun. 9 (2007) 159-163
[90] B. Onida, L. Borello, C. Busco, P. Ugliengo, Y.Goto, S.Inagaki, E.Garrone, J. Phys. Chem. B 109(2005) 11961-11966
[91] T. okayasu, H.-L. Zhang, D.G. Bucknall, and G. D. Briggs, Adv.mater. 14 (2004) 1081–1088.